Schweizerische Eidgenossenschaft
Confédération suisse
Confederazione Svizzera
Confederaziun svizra

Eidgenössisches Departement für Umwelt, Verkehr, Energie und Kommunikation UVEK
Département fédéral de l'environnement, des transports, de l'énergie et de la communication DETEC
Dipartimento federale dell'ambiente, dei trasporti, dell'energia e delle comunicazioni DATEC

Bundesamt für Strassen
Office fédéral des routes
Ufficio federale delle Strade

Durability and Fatigue Performance of Cold-Curing Structural Adhesives in Bridge Construction

Dauerhaftigkeit und Ermüdungsbeständigkeit von kalthärtenden strukturellen Klebstoffen im Brückenbau

Durabilité et résistance à la fatigue des adhésifs structuraux à basse température dans la construction des ponts

ÉCOLE POLYTECHNIQUE FÉDÉRALE DE LAUSANNE EPFL
M. Savvilotidou, MSc, dipl.-Ing. AUTh, GR
A. P. Vassilopoulos, Dr. sc. techn., dipl. Mech-Ing. UPatras, GR
T. Keller, Prof. Dr. sc. techn., dipl. Bau-Ing. ETH, CH

Research Project AGB 2012/012 commissioned by the Bridge Research Working Group (AGB)

October 2017 **687**

Der Inhalt dieses Berichtes verpflichtet nur den (die) vom Bundesamt für Strassen unterstützten Autor(en). Dies gilt nicht für das Formular 3 "Projektabschluss", welches die Meinung der Begleitkommission darstellt und deshalb nur diese verpflichtet.
Bezug: Schweizerischer Verband der Strassen- und Verkehrsfachleute (VSS)

Le contenu de ce rapport n’engage que les auteurs ayant obtenu l’appui de l’Office fédéral des routes. Cela ne s'applique pas au formulaire 3 « Clôture du projet », qui représente l'avis de la commission de suivi et qui n'engage que cette dernière.
Diffusion : Association suisse des professionnels de la route et des transports (VSS)

La responsabilità per il contenuto di questo rapporto spetta unicamente agli autori sostenuti dall’Ufficio federale delle strade. Tale indicazione non si applica al modulo 3 “conclusione del progetto”, che esprime l’opinione della commissione d’accompagnamento e di cui risponde solo quest’ultima.
Ordinazione: Associazione svizzera dei professionisti della strada e dei trasporti (VSS)

The content of this report engages only the author(s) supported by the Federal Roads Office. This does not apply to Form 3 ‘Project Conclusion’ which presents the view of the monitoring committee.
Distribution: Swiss Association of Road and Transportation Experts (VSS)

Schweizerische Eidgenossenschaft
Confédération suisse
Confederazione Svizzera
Confederaziun svizra

Eidgenössisches Departement für Umwelt, Verkehr, Energie und Kommunikation UVEK
Département fédéral de l'environnement, des transports, de l'énergie et de la communication DETEC
Dipartimento federale dell'ambiente, dei trasporti, dell'energia e delle comunicazioni DATEC

Bundesamt für Strassen
Office fédéral des routes
Ufficio federale delle Strade

Durability and Fatigue Performance of Cold-Curing Structural Adhesives in Bridge Construction

Dauerhaftigkeit und Ermüdungsbeständigkeit von kalthärtenden strukturellen Klebstoffen im Brückenbau

Durabilité et résistance à la fatigue des adhésifs structuraux à basse température dans la construction des ponts

ÉCOLE POLYTECHNIQUE FÉDÉRALE DE LAUSANNE EPFL
M. Savvilotidou, MSc, dipl.-Ing. AUTh, GR
A. P. Vassilopoulos, Dr. sc. techn., dipl. Mech-Ing. UPatras, GR
T. Keller, Prof. Dr. sc. techn., dipl. Bau-Ing. ETH, CH

Research Project AGB 2012/012 commissioned by the Bridge Research Working Group (AGB)

October 2017 **687**

Imprint

Research centre and project team

Project leader
Prof. Dr. Thomas Keller

Members
Maria Savvilotidou
Dr. Anastasios P. Vassilopoulos

Review board

President
J.-C. Putallaz

Members
Dr. M. Alvarez
S. Cuennet
Dr. H.-R. Ganz

Applicant

Federal Road Office (FEDRO)

Source

Table of contents

Summary

Structural adhesives have been used in bridge construction since the 1960s. State-of-the-art applications consist of bonding steel or carbon fiber-reinforced polymer (CFRP) strips or plates onto existing structures or bonding steel rebars into holes drilled into existing concrete structures for strengthening or upgrading purposes. More recent applications are bonding of glass fiber-reinforced polymer (GFRP) bridge decks onto steel main girders. Structural adhesives used in bridge construction are in most cases applied on the construction site and are thus mainly cold-curing systems based on thermosetting epoxy resins. Depending on the ambient temperature, curing and full development of the physical and mechanical properties may take more than one year for mechanical and even much longer for physical properties, such as the glass transition temperature (Tg).

In contrast to mechanical connections, adhesives allow the easy joining of different materials and adherends of different geometries. In adhesively-bonded joints the free edges are normally sealed to prevent direct exposure to humidity and ultraviolet (UV) radiation. In view of the long service life of bridges, up to 100 years, it cannot however be excluded that, sooner or later, an initial sealing may become ineffective and the adhesive may thus be exposed to moisture or even stagnant water during several decades. If sealing is not correctly applied this can already occur before the adhesive is fully cured. Furthermore, the adhesive may also be exposed to humidity if the adherends have a certain diffusivity (e.g. the polymer matrix of CFRP materials) or porosity as in the case of concrete, where the pore water solution is, in addition, alkaline. Depending on the joint type and its location in the bridge, the joint and thus the adhesive may also be exposed to significant fatigue loading. During their service life, adhesives may thus be subjected to various physical and chemical aging mechanisms, which may be active simultaneously with different effects on the physical and mechanical properties. Effects based on physical mechanisms, such as physical aging (densification) and plasticization due to humidity may be reversible after drying, in contrast to chemical mechanisms, such as molecular chain scission caused by, for instance, hydrolysis.

In this context, the aim of this research project was to extend the knowledge about the long-term mechanical behavior of cold-curing epoxy adhesives exposed to a bridge environment – i.e. to a 1) dry, 2) wet, 3) dried environment, and to 4) fatigue – over a service life of 100 years. The scope was limited to the adhesive behavior, the interface behavior between adhesives and adherends could not be taken into account within the frame of this project. In the case of a wet environment, the exposure to demineralized and alkaline water was investigated; the exposure to salt water was not considered since no detrimental effect on epoxy adhesives has been observed so far. The work is a continuation of a previous study (AGB 2005-008, report no. 654), where cold-curing structural epoxies were investigated during the first ten days of isothermal curing at low temperatures (5-20°C).

During this project, cold-curing and post-cured standardized specimens of the commercial epoxy adhesive Sikadur 330 were exposed to the different environments mentioned above up to two years. The aging behavior under the wet environment was further accelerated by the Arrhenius method, i.e. by exposure to elevated temperatures in water baths, in order to extrapolate the behavior up to 100 years. The mechanical investigation was based on quasi-static and fatigue tensile experiments, the physical investigations included Dynamic Mechanical Analysis (DMA) and Differential Scanning Calorimetry (DSC). The physical investigations mainly concerned Tg, where significant differences, up to 15°C, were found depending on the applied method. It was concluded that the Tg onset-value of the storage modulus, obtained from DMA, should be used for the structural characterization, since this value marks the beginning of significant losses of mechanical properties. Furthermore, a set of resistance factors applicable for adhesives is proposed, which takes into account the source of the adhesive properties, the method of adhesive application, the type of loading, the environmental conditions and fatigue.

In a dry environment of a sealed joint, thus protected from humidity and UV radiation, the main concurring aging mechanisms are physical aging and continuation of curing. Physical aging of epoxy adhesives occurs at aging temperatures lower than Tg, and is driven by a thermodynamic disequilibrium. During physical aging, i.e. approaching the thermodynamic equilibrium, an increase in mass density (densification), and thus a decrease in specific volume (volumetric relaxation), and a decrease in molecular configurational energy are observed. If the exposure temperature is low, physical aging effects may be active for several years. They may also be erased however, i.e. the adhesive is de-aged, if heating occurs. During the continuation of curing on the other hand, the specific volume and cross-link density increase. The experimental results during the first year revealed that physical aging was predominant in the earlier age and curing was predominant in the later age; both affected the physical and mechanical properties. The E-modulus exhibited a maximum in the earlier age due to a maximum mass density caused by physical aging. In the later age, when curing became predominant, mass density and thus the E-modulus decreased. After the first week, the E-modulus development became independent of the curing conditions, i.e. partly or fully cured. Tensile strength and failure strain depended mainly on the cross-link density and their development was thus influenced by the curing conditions and delayed in the earlier age due to physical aging. Eventually, all curing conditions resulted in similar tensile properties, i.e. maximum strength and failure strain and a reduced E-modulus after a maximum, after less than nine months of aging. However, the glass transition temperature still depended on the curing conditions and was not yet fully developed after one year. Based on these results, specifications about the required preconditioning of adhesive specimens for mechanical tests were established, which normally are required for the ultimate and serviceability limit state verifications in the design of adhesively-bonded joints.

In a wet environment, the main mechanism observed in epoxy adhesives so far was plasticization, resulting in a significant reduction of the glass transition temperature, stiffness and strength. These effects were found to be reversible however when the material was dried again. The effect of alkalinity, i.e. alkaline water exposure, on physical and mechanical epoxy resin properties has also already been investigated, although with contradictory results. The experimental results obtained herein confirmed a significant decrease of the glass transition temperature, tensile E-modulus and tensile strength, which could be attributed to plasticization. Plasticization changed the stress-strain behavior from almost linear under dry conditions to highly nonlinear at full saturation. A retention of 70% of the E-modulus and strength at an average 10°C reference temperature was predicted after a 100-year bridge service life at full immersion. The immersion in alkaline water had no detrimental effect. In the case of one-dimensional diffusion, moisture ingress and associated degradation of mechanical properties is limited to about 40 mm depth after 100 years. Depending on the joint type, this limit may be critical or not. In the case of a typical 300-500 mm long adhesive joint between a bridge deck and a top steel girder flange, the effect is marginal, while in the case of an only 1 mm thick adhesive joint between a CFRP layer and the bridge substrate the effect may become critical. However, even is this case, the maximal loss of mechanical properties is limited to about 30%, i.e. 70% of strength and stiffness are retained. The Tg under wet conditions remained in the range of 50-60°C. Depending on the exposition of the joint, e.g. for a CFRP-strip strengthening of the deck slab against negative moments below the asphalt, where temperature may rise up to 80°C, these values may be critical. After drying the immersed and fully saturated material, full recovery of the mechanical and physical properties was obtained.

Numerous studies exist on the fatigue behavior of adhesively-bonded joints with or without temperature and water effects. Fewer information exists on the investigation of the fatigue behavior of bulk structural adhesives, while very little information is available on the fatigue behavior of bulk adhesives subjected to wet conditions. The results obtained herein showed that the examined structural adhesive, even if degraded due to water uptake during 100 years, is capable of resisting fatigue stresses caused by typical bridge fatigue loads. Fatigue life between 2 and 10 million cycles was reached without failure at maximum stress levels higher than 5 MPa (at R=0.1). The plasticization and consequently the softening due to water uptake was responsible for the main differences between the behavior of the wet and the other two specimen sets, i.e. dry and dried specimens. The wet, i.e. fully saturated specimens exhibited the shortest fatigue life while the dried specimens showed a longer life compared to the dry ones, i.e. a positive effect of a small amount of remaining water. In contrast to steel for instance, the slopes of the S-N (stress vs. number of cycle) curves were much lower, however, the adhesive did not exhibit any fatigue limit.

As mentioned above, this project focused on the investigation of the behavior of bulk adhesives and did thus not yet consider the performance of adhesively-bonded joints, e.g. between concrete, steel or CFRP strengthening elements. Experimental work on joints has shown that, in many cases, the interface behavior may be more critical than the adhesive behavior. Furthermore, the above results are valid for the two-component epoxy adhesive Sikadur 330. They require further validation for different adhesive products.

Zusammenfassung

Strukturelle Klebstoffe werden im Brückenbau seit den 1960er-Jahren verwendet. Heute gebräuchliche Anwendungen sind das Aufkleben von Stahl- oder Kohlefaserverbund- (CFK) Lamellen auf bestehende Tragwerke oder das Einkleben von Anschlussbewehrung in Bohrungen von Stahlbetonbauteilen, beides meist zu Verstärkungszwecken. Jüngste Anwendungen sind das Aufkleben von Glasfaserverbund- (GFK) Brückenplatten auf Stahl-Hauptträger. Im Brückenbau werden Klebeverbindungen meist auf der Baustelle vorgenommen, deswegen können in der Regel nur kalthärtende Klebstoffe, meist auf Epoxidharzbasis, eingesetzt werden. In Abhängigkeit von der Umgebungstemperatur kann die Aushärtung und somit die vollständige Entwicklung der Klebstoff-Eigenschaften mehr als ein Jahr für die mechanischen und sogar wesentlich länger für die physikalischen Eigenschaften dauern, insbesondere für die Glasübergangstemperatur (T_g).

Im Gegensatz zu mechanischen Verbindungen erlauben Klebeverbindungen das einfache Fügen von verschiedenen Materialien und Bauteilen mit unterschiedlichen Geometrien. Bei Klebeverbindungen sind die freien Ränder normalerweise abgedichtet um eine Exposition gegenüber Feuchtigkeit und Ultraviolett- (UV-) Strahlung zu verhindern. Angesichts der langen Nutzungsdauer von Brücken, bis zu 100 Jahren, ist es jedoch denkbar, dass die Abdichtung früher oder später unwirksam wird und der Klebstoff somit Feuchtigkeit oder gar stagnierendem Wasser ausgesetzt wird, und dies im ungünstigsten Fall während Jahrzehnten. Wenn die Abdichtung nicht korrekt aufgebracht wird, kann dies bereits bevor der vollständigen Aushärtung des Klebstoffs geschehen. Ein Klebstoff kann auch Feuchtigkeit ausgesetzt werden wenn die zu verbindenden Fügeteile ein gewisses Diffusionsvermögen aufweisen (z.B. die Polymermatrix von CFK Materialen) oder porös sind, wie im Stahlbeton, mit zusätzlich alkalischer Porenwasserlösung. In Abhängigkeit der Art der Klebeverbindung und ihrer Anordnung im Brückentragwerk kann diese im Weiteren einer wesentlichen Ermüdungsbeanspruchung unterliegen. Klebstoffe können somit während ihrer Nutzungsdauer unterschiedlichsten physikalischen und chemischen Alterungsprozessen ausgesetzt sein, die häufig gleichzeitig aktiv sind und unterschiedliche Auswirkungen auf die physikalischen und mechanischen Eigenschaften haben können. Auswirkungen basierend auf physikalischen Prozessen, wie physikalische Alterung (Verdichtung) oder Plastifizierung aufgrund von Feuchtigkeit, können nach erfolgter Trocknung reversibel sein, im Gegensatz zu jenen von chemischen Prozessen, wie molekulare Kettenaufspaltung aufgrund von Hydrolyse beispielsweise.

In diesem Kontext war die Zielsetzung dieses Forschungsprojektes das Wissen zum langzeit-mechanischen Verhalten von kalthärenden Epoxidklebstoffen zu erweitern, und dies unter spezifischen Brückenexpositionen wie 1) trockene, 2) feuchte, 3) (nach Sättigung) getrocknete Exposition, sowie 4) Ermüdung, während einer Nutzungsdauer bis zu 100 Jahren. Der Projektrahmen war auf das Verhalten des Klebstoffs selbst beschränkt, das Verhalten der Verbundflächen (Interfaces) zwischen Klebstoff und Fügeteilen war nicht Gegenstand der Untersuchung. Im Falle einer feuchten Umgebung wurde die Exposition gegenüber reinem und alkalischem Wasser untersucht; die Exposition gegenüber Salzwasser wurde nicht berücksichtigt, da bisher keine schädlichen Auswirkungen auf Epoxidklebstoffe beobachtet wurden. Die vorliegende Arbeit ist eine Fortsetzung eines vorgängigen Projektes (AGB 2005-008, Bericht Nr. 654), in dem kalthärtende Epoxidklebstoffe während dem Aushärten in den ersten zehn Tagen unter tiefen Temperaturen (5-20°C) untersucht wurden.

Im Rahmen dieses Projektes wurden sich in Aushärtung befindende und bereits ausgehärtete genormte Prüfkörper des Epoxidklebstoffes Sikadur 330 während bis zu zwei Jahren den obenerwähnten Expositionen ausgesetzt. Das Alterungsverhalten unter feuchter Exposition wurde weiter gemäss der Arrhenius-Methode beschleunigt, d.h. die Prüfkörper wurden in Wasserbädern erhöhten Temperaturen ausgesetzt um das

Verhalten bis auf 100 Jahre extrapolieren zu können. Mechanisch wurde das Zugverhalten unter quasi-statischer und Ermüdungsbeanspruchung untersucht, die physikalischen Experimente umfassten Dynamische Mechanische Analyse (DMA) sowie Differentiale Scanning Kalorimetrie (DSC). Die physikalischen Untersuchungen betrafen hauptsächlich die Glasübergangstemperatur T_g, wobei je nach Methode erhebliche Differenzen, bis zu 15°C, festgestellt wurden. Der Schluss wurde gezogen, dass für T_g der Onset-Wert des DMA Speicher-Moduls verwendet werden sollte, da nur dieser Wert den Beginn des signifikanten Abfalls der mechanischen Eigenschaften kennzeichnet. Im Weiteren wird ein Set von Widerstandsbeiwerten für die Klebstoffbemessung vorgeschlagen, welches die Quelle der mechanischen Eigenschaften, Applikationsmethode, Beanspruchungsart sowie Exposition und Ermüdungsbeanspruchung berücksichtigt.

Im Falle einer trockenen Exposition unter einer abgedichteten Verbindung, d.h. geschützt vor Feuchtigkeit und UV-Strahlung, sind die hauptsächlichen und gleichzeitig ablaufenden Alterungsprozesse physikalische Alterung und fortschreitende Aushärtung. Eine physikalische Alterung von Epoxidklebstoffen basiert auf einem thermodynamischen Ungleichgewicht und erfolgt bei Temperaturen unterhalb von T_g. Um sich dem thermodynamischen Gleichgewicht anzunähern nimmt die Massendichte zu, das spezifische Volumen nimmt entsprechend ab (bezeichnet als volumetrische Relaxation) und auch die molekulare Konfigurationsenergie nimmt ab. Bei relativ geringer Umgebungstemperatur können die Auswirkungen der physikalischen Alterung mehrere Jahre andauern. Die Auswirkungen können jedoch durch Erwärmung wieder rückgängig gemacht werden. Die fortschreitende Aushärtung andererseits erhöht das spezifische Volumen und die Vernetzungsdichte. Die experimentellen Resultate während dem ersten Jahr haben ergeben, dass in der Anfangsphase die Auswirkungen der physikalischen Alterung überwiegen und jene der fortschreitenden Aushärtung in der späteren Phase; beide beeinflussten dabei die physikalischen und mechanischen Eigenschaften. Der E-Modul wies ein Maximum in der Anfangsphase auf, aufgrund des durch die physikalische Alterung verursachten Maximums in der Massendichte. In der späteren Phase, als die Aushärtung dominant wurde, nahmen Massendichte und E-Modul ab. Nach einer Woche wurde der Verlauf der Entwicklung des E-Moduls unabhängig von den Aushärtungsbedingungen, d.h. erst teilweise oder vollständig ausgehärtet. Zugfestigkeit und Bruchdehnung hingen in erster Linie von der Vernetzungsdichte ab und ihr Verlauf wurde deswegen von den Aushärtungsbedingungen beeinflusst; er wurde anfangs durch die physikalische Alterung verzögert. Schlussendlich, nach weniger als neun Monaten, wurden aber unter allen Aushärtungsbedingungen ähnliche Eigenschaften erreicht, d.h. maximale Zugfestigkeit und Bruchdehnung und ein gegenüber der Anfangsphase etwas reduzierter E-Modul. Die Glasübergangstemperatur hingegen war nach einem Jahr noch nicht voll entwickelt und immer noch von den Aushärtungsbedingungen abhängig. Basierend auf diesen Resultaten wurden Spezifikationen hinsichtlich den notwendigen Aushärtungsbedingungen von Prüfkörpern für mechanische Prüfungen definiert, um die für den Nachweis der Tragsicherheit und Gebrauchstauglichkeit erforderlichen Klebstoff-Materialkennwerte zu bestimmen.

In einer feuchten Umgebung war der bisher bei Epoxidklebstoffen hauptsächlich beobachtete Alterungsprozess die Plastifizierung, die eine erhebliche Reduktion von Steifigkeit, Festigkeit und Glasübergangstemperatur zur Folge hatte. Diese Auswirkungen waren jedoch nach der Trocknung des Materials reversibel. Die Auswirkung von Alkalität, d.h. alkalischer Wasserexposition auf die physikalischen und mechanischen Eigenschaften von Epoxidharzen wurde auch schon untersucht, die Resultate waren allerdings widersprüchlich. Die in diesem Projekt erhaltenen Resultate bestätigten die erhebliche Abnahme von Glasübergangstemperatur, E-Modul und Zugfestigkeit, die deshalb auf den Plastifizierungsprozess zurückgeführt werden können. Die Plastifizierung veränderte auch das Spannungs-Dehnungsverhalten von beinahe linear unter trockener zu stark nichtlinear unter voll gesättigter Exposition. Nach einer vollständig eingetauchten Wasserexposition unter einer 10°C Referenztemperatur, während einer hundertjährigen Nutzungsdauer, wurden verbleibende E-Modul- und Festigkeitswerte von 70% der Anfangswerte unter trockenen Bedingungen extrapoliert. Die Alkalität des Wassers hatte keinen nachteiligen Einfluss auf diese Resultate. Im Falle einer eindimensionalen Diffusion ist die Feuchtigkeitseindringtiefe in den Klebstoff und die damit verbundene

Länge der Abnahme der mechanischen Eigenschaften auf ca. 40 mm nach 100 Jahren begrenzt. In Abhängigkeit der Art der Klebeverbindung kann diese Länge kritisch sein oder nicht. Im Falle einer 300-500 mm langen Klebeverbindung zwischen einer Brückenplatte und dem oberen Flansch eines Stahlträgers beispielsweise sind die Auswirkungen gering, während im Falle einer nur 1 mm dicken Klebeverbindung zwischen CFK Lamellen und Brückenkonstruktion die Auswirkungen erheblich sein können. Allerdings beträgt auch in diesem Fall die Abnahme der mechanischen Eigenschaften nicht mehr als etwa 30%, d.h. ca. 70% der Steifigkeit und Festigkeit bleiben erhalten. Die T_g-Werte unter feuchten Bedingungen verblieben im Bereich von 50-60°C. Abhängig von der Exposition der Klebeverbindung können diese Werte kritisch werden, z.B. im Falle einer CFK Lamellenverstärkung für negative Momente auf der Oberseite einer Brückenplatte unter dem Asphalt, wo die Temperaturen bis 80°C ansteigen können. Nach der Trocknung des Klebstoffs erholten sich jedoch die physikalischen und mechanischen Eigenschaften vollständig.

Zahlreiche Arbeiten existieren zum Ermüdungsverhalten von Klebeverbindungen mit oder ohne Exposition gegenüber Temperaturen und Feuchtigkeit. Weniger untersucht wurde bisher das Ermüdungsverhalten von reinen Klebstoffen und sehr wenige Kenntnisse bestehen zum Ermüdungsverhalten von Feuchtigkeit ausgesetzten Klebstoffen. Die erhaltenen Resultate haben gezeigt, dass der untersuchte Klebstoff auch nach Schädigung während 100 Jahren Wasserlagerung noch in der Lage ist, Ermüdungsspannungen zu widerstehen, wie sie von typischen Brücken-Ermüdungseinwirkungen verursacht werden. Unter maximalen Spannungen über 5 MPa (bei R=0.1) wurden zwischen 2 und 10 Millionen Lastwechsel ohne Versagen erreicht. Die Plastifizierung und somit die Steifigkeitsabnahme aufgrund der Wasseraufnahme war der Hauptgrund für das unterschiedliche Verhalten der gesättigten und der trockenen sowie getrockneten Proben. Während die vollständig gesättigten Proben die geringste Ermüdungslebensdauer aufwiesen, erreichten die getrockneten Proben eine längere Lebensdauer als die trockenen Proben, was durch einen positiven Effekt einer kleinen verbleibenden Restfeuchtigkeit in den getrockneten Proben erklärt wurde. Im Gegensatz zu Stahl beispielsweise waren die Neigungen der S-N Kurven (Spannung gegen Anzahl Lastwechsel) wesentlich geringer, der Klebstoff wies jedoch keine Dauerfestigkeitsgrenze auf.

Wie bereits erwähnt, fokussierte das vorliegende Projekt auf die Untersuchung des reinen Klebstoffs und beinhaltete nicht das Verhalten von gesamten Klebeverbindungen, z.B. zwischen Stahl, Beton und CFK Verstärkungslamellen. Experimentelle Resultate von Klebeverbindungen haben gezeigt, dass vielfach das Verhalten der Verbundflächen (Interfaces) kritischer sein kann als jenes des Klebstoffs. Im Weiteren sind die oben zusammengefassten Resultate in erster Linie für den Zweikomponenten-Epoxidklebstoff Sikadur 330 gültig und bedürfen einer weiteren Validierung für andere Klebstoffprodukte.

Résumé

Les adhésifs structurels sont utilisés dans la construction de ponts depuis les années 1960. Les applications traditionnelles consistent aujourd'hui à coller des bandes ou plaques en acier ou en polymère renforcé par des fibres de carbone (CFRP) sur des structures existantes ou alors à coller des barres d'acier de liaison dans des percements effectués dans des structures en béton existantes, afin de renforcer ou améliorer les performances structurelles. Des applications plus récentes consistent à coller des dalles de pont en polymère renforcé par des fibres de verre (GFRP) sur des poutres maîtresses en acier. Les adhésifs structuraux utilisés dans la construction de ponts sont généralement appliqués sur le chantier et sont donc principalement des systèmes de durcissement à froid à base de résines époxydes thermodurcissables. Le durcissement et le développement complet des propriétés physiques et mécaniques de l'adhésif dépendent de la température ambiante et nécessitent plus d'un an en ce qui concerne les propriétés mécaniques et même bien au-delà pour les propriétés physiques, comme par exemple la température de transition vitreuse (Tg).

Contrairement aux connexions mécaniques, les adhésifs facilitent l'assemblage de différents types de matériaux et d'éléments de géométries différentes. Les bords libres des joints collés sont généralement scellés afin d'empêcher l'exposition directe à l'humidité et aux rayons ultraviolets (UV). Compte tenu de la durée de vie des ponts, pouvant atteindre jusqu'à 100 ans, il est impossible d'exclure que, tôt ou tard, un scellement puisse devenir inefficace et que l'adhésif puisse ainsi être exposé à l'humidité ou même à de l'eau stagnante pendant plusieurs décennies dans les cas les plus défavorables. En cas d'application incorrecte de l'étanchéité, cela peut se produire avant même que l'adhésif ne soit complètement durci. L'adhésif peut également être exposé à l'humidité lorsque les substrats ont une certaine perméabilité (par exemple la matrice polymère de matériaux CFRP) ou porosité, comme dans le cas du béton où la solution aqueuse des pores est en outre alcaline. Selon le type de joint et son emplacement dans le pont, le joint collé et par conséquent l'adhésif peuvent aussi être exposés à des sollicitations de fatigue importantes. Ainsi, pendant leur durée de vie, les adhésifs peuvent être soumis à divers mécanismes physiques ou chimiques de vieillissement pouvant agir simultanément et ayant différents effets sur leurs propriétés physiques et mécaniques. Les effets causés par des mécanismes physiques tels que le vieillissement physique (densification) et la plastification due à l'humidité peuvent être réversibles après séchage, contrairement à ceux occasionnés par des mécanismes chimiques tel que la scission des chaînes moléculaires provoquée par hydrolyse.

Dans ce contexte, l'objectif de ce projet de recherche était d'élargir les connaissances sur le comportement mécanique à long terme des adhésifs époxydes durcissant à froid et exposés à un environnement de pont, c'est-à-dire à un environnement 1) sec, 2) humide, 3) séché (après saturation), et à 4) la fatigue - sur une durée de vie de 100 ans. Le cadre du projet s'est limité au comportement de l'adhésif, le comportement de l'interface entre l'adhésif et les substrats ne faisant pas partie de cette étude. Dans le cas d'un environnement humide, l'exposition à l'eau déminéralisée et alcaline a été investiguée. L'exposition à l'eau salée n'a pas été considérée puisqu'aucune dégradation n'a été observée jusqu'à présent sur les adhésifs époxydes. Ce travail constitue la suite d'une recherche précédente (AGB 2005-008, rapport n° 654), dans laquelle les adhésifs époxydes structuraux durcissant à froid ont été étudiés lors des dix premiers jours de durcissement isotherme à basse température (5-20°C).

Au cours de ce projet, des éprouvettes normalisées d'adhésif époxyde Sikadur 330 durcies à froid et post-durcies ont été exposées aux divers environnements mentionnés ci-dessus pendant une durée maximale de deux ans. Le comportement au vieillissement en environnement humide a de plus été accéléré par la méthode d'Arrhenius, soit par exposition à des températures élevées dans des bains d'eau, afin d'extrapoler le comportement jusqu'à 100 ans. L'investigation mécanique s'est basée sur des essais de traction quasi-statique et de fatigue et les investigations physiques ont compris l'analyse mécanique dynamique (DMA) et la calorimétrie différentielle à balayage (DSC). Les

investigations physiques ont concerné principalement la température de transition vitreuse Tg, pour laquelle des différences significatives, pouvant atteindre 15°C, ont été trouvées selon la méthode appliquée. En conclusion, la valeur on-set Tg du module de stockage, obtenue à partir du DMA, devrait être utilisée pour la caractérisation structurale de l'adhésif car cette valeur indique à elle seule le début de pertes significatives des propriétés mécaniques. En outre, une série de facteurs de résistance applicables aux adhésifs est proposée, tenant compte de la source des propriétés de l'adhésif, de sa méthode d'application, du type de chargement, des conditions environnementales et des sollicitations de fatigue.

Dans le cas d'un environnement sec et d'un joint étanche, protégé de l'humidité et du rayonnement UV, les principaux mécanismes de vieillissement concomitants sont le vieillissement physique et la progression de la polymérisation. Le vieillissement physique des adhésifs époxydes se produit à des températures inférieures à Tg et est dicté par un déséquilibre thermodynamique. Le vieillissement physique, c'est-à-dire l'approche de l'équilibre thermodynamique, entraîne une augmentation de la densité (densification), ainsi qu'une diminution du volume spécifique (relaxation volumétrique) et une diminution de l'énergie orbitale moléculaire. Les effets du vieillissement physique peuvent être actifs pendant plusieurs années lorsque la température d'exposition est faible. Ils peuvent également être gommés lorsque l'adhésif est réchauffé. D'autre part, au cours de la progression de la polymérisation, le volume spécifique et la densité des liaisons entre chaînes moléculaires augmentent. Les résultats expérimentaux au cours de la première année ont révélé que le vieillissement physique était prédominant au jeune âge tandis que la polymérisation était prédominante ultérieurement; les deux mécanismes ont affecté les propriétés physiques et mécaniques. Le module d'élasticité était maximal au jeune âge en raison d'une densité maximale due au vieillissement physique. Ultérieurement, lorsque la polymérisation devint prédominante, la densité et donc le module d'élasticité ont diminué. Après la première semaine, le développement du module d'élasticité était devenu indépendant des conditions de polymérisation, que cette dernière soit partielle ou totale. La résistance à la traction et la déformation de rupture dépendaient principalement de la densité des liaisons entre chaînes moléculaires. Leur développement était donc influencé par les conditions de polymérisation et, au jeune âge, retardé en raison du vieillissement physique. Finalement et après moins de neuf mois de vieillissement, les différentes conditions de polymérisation ont conduit à des propriétés de traction similaires, c'est-à-dire une résistance à la traction et une déformation de rupture maximales ainsi qu'un module d'élasticité réduit. Toutefois, la température de transition vitreuse dépendait toujours des conditions de polymérisation et n'était pas encore complètement développée après un an. En se basant sur ces résultats, des spécifications concernant le pré-conditionnement des éprouvettes d'adhésif pour les essais mécaniques ont été établies, ce qui est normalement requis pour les vérifications des états limites ultimes et de service réalisées lors de la conception de joints collés.

En environnement humide, le mécanisme principal observé dans les adhésifs époxydes est la plastification, entraînant une réduction significative de la température de transition vitreuse, de la rigidité et de la résistance. Cependant, ces effets se sont révélés réversibles lorsque le matériau est à nouveau séché. L'effet de l'alcalinité, c'est-à-dire à l'exposition à une eau alcaline, sur les propriétés physiques et mécaniques de la résine époxyde a aussi été étudié, menant à des résultats contradictoires. Les résultats expérimentaux obtenus dans cette recherche ont confirmé une diminution significative de la température de transition vitreuse, du module d'élasticité et de la résistance à la traction, ce qui pourrait être attribué à la plastification. La plastification a modifié la loi de comportement (contrainte-déformation), de quasi-linéaire en environnement sec à fortement non-linéaire en environnement humide, complètement saturé. Un maintien de 70% du module d'élasticité et de la résistance à une température moyenne de référence de 10°C a été prédit après une durée de vie du pont de 100 ans en immersion totale. L'immersion dans l'eau alcaline n'a montré aucune dégradation. Dans le cas d'une diffusion unidimensionnelle, la progression de l'humidité et la dégradation correspondante des propriétés mécaniques sont limitées à 40 mm de profondeur après 100 ans. Selon le type de joint cette limite peut ou non devenir critique. L'effet est marginal dans le cas d'un joint collé de 300 à 500 mm de longueur entre une dalle de pont et l'aile supérieure d'une poutre en acier, alors que l'effet peut être critique dans le cas d'un joint de 1 mm d'épaisseur entre une couche de CFRP et le substrat d’un pont. Cependant, même dans ce cas, la perte maximale des propriétés mécaniques est limitée à environ 30%, ce qui veut dire que 70% de la résistance et de la rigidité sont conservées. La Tg en environnement humide est restée dans la plage de 50 à 60°C. Ces valeurs peuvent devenir critiques selon l'exposition du joint, comme dans le cas d’un renforcement à la partie supérieure d’une dalle de pont, avec des bandes de CFRP, pour reprendre les moments négatifs. La température sous l'asphalte peut y atteindre 80°C. Une récupération complète des propriétés mécaniques et physiques a été observée après séchage du matériau immergé entièrement saturé.

Il existe de nombreuses études sur le comportement à la fatigue des joints collés, prenant ou pas en considération l’effet de la température et de l’eau. Quelques informations existent concernant le comportement à la fatigue des adhésifs structuraux, alors que très peu d'information est disponible sur le comportement à la fatigue des adhésifs soumis à des conditions d’humidité. Les résultats obtenus dans ce projet ont montré que l'adhésif structurel examiné, bien qu’il soit dégradé suite à l’absorption d’eau pendant une durée de 100 ans, est capable de résister aux contraintes de fatigue auxquelles un pont est soumis au cours de sa durée de vie. Une durée de vie de fatigue entre 2 et 10 millions de cycles a été atteinte sans rupture pour des contraintes maximales supérieures à 5 MPa (sous (R=0.1). La plastification et, par conséquent, l'adoucissement dû à l'absorption d’eau étaient responsables des différences principales entre le comportement des échantillons à l’état humide et celui des deux autres lots d’échantillons, c'est-à-dire ceux secs et séchés. Les échantillons humides, et donc entièrement saturés, présentaient la plus faible durée de vie à la fatigue tandis que les échantillons séchés montraient une durée de vie plus longue que les échantillons secs, indiquant l’effet favorable d'une faible quantité d'eau restante. Contrairement à l'acier par exemple, les pentes des courbes S-N (contrainte par rapport au nombre de cycles) étaient beaucoup plus faibles. Néanmoins, l'adhésif ne présentait aucune limite de fatigue.

Comme mentionné précédemment, ce projet a porté sur l'étude du comportement des adhésifs et n'a donc pas traité du comportement des joints collés, comme par exemple entre des éléments de renforcement en béton, acier ou CFRP. Les études expérimentales de joints collés montrent que le comportement à l'interface est souvent plus critique que celui de l'adhésif. En outre, les résultats présentés ci-dessus sont valables pour l'adhésif époxyde à deux composants Sikadur 330 et nécessiteraient une validation supplémentaire pour d’autres produits adhésifs.

1 Introduction

1.1 Context and motivation

Structural adhesives are being increasingly used in bridge construction due to their ability to join different materials and geometrical shapes easily and effectively. Frequent examples are externally bonded carbon fiber-reinforced polymer (CFRP) strips for strengthening purposes or the anchoring of steel rebars in existing concrete components [1-2]. More recent applications are the bonding of bridge decks to steel girders [3].

As a result of the outdoor application on the construction site required in most cases and the often large bonding surfaces, cold-curing adhesive systems based on thermosetting epoxy resins are normally used. When employed with the appropriate curing agents, epoxies are able to cure, i.e. induce polymer crosslinking reactions and thus harden, at ambient temperatures. They are usually characterized by minimal shrinkage and swelling, significant resistance to chemicals and hydrolysis, and excellent adhesion to a broad range of materials at moderate costs [5]. Furthermore, adhesive joints are normally sealed and thus protected against humidity and ultraviolet (UV) radiation.

However, in outdoor structural applications such as bridges, environmental exposure may affect durability due to a) the long service life of bridges of up to 100 years, during which a sealing protection may become ineffective, b) the slow curing if subjected to low temperatures, and c) the possible non-compliance with the demanding manufacturing requirements concerning thickness control, surface preparation, cleanliness, humidity and temperature.

The most common environmental actions that may affect durability and performance in bridge applications are temperature, moisture, alkaline environment, de-icing salt solutions, freeze-thaw cycles, and UV radiation [6]. As a result of these environmental actions, the adhesive is subjected to both chemical and physical changes to the polymeric network, the former normally being irreversible and the latter reversible, both however leading to often considerable changes in mechanical and physical properties. These changes are attributed to physical and chemical aging mechanisms, e.g. physical aging, plasticization, hydrolysis, and post-curing, as discussed in the following [7].

The main consequences of curing epoxy adhesives at ambient temperature are long curing times of the order of weeks and often incomplete cross-linking reactions [8]. Moderate glass transition temperatures, T_g, are thus developed, often lower than 65°C [9], particularly if bonding occurs at low temperatures [8]. The T_g should ideally be approximately 20°C above the ambient temperature [10] in order not to affect the mechanical properties. Apart from curing, there is evidence that temperatures below the T_g may activate physical aging effects on the epoxy properties. This mechanism concerns a slow and gradual rearrangement of polymer chains into a denser network [11, 12]. The concurring mechanisms of curing progression and physical aging are however not yet well understood and thus need further investigation.

Temperatures above the T_g lead to a rapid reduction in both stiffness and strength due to changes in the molecular mobility [9, 13]. Temperatures significantly exceeding the T_g may also induce thermal aging [14], a mechanism which however does not occur under bridge conditions. Furthermore, UV radiation combined with oxygen can cause considerable thermo- or photo-oxidation [15], although the penetration and damage depth into the adhesive is normally small [14]. Since the adhesive layer is protected by the adherends and the sealing at the edges, this mechanism does not normally occur or if it does, its effects can usually be neglected in the case of a defect in the sealing.

The presence of water or moisture is known to affect the performance of epoxies. It diffuses into the polymeric network leading to segmental mobility and plasticization effects, which result in a reduction of strength, stiffness and the T_g [5, 16-19]. In the presence of moisture, the Tg may thus approach the service temperature. Furthermore, for adhesives in contact with concrete adherends the exposure may be alkaline. Existing works have shown contradictory results of the effect of alkaline solutions on epoxy properties [20, 21]. The effect of this action thus needs further investigation.

When de-icing salt is applied on the deck during winter or in the case of bridges in marine environments, the epoxy adhesive may be exposed to saline solutions. However, sodium chloride solutions, containing large hydrated ions, were found to prohibit the water absorption and related property degradation compared to pure water [20, 22]. However, combined effects may occur during freeze-thaw cycles in the presence of neutral or saline water and may lead to resin microcracking and thus interface damage in the joint [23].

Further to the aforementioned durability concerns, adhesively-bonded joints have to sustain millions of fatigue cycles [24] during their operational lifetime on a bridge, which however are of low cyclic stress level [8, 25]. The sensitivity to fatigue depends on the joint type. A deck-to-girder connection is normally not sensitive as the stresses in the adhesive layer are low due to the large bonding surfaces. In the case of a CFRP strengthening strip or a bonded steel rebar, however, the stresses due to traffic loads may be high. Moreover, due to the often large adhesive thicknesses and volumes in the case of bridge joints, the fatigue performance of the bulk adhesive should be studied separately. Numerous studies do exist concerning the fatigue behavior of adhesively-bonded joints, but little information is available regarding the fatigue behavior of bulk adhesives [26], and even less on the fatigue behavior of bulk structural adhesives subjected to environmental effects [27].

Finally, owing to the very limited information in existing codes [28] related to the design of cold-curing adhesive joints in specific applications such as bridges, practical recommendations need to be established in order to design safe, robust and durable joints.

The above short review is complemented in the following chapters to provide a thorough state-of-the art summary of existing knowledge regarding the durability of cold-curing structural epoxy adhesives. Based on this review, the potential alteration mechanisms relevant in a bridge environment were extracted from the whole set of possible mechanisms and will be investigated in the following. These mechanisms are physical aging, curing progression, exposure to low and elevated temperatures and plasticization in a dry or wet environment. While most of them are detrimental, the progression of curing has a positive effect. Excluded were thermal aging, salinity and UV for the abovementioned reasons. Freeze-thaw exposure is also relevant but may rather have effects on the whole joint, i.e. particularly the interfaces. This effect on bulk adhesives was thus not considered in this work. A main difficulty regarding the investigation of the above extracted mechanisms is that they cannot be analyzed individually but always occur simultaneously. The effect of fatigue on an aged bulk epoxy adhesive is also investigated.

1.2 Objectives

The general objective of this research was the study of the durability and long-term behavior of a widely applied cold-curing epoxy adhesive in bridge applications. The following specific objectives have been defined:

1) Identification of the main aging mechanisms and the influential environmental actions and their ranges in a bridge environment.
2) Investigation of the effects of aging in a dry environment on the development of physical and mechanical properties.
3) Quantification of the long-term effects of aging in a wet environment on the development of physical and mechanical properties.

4) Study of the effect of the curing degree on the development of physical and mechanical properties.
5) Investigation of the combined fatigue-environmental effect on long-term mechanical behavior.
6) Implementation of the results in bridge design.

1.3 Methodology

In order to attain the objectives listed above, extensive experimental work was carried out and theoretical methods originating from polymer and structural engineering were applied, as shown in Fig. 1.1 and described below:

<u>Literature review</u> (Objective 1)

- Based on a comprehensive literature review, the critical environmental actions on epoxy adhesives in a bridge environment were derived. A corresponding experimental campaign was designed and the laboratory conditionings were established. These comprised material exposures at different curing degrees to temperature, moisture and alkalinity.
- Due to the low rate of material changes caused by the aging mechanisms in service, an accelerated conditioning at elevated (30 and 50°C) temperatures was also conducted.

<u>Experimental investigations</u> (Objectives 2-5)

- Specimens with different curing degrees, dry, wet, at neutral or high pH, and dried, were conditioned.
- The monitoring of the changes in physical material properties was carried out using Differential Scanning Calorimetry (DSC) and Dynamic Mechanical Analysis (DMA) performed at regular times over a two-year span.
- The mechanical behavior of the adhesive was investigated by carrying out standard quasi-static tensile experiments and tension-to-tension fatigue experiments performed over the same two-year span.
- The specimens' failure surfaces were analyzed after different time spans during the investigated conditionings and the observed failure mechanisms were related to water or fatigue loading effects.

<u>Modeling</u> (Objectives 2-5)

- Analytical models were used to simulate quasi-static and fatigue behavior.
- For the long-term modeling of mechanical properties for up to 100 years, the Arrhenius method was applied.
- Fickian modeling was employed to derive diffusion parameters related to the exposure of wet specimens and allowed the numerical modeling of the mass diffusion into the adhesive layer of typical bridge joints.
- The relationship between water uptake and degradation of mechanical properties was established.

<u>Implementation in bridge design</u> (Objective 6)

- Existing resistance factors from design codes corresponding to environmental conditions were assessed based on the obtained mechanical property retentions.
- In order to cover the obtained time-dependent mechanical property variations in dry specimens, preconditioning procedures for test specimens were derived for ultimate limit state (ULS) and serviceability limit state (SLS) verification.

1.4 Report organization

The report comprises six chapters; the content of the main Chapters 2-5 is summarized in Fig. 1.1.

Chapter 1 introduces the specific problems addressed in this study, related to the durability of structural adhesives with applications in bridge construction and a bridge environment.

Chapters 2 presents a review of literature and relevant experimental investigations associated with the aging of structural adhesives in dry bridge environments. The physical aging and curing continuation of a cold-curing epoxy adhesive were monitored for one year in the laboratory under representative bridge conditions. Their effects on the development of the physical properties, such as the relaxation enthalpy, ΔH_{rel}, and the glass transition temperature, T_g, and of the tensile mechanical properties were addressed in the earlier and later ages.

Chapter 3 presents an extensive experimental investigation of the effects of curing and plasticization, the latter caused by exposure to humidity and alkalinity, on the physical and mechanical properties of a structural epoxy adhesive in representative wet bridge environments over a period of two years. Accelerated aging through exposure to elevated temperatures and corresponding modeling based on Arrhenius principles were used to predict the long-term mechanical behavior for a bridge service life of up to 100 years. The potential recovery of properties after drying was also addressed.

Chapter 4 presents experimental investigations and the modeling of the fatigue behavior of a cold-curing epoxy adhesive after long-term aging in dry and wet bridge environments. The adhesive was examined under a) dry conditions after reaching full property development, b) under saturated wet conditions with 70% tensile strength retention (corresponding to 100 years of aging) and c) in the dried state after full strength recovery. Low-cycle tension-tension fatigue of up to 10^7 cycles was applied within the serviceability load ranges of a bridge. The effects of water content on fatigue life, the fatigue damage accumulation, and the fatigue stiffness were described and thoroughly discussed.

Chapter 5 provides practical examples and recommendations related to the design of adhesively-bonded bridge joints. Typical joints were analyzed concerning sensitivity to moisture ingress and the associated degradation of mechanical properties. The adhesive resistance factors at ultimate limit state (ULS) and serviceability limit state (SLS) were assessed based on the experimental results obtained here regarding environmental conditions. The fatigue behavior of the adhesive was compared with that of CFRP and steel materials. Specifications concerning the preconditioning of test specimens were derived. The development of the T_g in dry and wet environments was addressed.

Chapter 6 comprises a summary of these research findings and recommendations for future research.

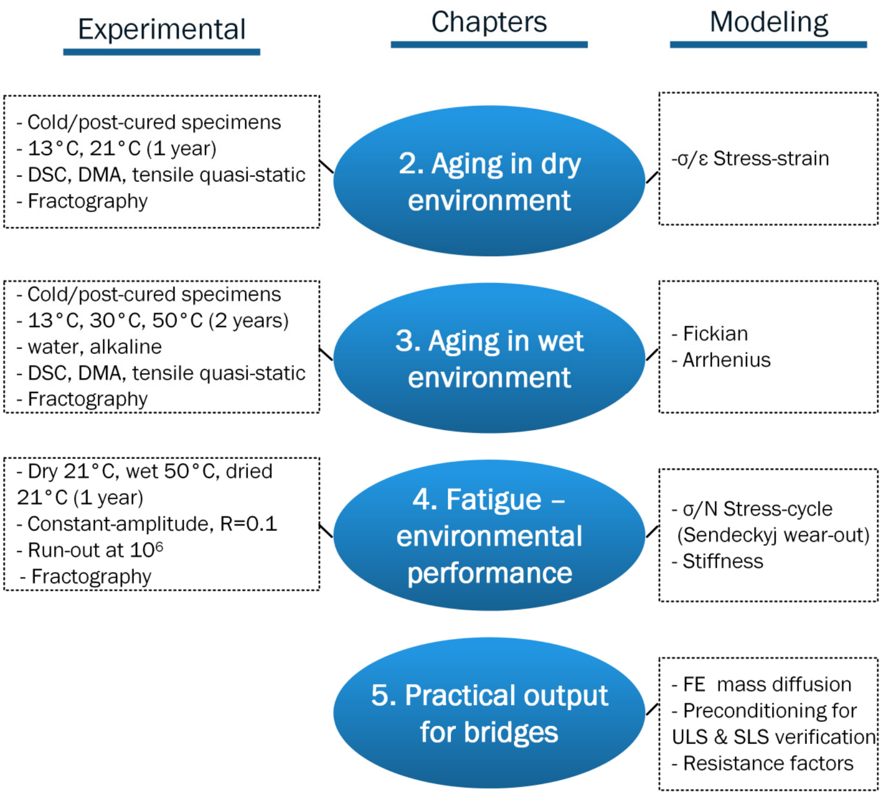

Fig. 1.1 *Overview of work and report organization.*

Results of this work have been published or submitted in three journal papers. The papers are listed below and correspond to the 2 to 4 main chapters.

1.5 List of publications

1. M. Savvilotidou, A. P. Vassilopoulos, M. Frigione, T. Keller, Effects of aging in dry environment on physical and mechanical properties of a cold-curing structural epoxy adhesive for bridge construction, Constr. Build. Mater. 140 (2017) 552–561.

2. M. Savvilotidou, A. P. Vassilopoulos, M. Frigione, T. Keller, Development of physical and mechanical properties of a cold-curing structural adhesive in a wet bridge environment, Constr. Build. Mater. 144 (2017) 115–124.

3. M. Savvilotidou, T. Keller, A. P. Vassilopoulos, Fatigue performance of a cold-curing structural epoxy adhesive subjected to moist environments, Int. J. Fatigue, 103 (2017) 405–414.

1.6 References

[1] T. C. Miller, M.J. Chajes, D. R. Mertz, J.N. Hastings, Strengthening of a Steel Bridge Girder Using CFRP Plates, J. Bridge Eng. 6 (2001) 514–522.

[2] C. C. Choo, Ching Chiaw, I.E. Harik, Performance Evaluation of Concrete Bridge Decks Reinforced with MMFX and SSC Rebars, Kentucky Transportation Center Research Report 191, 2006.

[3] T. Keller, J. Rothe, J. de Castro, M. Osei-Antwi, GFRP-Balsa Sandwich Bridge Deck: Concept, Design, and Experimental Validation, J. Compos. Constr. 18 (2013) 04013043 (1-10).

[4] D.J. Dunn, Engineering and structural adhesives, Rapra review report 15 (2004) 1–28.

[5] M. Frigione, Ageing of fibre-reinforced polymers for construction applications, JEC composites magazine 106 (2016) 46–49.

[6] V.M. Khabari et al., Durability gap analysis for fiber reinforced polymers in civil engineering, J. Comp. Const. 7 (2003) 238–247.

[7] A.J. Kinloch, Durability of structural adhesives, App. Sci. Publishers, London & New York, 1983.

[8] O. Moussa, T. Keller, Thermophysical and thermomechanical behavior of cold-curing structural adhesives in bridge construction, Rapport OFROU 654, Switzerland, 2013.

[9] Frigione, M., Lettieri, M., Mecchi, A.M. (2006), Environmental effects on epoxy adhesives employed for restoration of historical buildings. J. Mat. Civil Eng., 18: 715–722.

[10] L.C. Hollaway, A review of the present and future utilization of FRP composites in the civil infrastructure with reference to their important in-service properties, Constr. Build. Mater., 24 (2010) 2419–2445.

[11] L. Barral, J. Cano, J. López, et al., Physical Aging of a Tetrafunctional/phenol Novolac Epoxy Mixture Cured with Diamine. DSC and DMA measurements, J. Therm. Anal. Calorim. 60 (2000) 391-399.

[12] M. Frigione, C. Naddeo, D. Acierno, Cold-Curing Epoxy Resins: Aging and Environmental Effects. I - Thermal Properties, J. Polym. Eng. 21 (2001) 23–51.

[13] R.D. Adams and J. Comyn, Joining using adhesives, Assembly automation, 20 (2000) 109–117.

[14] J. R. White, Polymer ageing: physics, chemistry or engineering? Time to reflect,” Comptes Rendus Chimie, 9 (2006) 1396–1408.

[15] P. Musto, G. Ragosta, M. Abbate, G. Scarinzi, Photo-Oxidation of High Performance Epoxy Networks: Correlation between the Molecular Mechanisms of Degradation and the Viscoelastic and Mechanical Response, Macromolecules, 41 (2008) 5729–5743.

[16] G.C. Mays, A.R. Hutchinson, Adhesives in civil engineering, Cambridge university press, 1992.

[17] M.P. Zanni-Deffarges, M.E.R. Shanahan, Diffusion of water into an epoxy adhesive: comparison between bulk behavior and adhesive joints, Int. J. Adhes. Adhes. 15 (1995) 137–142.

[18] A.F. Abdelkader, J.R. White, Water absorption in epoxy resins: The effects of the crosslinking agent and curing temperature, J. Appl. Polym. Sci., 98 (2005) 2544–2549.

[19] P. Nogueira et al., Effect of water sorption on the structure and mechanical properties of an epoxy resin system, J. Appl. Polym. Sci., 80 (2001) 71–80.

[20] Q. Yang, G. Xian, V.M. Karbhari, Hygrothermal ageing of an epoxy adhesive used in FRP strengthening of concrete, J. Appl. Polym. Sci. 107 (2008) 2607–2617.

[21] L. Wolff, K. Hailu, M. Raupach, Mechanisms of Blistering of Coatings on Concrete, International Symposium Polymers in Concrete, Portugal, 2006.

[22] P. Silva, P. Fernandes, J. Sena-Cruz, J. Xavier, F. Castro, D. Soares, V. Carneiro, Effects of different environmental conditions on the mechanical characteristics of a structural epoxy, Composites Part B 88 (2016) 55–63.

[23] J. W. Shi, H. Zhu, G. Wu, Z. S. Wu, Tensile behavior of FRP and hybrid FRP sheets in freeze–thaw cycling, Composites Part B 60 (2014) 239–247.

[24] EN 1991-2 Eurocode 1. Actions on structures - Part 2: Traffic loads on bridges.

[25] A. R. Hutchinson, Durability of structural adhesive joints, PhD thesis, University of Dundee, 1986

[26] G. Tao, Z. Xia, Ratcheting behavior of an epoxy polymer and its effect on fatigue life, Polym. Test. 26 (2007) 451–460

[27] L. J. Broutman S. K. Gaggar 1972, Fatigue behavior of epoxy and polyester resins, Int. J. Polym. Mater. Po. 1 (1972) 295–316.

[28] J. L Clarke, Structural design of polymer composites - Eurocomp Design Code and Handbook, E & FN Spon, London, 1996.

2 Aging in dry environment

2.1 Overview

Structural adhesives have been used in bridge construction for strengthening purposes for decades, e.g. for bonding carbon fiber-reinforced polymer (CFRP) plates or strips onto existing structures. A more widespread application in new construction however is still restricted due to a lack of knowledge concerning their long-term mechanical behavior over a required service life of up to 100 years [1]. Structural adhesives used in bridge construction are in most cases applied on the construction site and are thus mainly cold-curing systems based on thermosetting epoxy resins. Aliphatic amines are commonly used as curing agents for this purpose, since they are also able to react with epoxies at low temperatures, i.e. during winter. Covalent bonds form between the epoxide and the amine groups, resulting in a highly cross-linked, rigid and amorphous epoxy network. However, several weeks – or even months – of curing are necessary to assure a reasonably high curing degree and a moderate glass transition temperature (T_g), which is usually lower than 65°C, particularly if bonding occurs at low temperatures of minimum 5-10°C [2-6].

During their service life, cold-curing epoxies are subjected to various physical and chemical aging mechanisms, which may be active simultaneously with different effects on the physical and mechanical properties, mainly depending on temperature, humidity and UV exposure [7, 8]. Effects based on physical mechanisms, such as plasticization and physical aging (densification), may be reversible [3, 9]; cold-curing epoxies exposed to natural weathering for 36 months showed partially reversible changes in both physical and mechanical properties [7]. However, effects based on chemical mechanisms, e.g. further cross-linking due to continuation of curing [2, 9], or chain scissions due to long-term water attack or high temperature and UV exposure, are not reversible [7].

In bridge construction, cold-curing adhesive joints, if properly designed and executed, are normally not exposed to humidity, high temperature and UV radiation. The main aging mechanisms that still occur in such dry environments, at low or moderate outdoor temperatures (well below T_g), are physical aging and continuation of curing. In this respect however, most of the works published on physical aging concern hot-cured epoxy resins, i.e. cured at elevated temperatures (often above 100°C) by artificial heating and works about cold- or outdoor-curing are rare [2-11]. Moreover, apart from a few works where investigations have been conducted during several months or years [3, 7-9, 12], most of the available studies are limited to a few days of aging. There is thus a lack of knowledge regarding the effects of physical aging and simultaneous continuation of curing on the physical and mechanical properties of cold-curing structural epoxy adhesives exposed to dry outdoor temperature conditions, as is the case in bridge applications.

Physical aging of epoxy adhesives occurs in the glassy state, i.e. after vitrification and at aging temperatures (T_a) lower than T_g, and is driven by a thermodynamic disequilibrium in this state [13]. During aging, i.e. approaching the thermodynamic equilibrium, an increase in mass density (densification), and thus a decrease in specific volume (volumetric relaxation) (v), and a decrease in molecular configurational energy are observed [3, 12-16]. The difference between T_a and T_g and the thermal history have a strong influence on the rate of physical aging. If the exposure temperature is low, physical aging effects may be active for several years [3, 12-14, 17-21]. They may also be erased however, i.e. the adhesive is de-aged, if heating occurs at temperatures above T_g, i.e. in the rubbery state, and subsequently cooled down into the glassy state, where physical aging begins [3, 14-16]. To quantify physical aging, the specific enthalpy (h) is an appropriate physical metric, since it considers both volume changes and molecular configurational changes (at constant volume) [15]. Similar to the decrease in specific volume, specific enthalpy decreases with time due to physical aging.

The interdependence of all these parameters is illustrated in Fig. 2.1, which shows in the upper part the specific volume (v) or specific enthalpy (h) vs temperature (T) and in the lower part the specific heat capacity (C_p) vs temperature (according to [15]). Indicated in the upper part are the thermodynamic equilibrium lines of an amorphous and crystalline polymer, and the region in between represents free volume. The curve v_0-h_0-t_0 describes an unaged epoxy at time t_0, either after vitrification and then heated from the glassy into the rubbery state, or hot-cured or de-aged at high temperature in the rubbery state and then cooled down into the glassy state. The curve deviates at the transition from the rubbery to the glassy state, i.e. at the glass transition temperature ($T_{g,0}$), from the amorphous equilibrium line and the adhesive thus includes additional free volume in the glassy state. At this transition, i.e. $T_{g,0}$, the specific heat capacity also increases. The unaged epoxy then starts physically aging at temperature (T_a) during the times $t_2 > t_1$, i.e. the specific volume and specific enthalpy decrease to $v_2 < v_1 < v_0$ and $h_2 < h_1 < h_0$. If the temperature subsequently increases into the rubbery state, the curves overshoot the amorphous equilibrium line, which is expressed by additional endothermic peaks in the specific heat capacity vs temperature curves ($\Delta H_{rel,2} > \Delta H_{rel,1}$) and an increase in the glass transition temperature ($T_{g,2} > T_{g,1} > T_{g,0}$). Specific heat capacity vs temperature curves can be obtained by Differential Scanning Calorimetry (DSC) [22]. An increasing ΔH_{rel} has been found with increasing physical aging periods of both cold-curing [3, 13] and hot-cured epoxies [13, 17-18].

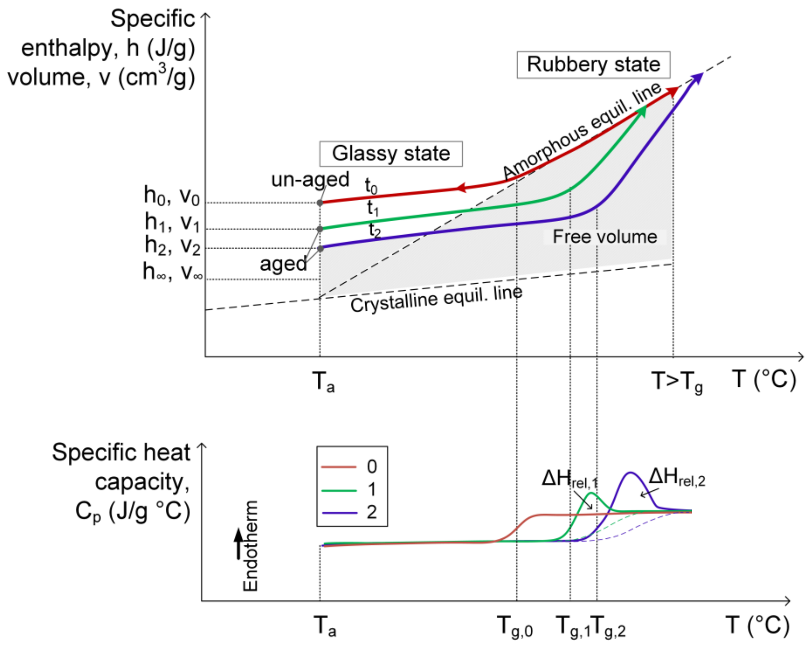

Fig. 2.1 *Specific volume, specific enthalpy and specific heat capacity vs temperature during heating and cooling cycles of epoxy adhesive.*

Concerning the mechanical properties, since physical aging decreases the specific volume, the E-modulus increases accordingly [9, 12, 19]. Furthermore, the yield compressive strength increases with physical aging [17, 19], while the tensile strength normally decreases as a result of the embrittlement and potential microcracking [23]. After de-aging through exposures above T_g, however, the mechanical properties almost completely recover [17].

The continuation of curing, i.e. increasing of the curing degree, in contrast to physical aging, decreases the mass density (and thus increases the specific volume) but increases the cross-link density, defined as the number of chemical cross-links per unit volume [24]. In accordance with the increase of the specific volume the E-modulus decreases during curing [12, 25-29]. The glass transition temperature and strength, however, increase with increasing cross-link density, i.e. curing degree [2, 10].

In this chapter, the physical and mechanical behaviors of cold-curing epoxy adhesive specimens are investigated during an aging period of up to 12 months in a dry environment. Post-cured epoxy specimens, i.e. heated for short times at temperatures not much higher than their T_g, are used as reference in order to derive the different behaviors at cold curing, compared to hot-cured conditions where the knowledge is much broader. The physical and mechanical property changes are discussed on the basis of the sequence or concurrence of the above-described aging mechanisms, i.e. physical aging and continuation of curing. The current work is a continuity of the previous study [2, 10, 11], where cold-curing structural epoxies were physically and mechanically investigated during the first ten days of isothermal curing at low temperatures (5-20°C). Post-curing treatments had also served as reference.

2.2 Experimental program

2.2.1 Materials and conditioning

The epoxy adhesive used in this study was Sikadur-330, supplied by SIKA Schweiz AG. The primary commercial use of this cold-curing adhesive or resin is manual application to surfaces in order to bond FRP strips and impregnate FRP fabrics employed to strengthen existing concrete or steel structures. Sikadur-330 is a thixotropic bi-component adhesive comprising a bisphenol-A-based epoxy resin and a hardener consisting of aliphatic amines. Its viscosity is approximately 6000 mPa·s (at 23 °C), according to the product data sheet. A small quantity, less than 20% per weight, of silica-based fillers has been identified by burn-off tests and optical microscopy observations [10]. The glass transition temperature of specimens cured for two weeks under laboratory conditions was 43.7°C (based on DSC) [10].

The adhesive was produced with a 4:1 resin-to-hardener mixing ratio, suggested by the manufacturer. After stirring each part thoroughly, the hardener was poured into the base resin and they were stirred together for at least three minutes (at laboratory temperature) with a mixing spindle attached to a slow-speed electric drill (to minimise air entrapment), until the material was a uniform grey color. The mixture was then poured into a clean container and stirred again for approximately one more minute, according to the adhesive supplier’s specification. Subsequently, the adhesive was poured into aluminum molds or applied using a spatula onto a Teflon work surface to form thin sheets. No vacuum application was used to minimize voids in order to simulate the actual adhesive application under on-site bridge conditions.

Both cold-curing and post-cured specimens were manufactured according to the different conditioning processes shown in Tab. 2.1. Specimens C13 and C21, directly after pouring, were conditioned at a low 13°C and moderate 21°C temperature. The post-cured P21 reference specimens, after curing for five or seven days at 21°C, were post-cured for three days at 60°C and then allowed to cool in the air and age at 21°C.

A total of 172 specimens were subjected to the above conditions, 112 for the mechanical and 60 for the physical characterization, for a period of up to 350 days. For all specimens, the aging time zero (t_a=0) corresponds to their fabrication day.

2.2.2 Methods of characterization and specimen types

Physical characterization was performed using Differential Scanning Calorimeter analyses (DSC) and Dynamic Mechanical Analyses (DMA). The former was used to mainly compare the cold-curing and post-cured conditions while the latter was used to compare the different cold-curing conditions. For the mechanical characterization standard tensile experiments were carried out, both at irregular frequencies, following the development of the properties. An overview of the experimental program is shown in Tab. 2.1.

Tab. 2.1 *Designation, characterization and conditioning*

Specimens	**Characterization**	**Conditioning** T_a **[°C]**	**Aging time** t_a **[days]**
C13	Physical (DMA)	13 ± 0.5	300
	Mechanical	13 ± 0.5	338
C21	Physical (DSC)	21 ± 3	327
	Physical (DMA)	21 ± 3	282
	Mechanical	21 ± 3	350
P21	Physical (DSC)	21 ± 3	5
		60 ± 0.5	8
		21 ± 3	331
	Mechanical	21 ± 3	7
		60 ± 0.5	10
		21 ± 3	316

DSC was selected to derive the thermo-physical characteristics, i.e. the glass transition temperature ($T_{g,DSC}$), enthalpy relaxation (ΔH_{rel}), residual heat (ΔH_{res}), and curing degree (α), for both cold-curing (C21) and post-cured epoxy conditions (P21). The experiments were performed using a Netzsch 204 F1 Phoenix thermoanalyzer. The samples, weighing between 10-20 mg, were cut from appropriately conditioned epoxy sheets of 1-mm thickness, placed into an aluminum pan, and weighed using a Mettler Toledo MT-5 microbalance. The samples were then covered with an aluminum lid and sealed with a manual press. Each DSC experiment was composed of two subsequent scans from -25°C to 250°C at a heating rate of 10°C/min under a nitrogen atmosphere, and an intermediate cooling at 20°C/min. Properties from two DSC experiments on two different samples of each condition and time have been obtained.

The $T_{g,DSC}$ has been determined as the glass transition midpoint on the first scan curve according to ASTM E1356, the area of the endothermic peak in the glass transition region is the enthalpy relaxation (ΔH_{rel}), while the residual heat (ΔH_{res}) of the cross-linking reaction is calculated from the broader exothermic peak area that follows on this curve, see Fig. 2.2. The ratio between ΔH_{res} and the total heat ($\Delta H_{res,tot} \approx 315$ J/g) measured for the uncured/fresh resin, as shown on the DSC curve in Fig. 2.3, indicated the degree of cure for each experiment. In the second scan curve, the relaxation peak and residual heat peak have disappeared, the former due to the de-aging during the first scan and the latter due to full curing during the first scan.

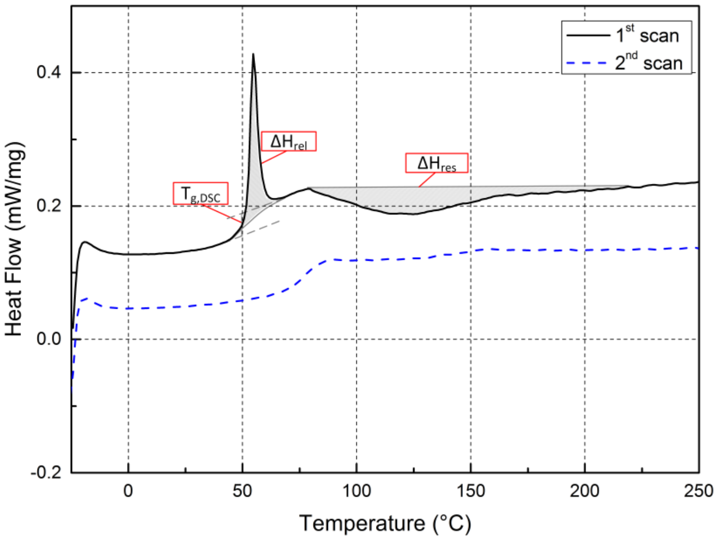

Fig. 2.2 *DSC responses from 1st and 2nd scans of Sikadur 330, C21 sample, aged during 14 days.*

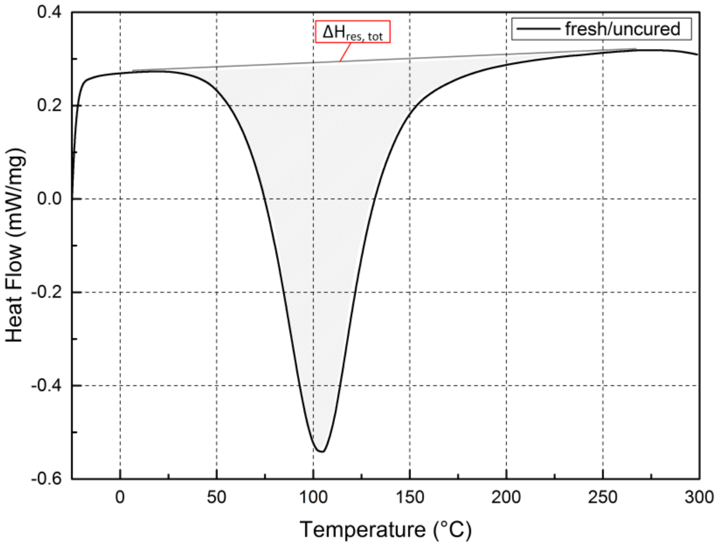

Fig. 2.3 *DSC response of fresh/uncured Sikadur 330.*

Dynamic Mechanical Analysis (DMA) was used to obtain the temperature-dependent viscoelastic properties i.e. storage and loss modulus, and the glass transition temperature for the cold-curing conditions (C13 and C21). Two values were considered for the glass transition temperature, the DMA onset value on the storage modulus curve ($T_{g,DMA,onset}$), used as reference in guidelines for structural FRP design [30], and the value at the peak of the loss modulus curve ($T_{g,DMA,LM}$), which reflects the onset of segmental motion on the molecular level [31], see Fig. 2.4. The experiments were performed with a TA Instruments Q800 dynamic mechanical analyzer in single cantilever configuration. Aluminum molds were used to fabricate the 35x10x3-mm epoxy specimens. Specimens were subjected to a constant strain amplitude of 20 µm at an oscillation frequency of 1 Hz, while the temperature increased from laboratory temperature (21±3°C) to 90°C with a heating rate of 1°C/min, in an air atmosphere. Properties from two DMA experiments performed on two different specimens of each condition and time have been obtained.

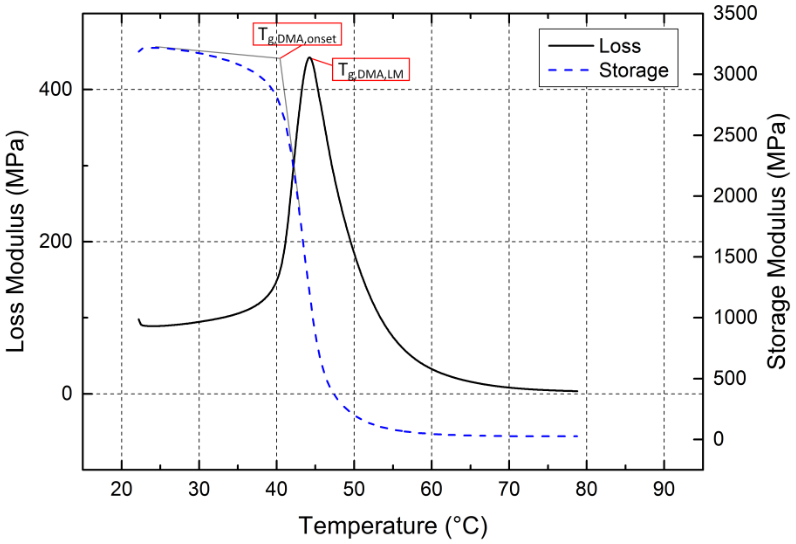

Fig. 2.4 *DMA responses of Sikadur 330, C13 specimen, aged during 34 days.*

Quasi-static tensile experiments were performed under laboratory conditions (i.e. at T=21±3°C and RH=40±10%) according to ASTM D638, using an MTS Landmark servo-hydraulic loading machine, calibrated at a maximum load capacity of 5 kN. The dog-bone-shaped specimens used for the mechanical experiments were fabricated in aluminum molds with geometry according to ASTM D638, as shown in Fig. 2.5. The specimens were clamped by flat-faced pneumatic metal grips and loaded under displacement control at a rate of 3.5 mm/min. The clamping pressure was regulated in order to prevent any slippage at the grips and to ensure that failure occurred within the length of the narrow section. For determining the E-modulus, the longitudinal strain was measured by using an MTS clip-on extensometer, with a gage length of 25±0.05 mm and a minimum accuracy of ±0.5% of the calculated strain, as shown in Fig. 2.5. A data acquisition system was used to record the time, machine displacement, strain and corresponding load. Nominal strengths, derived after dividing the maximum load by the initial cross section of each specimen, were used, while the strains were directly measured by the clip-on extensometer. Furthermore, the tensile E-modulus was calculated as the slope of the stress vs strain curve in the initial linear part, between 0.05% and 0.15% strain. Specimens that presented tab failure were not taken into account in the analysis and four specimens were considered for the mechanical characterization at each condition and time.

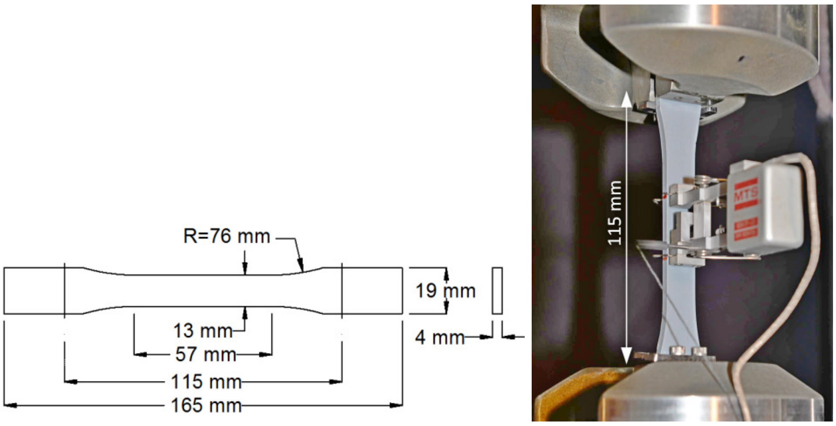

Fig. 2.5 *Tensile experiments, specimen dimensions and experimental set-up according to ASTM D638.*

2.3 Experimental results

2.3.1 Physical Characterization

A sequence of DSC curves for the first scans of C21 and P21 samples at increasing aging times are presented in Fig. 2.6 and Fig. 2.7 respectively. A shift of the ΔH_{rel} peak and the $T_{g,DSC}$ to higher temperatures with increasing aging time was observed for the cold-curing adhesive in Fig. 2.6, while ΔH_{res} decreased, indicating curing development. The same behavior was observed for the post-cured adhesive in Fig. 2.7 before the post-curing treatment, i.e. at five days. At nine days, after the treatment, curing was fully developed ($\Delta H_{res}=0$) and a slight shift of the ΔH_{rel} peak and the $T_{g,DSC}$ back to lower temperatures occurred with increasing aging time. The areas related to ΔH_{rel} after post-curing, i.e. at nine or more days, were smaller compared to the peak area before the treatment, i.e. at five days, and to those of C21 (Fig. 2.6), regardless of time.

A sequence of DMA storage modulus curves of C13 specimens at increasing aging times are shown in Fig. 2.8. The curves and related $T_{g,DMA,onset}$ values shifted to higher temperatures with increasing aging time, indicating the continuation of curing. Furthermore, the storage modulus at the glassy state increased with the aging time up to 125 days, but at 300 days showed a decrease to the 34-day level. The loss modulus development at the same aging times is shown in Fig. 2.9. The peaks and thus the related $T_{g,DMA,LM}$ values also shifted to higher temperatures with increasing aging time.

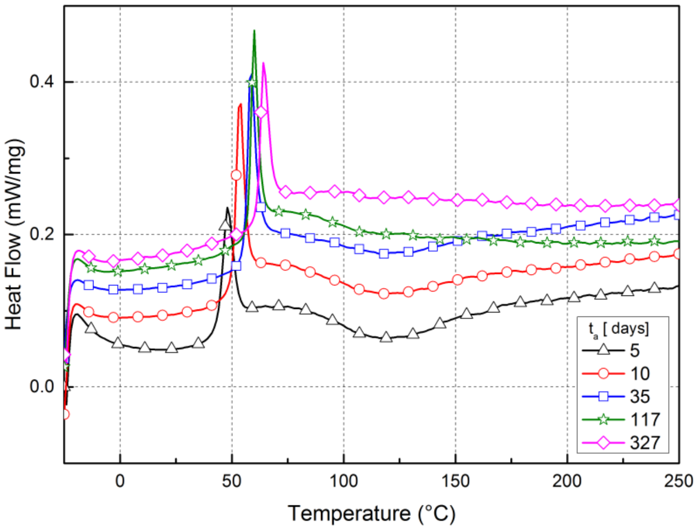

***Fig. 2.6** Sequence of DSC curves (1st scans) at increasing aging times - C21 samples.*

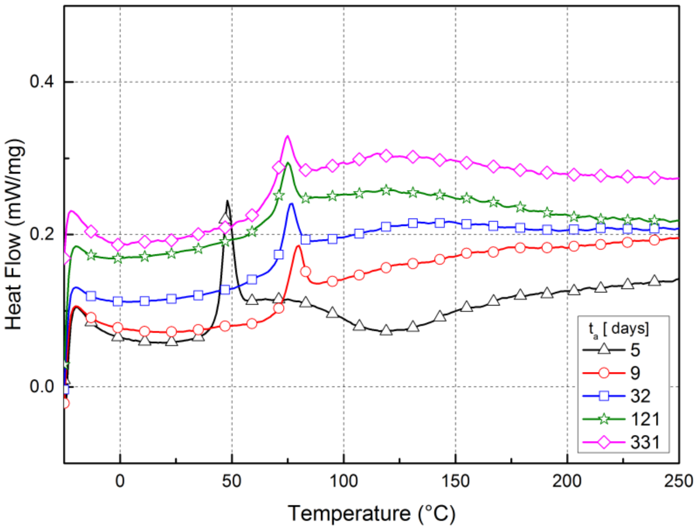

***Fig. 2.7** Sequence of DSC curves (1st scans) at increasing aging times - P21 samples.*

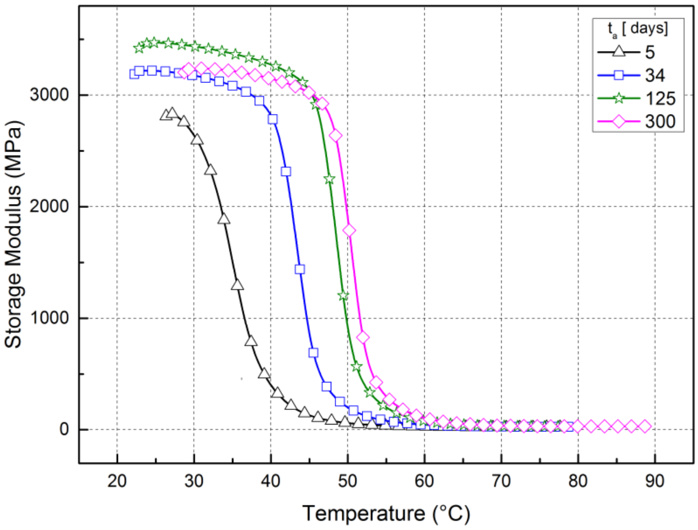

***Fig. 2.8** Sequence of DMA storage modulus curves at increasing aging times - C13 specimens.*

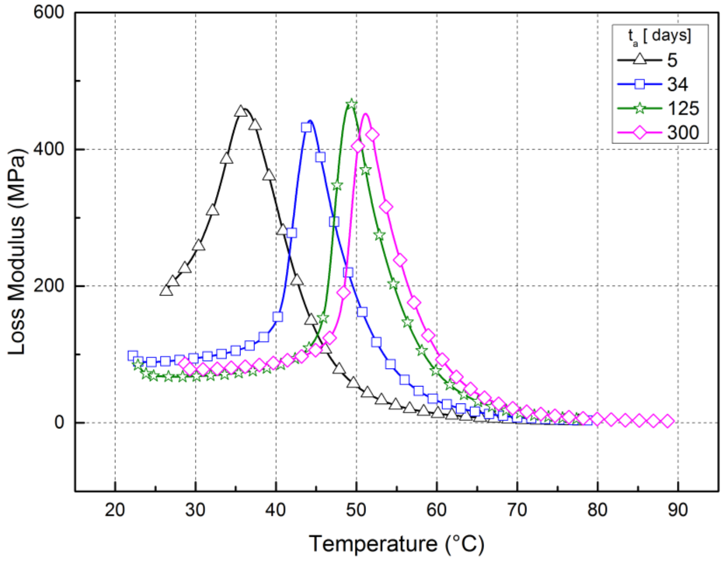

***Fig. 2.9** Sequence of DMA loss modulus curves at increasing aging times - C13 specimens.*

The thermo-physical properties measured at different aging times are presented in Fig. 2.10-Fig. 2.12 on a logarithmic scale to better represent the earlier age development. The curing degree (α) development of conditions C21 and P21 is shown in Fig. 2.10. A high curing degree of approximately 94% was achieved by all C21 and P21 samples during the first five days of curing (time corresponding to the first measurement). The P21 samples appeared fully cured (α=1) in the next measurements after post-curing (at nine days). After 327 days, the C21 samples also achieved an almost complete curing of 99% -100%, the development over time being almost linear on the logarithmic scale.

The glass transition temperature (T_g) development, according to the three different definitions, with increasing aging time is shown in Fig. 2.11 for all conditions. After five days, the T_g of all conditions ranged around 40°C. The values for the cold-curing specimens C13 and C21 then slowly developed while a jump to values above 70°C occurred after post-curing in the P21 specimens (at nine days). The rate of increase was lower at 13°C than at 21°C, as already observed in [11], due to the decelerated cross-linking. After almost one year, the C13 specimens achieved values of around 50°C while the C21 specimens reached around 55°C ($T_{g,DMA,LM}$). The values of the P21 specimens started slightly decreasing by approximately 7%, from the maximum value (72.4°C) at nine days and up to 331 days. The values obtained using DSC ($T_{g,DSC}$) were always higher than those obtained using DMA, while the lowest values were obtained from $T_{g,DMA,onset}$.

The variations of the relaxation enthalpy (ΔH_{rel}) over time of the C21 and P21 samples are shown in Fig. 2.12. The values of the cold-curing C21 increased up to a maximum after approximately 17 days and then started decreasing. At five days, the post-cured P21 started at the same values as those of the C21, but the former then decreased by 50% after post-curing (at nine days). Subsequently, similarly to C21 but on a lower level, a peak appeared at around 17 days, followed by a decrease and then a slight increase again after 121 days.

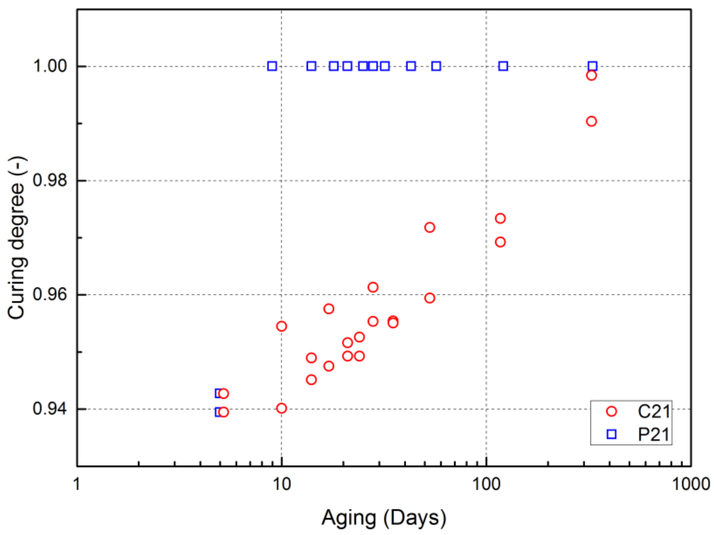

Fig. 2.10 Development of curing degree with aging time.

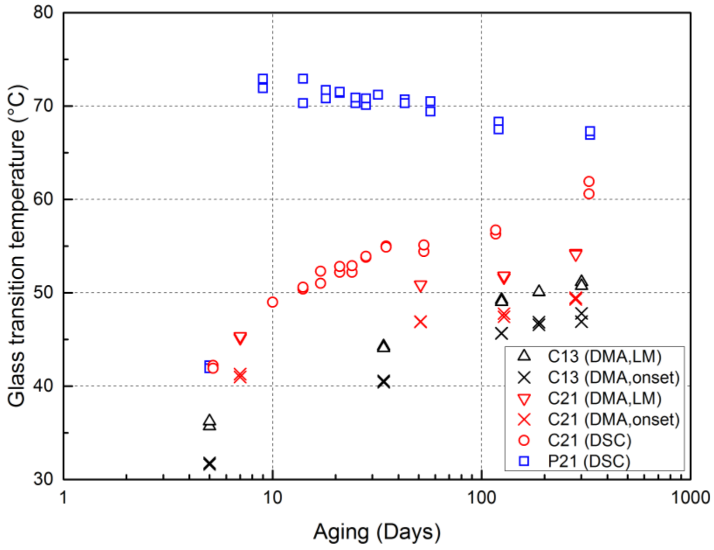

Fig. 2.11 Development of glass transition temperature with aging time.

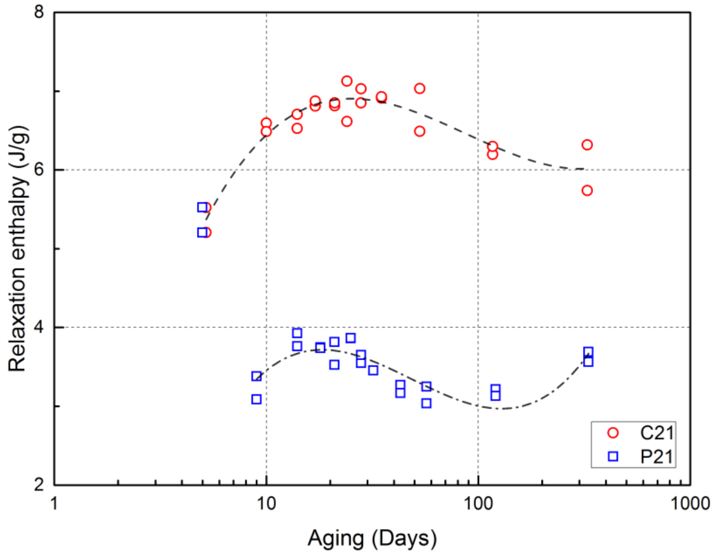

Fig. 2.12 Development of relaxation enthalpy with aging time.

2.3.2 Mechanical Characterization

The tensile modulus, strength and failure strain of all specimens C13, C21 and P21 are shown in Tab. 2.2-Tab. 2.4 and Fig. 2.13-Fig. 2.15 respectively as a function of time and on a logarithmic scale, again to better differentiate the results during the first days; average values and standard deviations are indicated.

Tab. 2.2 *Condition C13, average values and standard deviations of tensile properties*

Aging [Days]	E-modulus [MPa]	Strength [MPa]	Strain at failure [%]
5	3463 ± 305	27.0 ± 1.0	1.27 ± 0.20
6	4121 ± 227	29.4 ± 3.0	0.95 ± 0.17
34	4993 ± 126	28.6 ± 2.5	0.61 ± 0.06
37	5013 ± 161	29.6 ± 2.3	0.68 ± 0.08
101	5403 ± 56	33.5 ± 1.9	0.68 ± 0.05
131	5430 ± 371	32.9 ± 4.6	0.68 ± 0.11
181	4567 ± 143	31.8 ± 4.4	0.92 ± 0.23
264	4881 ± 146	38.0 ± 1.1	1.13 ± 0.13
338	4658 ± 189	36.9 ± 5.7	1.02 ± 0.21

Tab. 2.3 *Condition C21, average values and standard deviations of tensile properties*

Aging [Days]	E-modulus [MPa]	Strength [MPa]	Strain at failure [%]
7	4580 ± 55	27.0 ± 3.0	0.60 ± 0.08
12	4974 ± 198	34.8 ± 1.7	0.79 ± 0.04
88	5137 ± 217	31.7 ± 4.1	0.74 ± 0.15
181	4445 ± 79	29.5 ± 4.1	0.76 ± 0.13
261	4956 ± 151	40.5 ± 4.1	1.12 ± 0.16
350	4761 ± 252	40.3 ± 8.4	1.06 ± 0.27

Tab. 2.4 *Condition P21, average values and standard deviations of tensile properties*

Aging [Days]	E-modulus [MPa]	Strength [MPa]	Strain at failure [%]
10	4500 ± 116	41.8 ± 3.8	1.13 ± 0.13
14	5123 ± 20	42.5 ± 4.5	1.00 ± 0.13
25	4776 ± 103	46.4 ± 7.1	1.24 ± 0.33
90	5034 ± 299	46.9 ± 7.2	1.20 ± 0.26
142	4407 ± 172	40.0 ± 4.0	1.06 ± 0.13
156	4211 ± 238	40.4 ± 7.8	1.17 ± 0.31
160	4168 ± 235	37.8 ± 2.2	1.06 ± 0.10
162	4206 ± 107	37.8 ± 5.0	1.04 ± 0.20
176	4312 ± 282	40.6 ± 7.5	1.11 ± 0.27
197	4353 ± 109	46.3 ± 0.2	1.36 ± 0.01
201	4268 ± 142	43.8 ± 6.2	1.31 ± 0.37
212	4543 ± 407	43.2 ± 3.6	1.16 ± 0.15
257	4778 ± 138	32.4 ± 3.5	0.88 ± 0.15
316	4715 ± 234	37.3 ± 4.9	0.95 ± 0.17

The E-modulus of all specimens increased during the first 20 days, independently of the curing conditions. Subsequently, the C21 and P21 values remained stable while the C13 values further increased, before the values for all conditions exhibited a drop to a similar minimum value at around 180 days and then slightly increased again, independently of the curing conditions. The C13 specimens thus achieved the highest value of 5.4 GPa, at a peak that slightly shifted to a longer aging time compared to the peaks of the other conditions. Also shown in Fig. 2.13 is the DMA storage modulus at the glassy state of the

C13 and C21 specimens, which followed the same trend as the E-modulus measured by the tensile experiments.

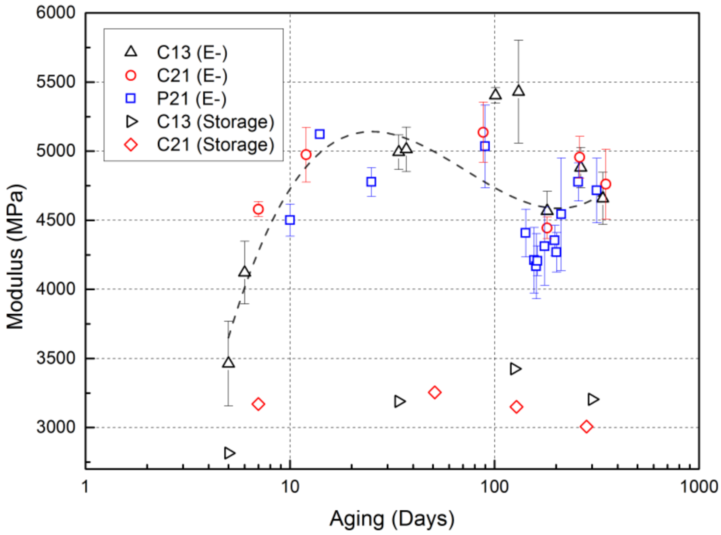

Fig. 2.13 *Tensile E-modulus and storage modulus vs aging time relationships.*

With regard to strength and failure strain, clear differences could be observed according to the curing conditions between the cold-curing specimens C13 and C21 and the post-cured specimens P21, see Fig. 2.14 and Fig. 2.15 respectively. The cold-curing specimens showed similar values independently of the curing temperature. At the aging time where the E-modulus reached a maximum, the strength development showed a slight valley and the failure strain development a clear valley, both approaching the values of the post-cured P21 specimens after 260 days, however. The latter exhibited a comparatively high scatter, but clearly did not show any valley. Generally, the strength and failure strain of the P21 remained almost constant with slightly lower values after 200 days.

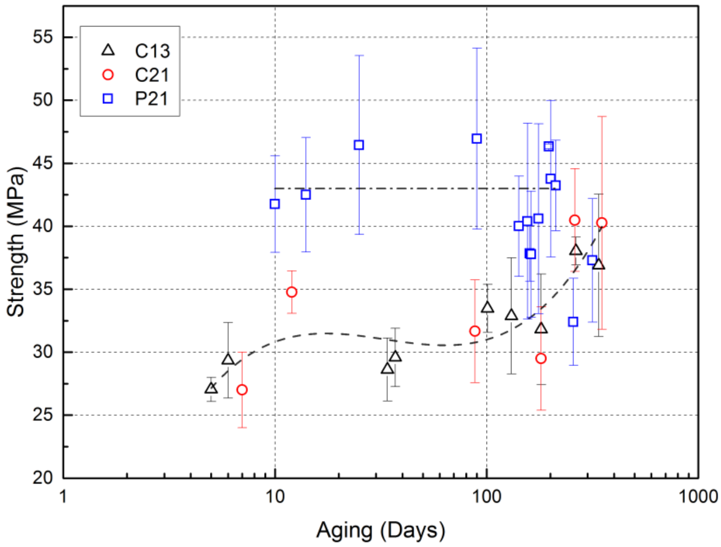

Fig. 2.14 *Tensile strength vs aging time relationship.*

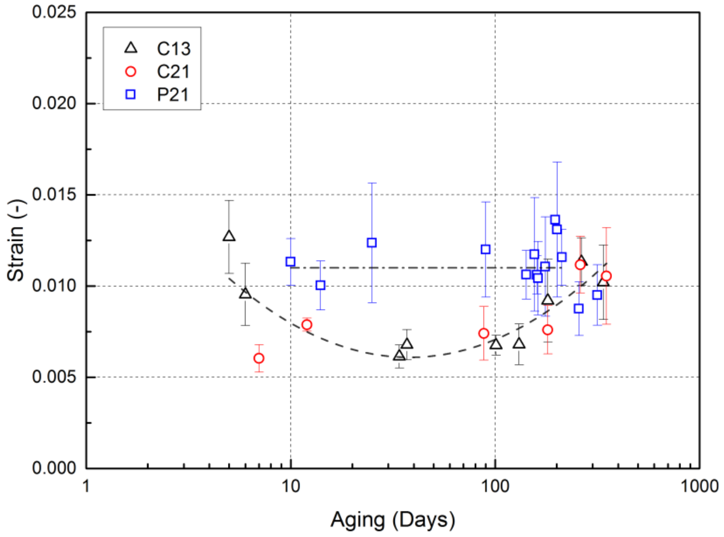

Fig. 2.15 *Tensile failure strain vs aging time relationship.*

Typical nominal stress vs strain responses are shown in Fig. 2.16-Fig. 2.18 for specimens of all conditions at different aging times. The E-modulus, strength and failure strain values of the C13 responses depended significantly on aging time, see Fig. 2.16, and their variations were in accordance with the peak and valley results shown in Fig. 2.13-Fig. 2.15. The curves changed from non-linear to almost linear with increasing E-modulus. The differences in E-modulus were less pronounced in the C21 specimens; the highest strength was achieved after 350 days as the post-cured specimen values were approached, see Fig. 2.17. The post-cured P21 responses almost overlapped, exhibiting the smallest variations with aging time.

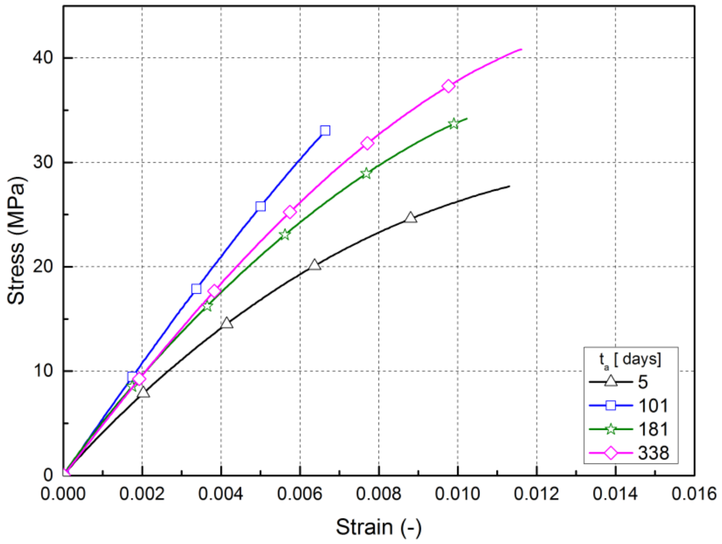

Fig. 2.16 *Nominal tensile stress vs strain responses at increasing aging times - C13 specimens.*

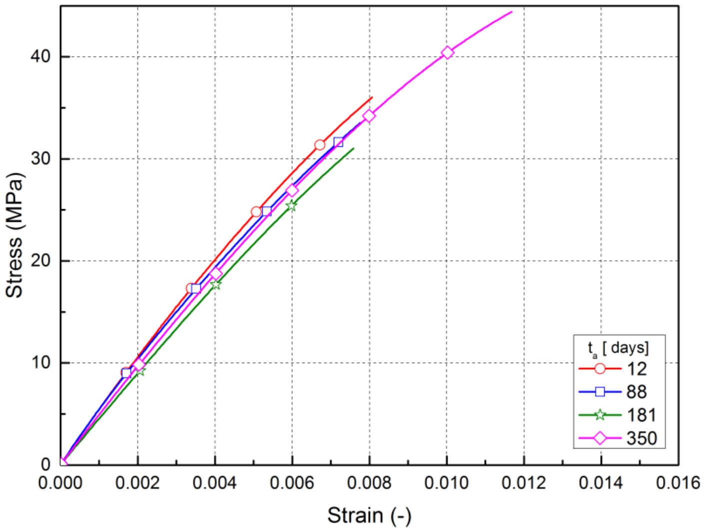

Fig. 2.17 *Nominal tensile stress vs strain responses at increasing aging times - C21 specimens.*

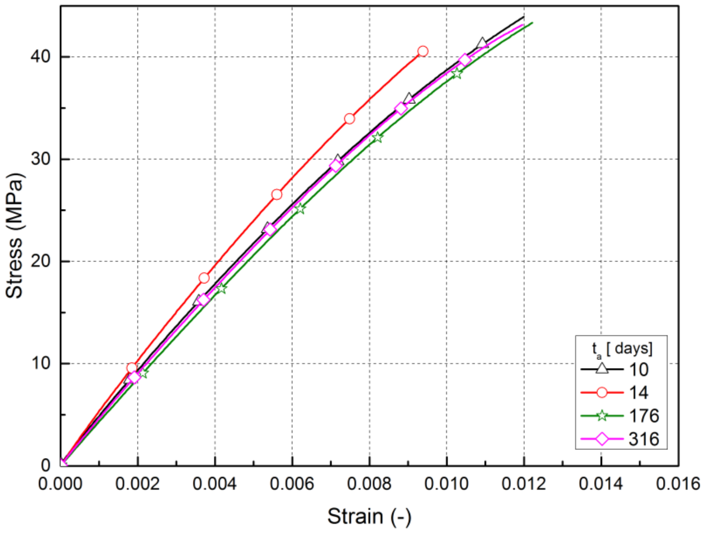

Fig. 2.18 *Nominal tensile stress vs strain responses at increasing aging times - P21 specimens.*

Typical fracture surfaces are shown in Fig. 2.19.

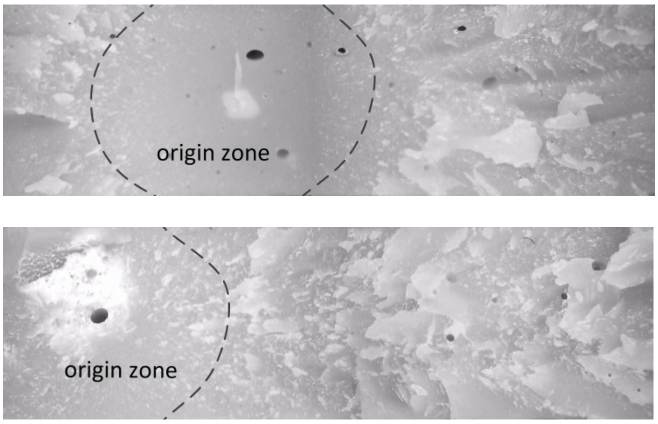

Fig. 2.19 *Fracture surface (13x4 mm^2) of cold-curing specimens C13 of lower strength at 131 days (top), and higher strength at 264 days of aging (bottom).*

They exhibited a flat origin zone and a much rougher propagation zone (according to [32]). In the origin zone, at lower strength a white dot with a regular shape and at higher strength a white dot with an irregular shape were in most cases visible. However, the size of the different zones and dots exhibited a large scatter and could not be correlated to the curing conditions or aging time. Furthermore, small voids were always present.

2.4 Discussion of experimental results

2.4.1 Physical Characterization

The physical characterization results showed that the glass transition temperature ($T_{g,DSC}$) of the cold-curing C21 specimens was very sensitive to small changes in the curing degree (α) at the end of cure, see Fig. 2.20. A small increase of 5% of the curing degree resulted in a 45% increase of the $T_{g,DSC}$. Similar results describing a non-linear increase of T_g with curing as from the earlier age have already been obtained in [11, 29, 33, 34]. Above it has been shown that the glass transition temperature increased due to both physical aging and continuation of curing. From Fig. 2.12 it can be concluded that physical aging was particularly active during the first 50 days and then decreased. During the first 50 days the $T_{g,DSC}$ increased to approximately 55 °C according to Fig. 2.11. The subsequent increase of the glass transition temperature at the end of cure was thus mainly caused by the continuation or completion of curing and less so by physical aging. Also shown in Fig. 2.20 is the P21 development, which, after the increase of α and $T_{g,DSC}$ due to post-curing, exhibited a slight decrease of the latter (at α=1, as already shown in Fig. 2.11). Similar results were found in [35-37] and attributed to residual stresses and inhomogeneous thermoset morphology caused by cooling after the post-curing.

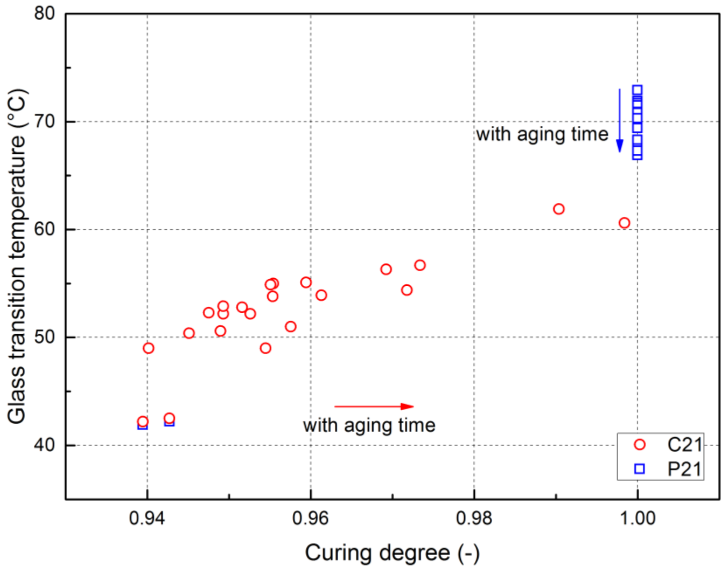

Fig. 2.20 *Curing degree vs glass transition temperature ($T_{g,DSC}$) relationship.*

Coming back to the illustration of the parameter interactions in Fig. 2.1, the simultaneously progressing physical aging and curing mechanisms may be represented as shown in Fig. 2.21. Physical aging shifted the curve of an already aging epoxy further downwards by decreasing the specific volume and enthalpy, as already shown in Fig. 2.1. Curing, however, increased the specific volume and may thus be represented by an analogous upward shift of the curve. Both mechanisms increased the glass transition temperature.

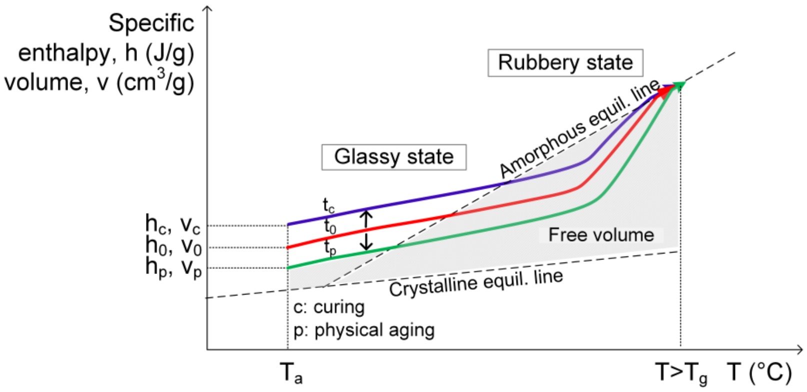

Fig. 2.21 *Schematic diagram of effect of curing and physical aging on specific enthalpy and volume.*

2.4.2 Mechanical Characterization

The peak in the E-modulus curves shown in Fig. 2.13 for all specimens almost coincided with the peak in the ΔH_{rel} responses shown in Fig. 2.12 for the C21 and P21 conditions. This confirmed the dependence of the epoxy E-modulus on the specific volume, the former varied according to the latter due to physical aging and continuation of cure. In the earlier age, physical aging was the predominant mechanism that led to the E-modulus increase, while after the peak, continuation of curing became predominant, decreasing the E-modulus. The new E-modulus increase after the minimum at 180 days could be an indication of the reactivation of physical aging. A similar increasing trend could be seen in the last measurements of the relaxation enthalpy of the P21 condition in Fig. 2.12. The physical aging rate measured in [29] for a hot-cured epoxy was also found to decrease with the extent of cure initially and to increase again with a further extent of cure. Similar results, i.e. an E-modulus peak at 90 days, followed by a decrease to lower values above 150 days, were shown in [12], however again for a hot-cured epoxy, at different initial curing degrees.

The measurements in this study started after five days, and the E-modulus was subsequently not significantly affected by the curing conditions. In the above-mentioned preceding study [2], investigations concerning the E-modulus development for a similar structural epoxy adhesive were conducted during the first 10 days of isothermal curing at different temperatures (T_a) from 5°C to 70°C. A strong influence of the curing temperature on E-modulus and strength development during the first six days was observed, which however subsequently disappeared, as in this study (excluding the strength of P21). The properties rapidly increased at high temperatures, while a delay in the process was observed during the first six days at low curing temperatures. The E-modulus differences may be attributed to different physical aging rates caused by the differences between T_a and T_g among the different curing conditions. At the lower temperatures, the molecular mobility was reduced, thus delaying the mechanism. After six days, however, the properties at lower temperatures approached those obtained at the highest temperature [2].

The relationship between the E-modulus and the glass transition temperature, i.e. the extent of cure (according to [29]), for all conditions is shown in Fig. 2.22 (only the average values are given). The curves of the cold-curing conditions C13 and C21 exhibited a similar shape as in Fig. 2.13. The E-modulus increased with increasing T_g, reaching a maximum, but as T_g approached higher values the E-modulus tended to decrease and eventually reached moderate values. At a lower curing temperature (C13), the peak was higher and shifted to lower T_g values, i.e. lower curing degrees, compared to C21. Similar results were found in [29], for a hot-cured epoxy however. An inverse trend was exhibited by the post-cured specimens P21 due to the T_g decreasing with aging time. The E-modulus showed a minimum at lower and then rose to a peak at higher T_g values, both however at a much higher T_g than under the cold-curing conditions. Overall, i.e. on average, the E-modulus was almost constant and independent of T_g above a T_g of around

45°C, i.e. above a curing degree of 0.94 (see Fig. 2.20); the variation was caused by the alternating predominance of either physical aging or curing. This result confirmed that the E-modulus was mainly dependent on mass and not cross-link density.

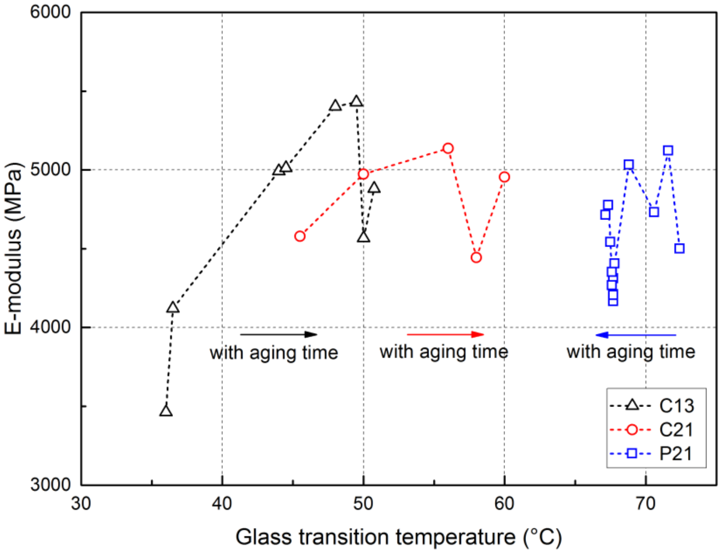

***Fig. 2.22** Tensile E-modulus vs glass transition temperature relationship.*

In contrast to the E-modulus development, the similar strength and failure strain of the cold-curing specimens C13 and C21 were significantly different from those of the P21 post-cured specimens. This could be attributed to their primary dependency on the cross-link density and not the mass density (on which the E-modulus mainly depended). Up to 180 days, the strength and failure strain, for both cold-curing conditions C13 and C21, followed a behavior inversely proportional to the E-modulus (compare Fig. 2.13, Fig. 2.14 and Fig. 2.15), i.e. the modulus peaks coincided with strength and failure strain valleys, evidencing the embrittlement induced by physical aging. Between 180 and 260 days, the values deviated from the inversely proportional behavior, i.e. strength and failure strain continued increasing and approached the P21 values, confirming that they were driven by the increasing cross-link density due to the continuation of curing, and not by the newly increasing mass density due to physical aging. A similar behavior of the tensile strength was observed in [25]. Up to 200 days, the strength and failure strain of the P21 were almost constant (on average) and high, as a result of their high level of cross-linking directly after post-curing. After 200 days, a new increase of the E-modulus of the P21 (see Fig. 2.13), possibly due to a new physical aging cycle, may explain the slight strength and strain decrease of the already fully cross-linked material. It should be further noted that, although the strength and failure strain of the C13, C21 and P21 specimens approached similar values above 260 days, their $T_{g,DSC}$ values were still different (compare Fig. 2.11, Fig. 2.14 and Fig. 2.15).

The relationship between the strength and the glass transition temperature for all conditions is shown in Fig. 2.23 (again only the average values are shown). On average, there was an exponential increase of strength with increasing T_g, and the variation was again caused by the alternating predominance of either physical aging or curing. This result however confirmed that strength development is generally driven by the increasing cross-link (and not mass) density.

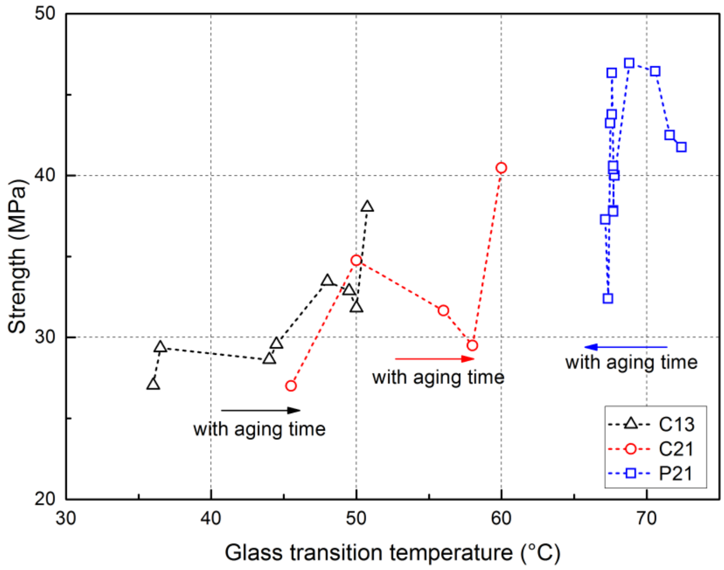

Fig. 2.23 *Tensile strength vs glass transition temperature relationship.*

2.5 Conclusions

The effect of physical aging and continuation of curing on the physical and mechanical properties of a cold-curing structural epoxy adhesive in a dry environment was investigated during the first year. The following conclusions have been drawn:

1) Physical aging and curing (i.e. continuation of cure) occur simultaneously in a cold-curing epoxy adhesive during the first year; the first mechanism increases the mass density (i.e. reduces the specific volume) while the second one reduces the mass density (i.e. increases the specific volume), but increases the cross-link density.
2) The physical and mechanical properties are driven by predominant physical aging in the earlier age and predominant curing in the later age during the first year.
3) The E-modulus mainly depends on the mass density and reaches a maximum in the earlier age due to physical aging. At the later age curing becomes predominant and the decreasing mass density decreases the E-modulus. After the first week, the E-modulus development becomes independent of the curing conditions, i.e. cold or hot/post-cured.
4) Tensile strength and failure strain change mainly with the cross-link density and their development is thus dependent on the curing treatment, i.e. cold or hot/post cured. With regard to the cold-curing conditions, the strength and failure strain development is delayed in the earlier age due to physical aging.
5) Eventually, all curing conditions (cold, or hot/post-cured) result in similar tensile properties, i.e. maximum strength and failure strain and a reduced E-modulus after a maximum, after less than nine months of aging. However, the glass transition temperature still depends on the curing conditions and is not yet fully developed after one year.

2.6 References

[1] EN1991 Eurocode 1: Actions on structures.

[2] O. Moussa, A.P. Vassilopoulos, J. de Castro, T. Keller, Early-age tensile properties of structural epoxy adhesives subjected to low-temperature curing, Int. J. Adhes. Adhes. 35 (2012) 9–16.

[3] M. Frigione, C. Naddeo, D. Acierno, Cold-Curing Epoxy Resins: Aging and Environmental Effects. I - Thermal Properties, J. Polym. Eng. 21 (2001) 23–51.

[4] M. Frigione, M. Lettieri, A.M. Mecchi, Environmental effects on epoxy adhesives employed for restoration of historical buildings, J. Mater. Civ. Eng. 18 (2006) 715–722.

[5] M. Frigione, M.A. Aiello, C. Naddeo, Water effects on the bond strength of concrete/concrete adhesive joints, Constr. Build. Mater. 20 (2006) 957–970.

[6] M. Lettieri, M. Frigione, Effects of humid environment on thermal and mechanical properties of a cold-curing structural epoxy adhesive, Constr. Build. Mater. 30 (2012) 753–760.

[7] M. Lettieri, M. Frigione, Natural and artificial weathering effects on cold-cured epoxy resins, J. Appl. Polym. Sci. 119 (2011) 1635–1645.

[8] P. Silva, P. Fernandes, J. Sena-Cruz, J. Xavier, F. Castro, D. Soares, V. Carneiro, Effects of different environmental conditions on the mechanical characteristics of a structural epoxy, Compos. Part B-Eng. 88 (2016) 55–63.

[9] M. Frigione, C. Naddeo, D. Acierno, Cold-Curing Epoxy Resins: Aging and Environmental Effects. Part II - Mechanical Properties, J. Polym. Eng. 21 (2001) 349–368.

[10] O. Moussa, A.P. Vassilopoulos, J. de Castro, T. Keller, Long-term development of thermophysical and mechanical properties of cold-curing structural adhesives due to post-curing, J. Appl. Polym. Sci. 127 (2013) 2490–2496.

[11] O. Moussa, A.P. Vassilopoulos, T. Keller, Effects of low-temperature curing on physical behavior of cold-curing epoxy adhesives in bridge construction, Int. J. Adhes. Adhes. 32 (2012) 15–22.

[12] J. Moosburger-Will, M. Greisel, S. Horn, Physical aging of partially crosslinked RTM6 epoxy resin, J. Appl. Polym. Sci. 131 (2014) 41121.

[13] S. Montserrat, Vitrification and physical aging on isothermal curing of an epoxy resin, J. Therm. Anal. 37 (1991) 1751–1758.

[14] J.R. White, Polymer aging: physics, chemistry or engineering? Time to reflect, Comptes Rendus Chimie. 9 (2006) 1396–1408.

[15] G.M. Odegard, A. Bandyopadhyay, Physical aging of epoxy polymers and their composites, J. Polym. Sci. B: Polym. Phys. 49 (2011) 1695–1716

[16] L.C.E. Struik, Physical aging in plastics and other glassy materials, Polym. Eng. Sci. 17 (1977) 165–173.

[17] W.D. Cook, M. Mehrabi, G.H. Edward, Aging and yielding in model epoxy thermosets, Polym. 40 (1999) 1209–1218.

[18] F. Fraga, C. Castro-Díaz, E. Rodríguez-Núñez, J.M. Martínez-Ageitos, Physical aging for an epoxy network diglycidyl ether of bisphenol A/m-xylylenediamine, Polym. 44 (2003) 5779–5784.

[19] C. G'Sell, G.B. McKenna, Influence of physical aging on the yield response of model DGEBA/poly(propylene oxide) epoxy glasses, Polym. 33 (1992) 2103–2113.

[20] X. Shi, B.M.D. Fernando, S.G. Croll, Concurrent physical aging and degradation of crosslinked coating systems in accelerated weathering, J. Coat. Technol. Res. 5 (2008) 299–309.

[21] Z. Ophir, J. Emerson, G. Wilkes, Sub-T g annealing studies of rubber-modified and unmodified epoxy systems, J. Appl. Phys. 49 (1978) 5032–5038.

[22] L. Barral, J. Cano, J. López, I. López-Bueno, P. Noguiera, M.J. Abad, C. Ramirez, Physical Aging of a Tetrafunctional/phenol Novolac Epoxy Mixture Cured with Diamine. DSC and DMA measurements, J. Therm. Anal. Calorim. 60 (2000) 391–399.

[23] E.S.W. Kong, Physical aging in epoxy matrices and composites, Adv. Polym. Sci. 80 (1986) 125–171.

[24] J.P. Fouassier, J.F. Rabek, Radiation Curing in Polymer Science and Technology–Volume III: Polymerization Mechanisms, third ed., Elsevier, Barking, 1993.

[25] V.B. Gupta, L.T. Drzal, C.Y.-C. Lee, M.J. Rich, The temperature-dependence of some mechanical properties of a cured epoxy resin system, Polym. Eng. Sci. 25 (1985) 812–823.

[26] F. Meyer, G. Sanz, A. Eceiza, I. Mondragon, J. Mijovic, The effect of stoichiometry and thermal history during cure on structure and properties of epoxy networks, Polym. 36 (1995) 1407–1414.

[27] V.B. Gupta, L.T. Drzal, C.Y.-C. Lee, M.J. Rich, The Effects of Stoichiometry and Structure on the Dynamic Torsional Properties of a Cured Epoxy Resin System, J. Macromol. Sci. Phys. B. 23 (1984) 435–466.

[28] J.B. Enns, J.K. Gillham, Effect of the extent of cure on the modulus, glass transition, water absorption, and density of an amine-cured epoxy, J. Appl. Polym. Sci. 28 (1983) 2831–2846.

[29] X. Wang, J. K. Gillham, Tg - temperature property (TgTP) diagram for thermosetting systems: anomalous behavior of physical properties vs. extent of cure, J. Coat. Technol. 64 (1992) 37–45.

[30] CUR commission C124, Recommendation 96: Fibre-Reinforced Polymers in Civil Load-bearing Structures, CUR Gouda, The Netherlands, 2003

[31] E.A. Turi, Thermal Characterization of Polymeric Materials, Volume I, second ed., Academic Press, New York, 1997

[32] J.R.M. d'Almeida, G.W. de Menezes, S.N. Monteiro, Ageing of the DGEBA/TETA epoxy system with off-stoichiometric compositions, Mater. Res. 6 (2003) 415–420.

[33] K.P. Pang, J.K. Gillham, Anomalous behavior of cured epoxy resins: Density at room temperature versus time and temperature of cure, J. Appl. Polym. Sci. 37 (1989) 1969–1991.

[34] O. Moussa, A.P. Vassilopoulos, T. Keller, Experimental DSC-based method to determine glass transition temperature during curing of structural adhesives, Constr. Build. Mater. 28 (2012) 263–268.

[35] Y. Zhang, R.D. Adams, L.F.M da Silva, Effects of Curing Cycle and Thermal History on the Glass Transition Temperature of Adhesives, J. Adhes. 90 (2014) 327–345.

[36] F. Meyer, G. Sanz, A. Eceiza, I. Mondragon, J. Mijovic, The effect of stoichiometry and thermal history during cure on structure and properties of epoxy networks, Polym. 36 (1995) 1407–1414.

[37] J. Mijović, Time-dependent changes in mechanical properties of neat and reinforced epoxy resins, J. Appl. Polym. Sci. 27 (1982) 2919–293

3 Aging in wet environment

3.1 Overview

Structural adhesives have been used in bridge construction since the 1960s [1]. Today, state-of-the-art applications consist of bonding steel or carbon fiber-reinforced polymer (CFRP) strips or plates onto existing reinforced concrete, steel or timber structures or bonding steel rebars into holes drilled into existing concrete structures for strengthening or upgrading purposes [2]. More recent applications are bonding of reinforced concrete or glass fiber-reinforced polymer (GFRP) bridge decks onto steel or concrete main girders [3]. In contrast to mechanical connections, in these applications adhesives allow the easy joining of different materials and adherends of different geometries.

Due to the often large bonding surfaces and usually outdoor applications, cold-curing adhesives are required for such joints. Thermosetting bisphenol epoxy resins are used in most cases since they cure at ambient temperatures if appropriate curing agents, i.e. aliphatic amines, are used. However, depending on the ambient temperature, curing and full development of the physical and mechanical properties may take up to one year for mechanical and even much longer for physical properties, such as the glass transition temperature [4].

Cold-curing epoxy bonded joints used in bridge construction are normally sealed to prevent exposure to humidity and UV radiation. The corresponding aging behavior of cold-curing structural epoxy adhesives under dry bridge conditions has already been investigated [4]. It has been shown that the material is exposed to concurring mechanisms, i.e. continuation of curing and physical aging, which both influence the physical and mechanical properties. In view of the long service life of bridges, up to 100 years, it cannot however be excluded that, sooner or later, an initially sealed joint may start leaking and the adhesive may thus be exposed to moisture or even stagnant water during several decades. If sealing is not correctly carried out this can already occur before the adhesive is fully cured. Furthermore, the adhesive may also be exposed to humidity if the adherends have a certain porosity (e.g. in the case of concrete) or diffusivity (e.g. the matrix of CFRP materials) [5]. In the former case, the concrete pore water is, in addition, alkaline and has a high pH value of approximately 12.5 [6]. A similar case occurs if wet concrete is poured onto a fresh and still wet epoxy adhesive, as in the installation of a lightweight concrete-GFRP sandwich bridge deck in order to improve the adherence of the lightweight concrete to a GFRP T-web face sheet [7].

The effect of humidity or water on the physical and mechanical properties of epoxy resins has already been investigated. Plasticization of the resin occurred, resulting in a significant reduction of the glass transition temperature, stiffness and strength [8-10]. These effects were found to be reversible however when the material was dried again [11, 12] and plasticization was thus considered as a physical degradation [9]. In contrast, irreversible chemical degradation has been observed in some cases and morphological effects such as cracking or material leaching were involved [11, 13-15]. In most of these studies, fully cured or almost fully cured materials were investigated, i.e. the effect of the curing degree on these degradation mechanisms and their related decreases of physical and mechanical properties have not yet been specifically addressed.

The effect of alkalinity, i.e. alkaline water exposure, on physical and mechanical epoxy resin properties has also already been investigated, although with contradictory results. Exposure to pure water and alkaline solutions during 5 [13], 18 [14] and 24 [16] months at different temperatures resulted in a higher decrease of tensile strength in the case of alkaline exposure (15% at 60°C [13], 86% at 40°C [14] and 5% at 23°C [16]) than in pure water (4% at 60°C [13], 37% at 40°C [14] and 43% at 23°C [16]). Another study however [17] did not find any effect of alkalinity, with water uptake in pure and alkaline water and resistances being the same.

Current knowledge concerning the long-term performance of cold-curing epoxies exposed to different environments is mainly based on laboratory investigations of a very limited duration of one to two years. Accelerated methods were thus developed whereby the physical and chemical processes are accelerated by higher temperatures or increased concentrations of solutions [18-20] in order to predict the long-term properties of polymers. The Arrhenius law, which is based on acceleration by increased temperature, is frequently used in this respect, and ASTM D3045 [21] provides corresponding guidance for polymers. With regard to bulk epoxies, the Arrhenius law has been applied in viscosity models [22], modeling of gelation and curing reactions [23], and diffusivity development during aqueous exposure [24].

In this chapter, based on the above-described scenario of adhesives not yet fully cured and exposed to a wet bridge environment, the effects of curing degree and exposure to humidity and alkalinity on the long-term physical and mechanical properties of a structural epoxy adhesive were investigated, as well as the potential recovery of properties after drying in order to consider the effect of a dry period following a wet period of weather. Since the investigations in Chapter 2 [4] showed that the same cold-curing epoxy adhesive as used in this chapter was almost fully cured after only one year of exposure in a dry environment, this study of the wet environment also investigated materials fully cured before exposure, in addition to partially cured materials. The long-term behavior was predicted based on the Arrhenius law. However, this method was only applicable for the fully cured materials since the elevated temperatures would have led to the rapid curing of partially cured materials.

3.2 Experimental program

3.2.1 Materials and conditioning

The commercial cold-curing epoxy adhesive Sikadur-330, supplied by SIKA Schweiz AG, was selected for this study as it is frequently used in structural civil engineering applications, e.g. for the bonding of carbon fiber-reinforced polymer (CFRP) plates or as impregnation resin for fabrics to strengthen existing structures. The thixotropic bi-component resin/adhesive comprises a bisphenol-A-based epoxy resin and a hardener consisting of aliphatic amines, and a small quantity, less than 20% per weight, of silica-based fillers [25]. Its viscosity is approximately 6000mPa·s at 23°C, according to the product data sheet.

The adhesive was produced under laboratory conditions (T=21± 3°C and RH=40±10%) with 4:1 resin to hardener mixing ratio, as suggested by the supplier. The adhesive was then poured into aluminum molds of specimen dimensions as described in the next section. To represent adhesive applications under on-site bridge conditions, no vacuum was applied to remove entrapped air. As explained above, post-cured (i.e. fully cured) and cold-curing (i.e. partially cured) specimens were manufactured. The post-cured specimens were left, after pouring, for seven days' curing under laboratory conditions, followed by three-day post-curing at 60±0.5°C in an oven. Directly after pouring, the cold-curing specimens were conditioned at a low temperature of 13°C for two days, i.e. the time necessary for demolding. The post-curing also dried the post-cured specimens, whereas for the cold-curing specimens drying before immersion was not possible.

After this first phase of conditioning, the specimens were immersed in different baths. Six baths were prepared for the post-cured specimens, i.e. three baths containing demineralized water at 13, 30 and 50°C (specimens PD13, PD30, PD50) and three baths with alkaline water at the same temperatures (specimens PA13, PA30, PA50), see Tab. 3.1. Three temperatures were thus selected in order to subsequently apply the Arrhenius law as mentioned above. The maximum temperature was limited to 50°C to clearly remain below the DMA onset of glass transition (approximately 65°C, obtained from reference P21) and thus not activate additional degradation mechanisms. The three alkaline baths had a pH value slightly fluctuating around 13.0, obtained from dissolving 0.25 mol/L KOH, 0.14 mol/L NaOH and 0.02 mol/L $Ca(OH)2$ in demineralized water. The cold-curing specimens (CD13) were immersed in demineralized water at low temperature, 13°C, in order to delay the curing progression. The temperatures of the seven baths in total were maintained with a precision of ±1.5°C. A total of 595 specimens were subjected to this second conditioning phase for a period of up to 24 months.

For the subsequent drying phase and evaluation of potential property recovery, only the PD50 specimens with the highest water uptake were investigated. These were removed from the bath at the end of the immersion period, i.e. in a fully saturated state, and subjected to drying, either in a laboratory environment, i.e. 21°C and RH=40±10% for up to 285 days, or at 50°C in an oven for up to 55 days.

Tab. 3.1 *Specimen designation, conditioning (C=cold-curing, P=post-cured) and immersion conditions*

Conditioning	Immersion medium	Temperature [°C]	Max. immersion time [days]
C13, P21 reference	None	13, 21	0 (dry)
CD13	Demineralized water, pH ≈ 7.0	13	754
PD13		13	740
PD30		30	737
PD50		50	557
PA13	Alkaline water, pH ≈ 13.0	13	726
PA30		30	730
PA50		50	684

3.2.2 Characterization methods and specimen types

The physical properties of the adhesive were obtained from Dynamic Mechanical Analysis (DMA) and Differential Scanning Calorimetry (DSC). The mechanical properties were derived from standard tensile experiments and the water uptake characteristics were obtained from gravimetric measurements. Reference values, i.e. properties before immersion, were obtained after five days of curing at 13°C for the cold-curing specimens (when the C13 specimens were sufficiently solid to be tested, see Tab. 3.1) and after the three-day post-curing and cooling to laboratory temperature (21°C) for the P21 specimens. Subsequent measurements, during immersion, were taken at irregular frequencies, according to the development of the properties.

DMA was used to obtain the temperature-dependent viscoelastic properties, i.e. loss and storage modulus and glass transition temperature (T_g). The temperature at the peak of the loss modulus curve, which reflects the onset of segmental motion on the molecular level [26], was selected as representing T_g. The experiments were performed with a TA Instruments Q800 dynamic mechanical analyzer in single cantilever configuration. Prismatic specimens of 35x10x3 mm^3 dimensions were subjected to a constant strain amplitude of 20 μm at an oscillation frequency of 1.0 Hz, while the temperature increased from laboratory temperature (21°C) to 100°C with a heating rate of 1°C/min in an air atmosphere. Properties were obtained from two DMA experiments performed on two different specimens for each condition and time.

DSC was used to measure the residual heat of the exothermic reaction (ΔH_{res}) and thus estimate the curing degree (α) of the resin based on ΔH_{res} and the total heat ($\Delta H_{res,tot}$ =296J/g), measured for the uncured/fresh resin. A heat-flux differential scanning calorimeter (DSC-TA Q100) connected to a thermal analyzer was used. Dynamic scans from -25 to 280°C, at a heating rate of 10°C/min, were performed under a nitrogen atmosphere. The samples, weighing between 5 and 10 mg, were cut from the conditioned specimens. Properties were obtained from two DSC experiments on two different samples for each condition and time.

Quasi-static tensile experiments were performed under laboratory conditions according to ASTM D638 [27], using an MTS Landmark servo-hydraulic loading machine, calibrated at a load capacity of 5 kN. The dog-bone-shaped specimens, shown in Fig. 3.1, were loaded under displacement control at a rate of 3.5 mm/min. The longitudinal strain was obtained from an MTS clip-on extensometer with a gage length of 25±0.05 mm and an accuracy of ±0.5% of the calculated strain. Nominal strength, i.e. based on the initial cross section of each specimen, was considered. The tensile E-modulus was calculated as the slope of the stress-strain curve in the initial linear part, between 0.05% and 0.15% strain. Four or five specimens were considered for the mechanical characterization for each condition and time. Specimens that presented tab failure were not taken into account in the analysis.

Gravimetric measurements were performed on the prismatic (DMA) and dog-bone (tensile) specimens using an analytical balance (Mettler Toledo) of 0.001 g accuracy. All specimens were weighed prior to immersion. Five prismatic (DMA) specimens from each bath were regularly weighed to assess the amount of water absorbed during immersion and derive the diffusion coefficients according to ASTM D570 [28]. The corresponding drying curves were obtained from three prismatic specimens at each drying temperature. Furthermore, all immersed and drying specimens (prismatic and dog-bone-shaped) were weighed before the DMA and tensile experiments, in order to correlate the changes in properties with the amount of water absorbed.

Images of the fracture surfaces of the tensile specimens were taken using a digital handheld microscope Dino-Lite AD7013MZT. This microscope is equipped with a 5-megapixel sensor with an adjustable polarizer on an aluminum alloy body with an interchangeable nozzle feature. It provides up to 240x magnification and resolution of 2592x1944 pixels.

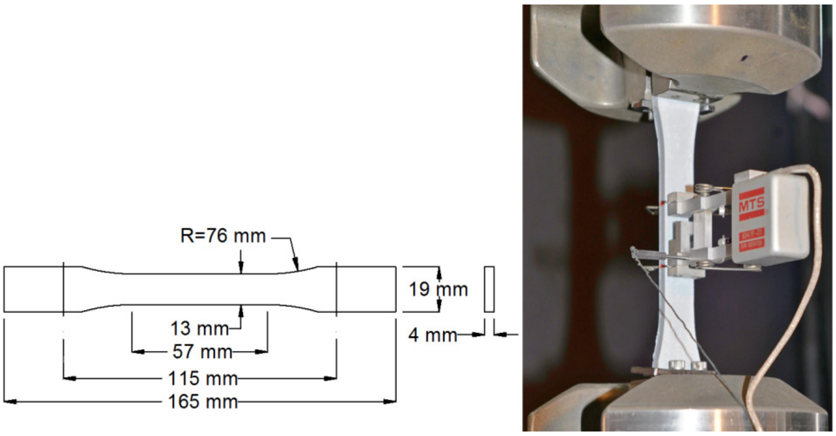

Fig. 3.1 *Specimen dimensions and experimental set-up of tensile experiments.*

3.3 Experimental results and discussion

In the following, after reporting the results obtained from the reference specimens before immersion, the physical and mechanical properties development of the fully (post-) cured immersed specimens (PD and PA) are discussed. Subsequently, the results obtained for the cold-curing immersed specimens are analyzed and compared to those of similar specimens aging in a dry environment, obtained in the previous work [4]. This comparison allowed the effects of the concurring curing and plasticization mechanisms on the physical and mechanical properties to be separated. Finally, the results obtained from the drying process are reported.

3.3.1 Reference specimens before immersion

The physical and mechanical properties of the specimens before immersion are listed in Tab. 3.2. No residual heat could be detected on the DSC scans of the post-cured specimens, confirming full curing of the resin.

***Tab. 3.2** Reference properties of specimens before immersion (physical property averages from two measurements)*

Conditioning	T_g [°C]	ΔH_{res} [J/g]	α [-]	E-modulus [MPa]	Strength [MPa]
C13	36.0	38.5	0.87	3463 ± 305	27.0 ± 1.0
P21	74.7	0	1.00	4526 ± 125	43.3 ± 3.5

The cold-curing specimens already exhibited a significant curing degree of 0.87 after five days of curing at 13°C. However, T_g and the tensile strength did not yet reflect this curing degree, as already observed in [4].

3.3.2 Post-cured specimens during immersion

Water uptake and diffusion coefficients

During the immersion period, the increase in weight (Δw_t) due to the absorbed demineralized or alkaline water was calculated to the nearest 0.001g as follows:

$$\Delta w_t\ (\%) = \frac{w_t - w_{t0}}{w_{t0}} \cdot 100 \qquad (3.1)$$

where w_t and w_{t0} are the specimen weights at immersion time (t) and prior to immersion (t_0) respectively. The results for the six post-cured and the cold-curing conditioning cases, in relation to the root of immersion time (according to ASTM D570 [28]), are shown in Fig. 3.2.

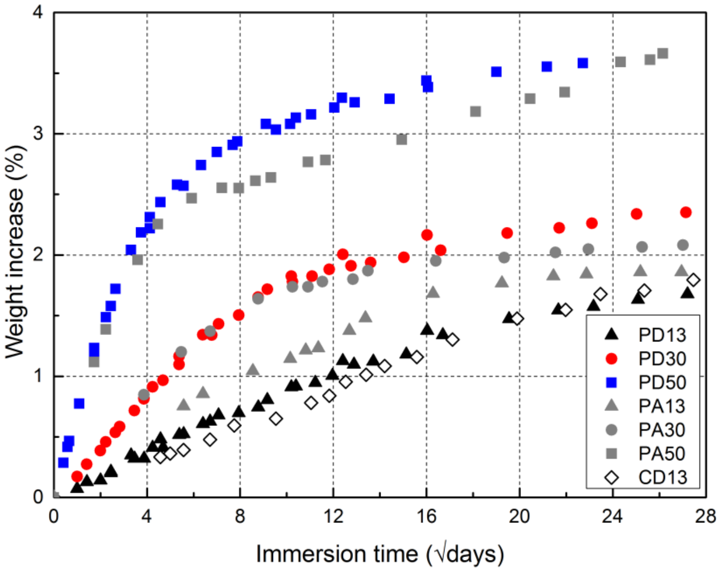

***Fig. 3.2** Weight increase of prismatic specimens vs root of immersion time, all conditioning cases (see Tab. 3.1), average from five specimens.*

All conditioning cases exhibited the typical initially linear and subsequently leveling-off weight increase when approaching saturation. The increase in weight per two-week period for three consecutive weighings was less than 1% of the total increase in weight or 5 mg for the last weight measurements. Therefore, according to ASTM D570, the specimens were considered saturated. The resulting weight increases at saturation ($\Delta w_{t\infty}$) are summarized in Tab. 3.3.

***Tab. 3.3** Diffusion coefficients and saturation results (average from five specimens)*

Conditioning	**D [mm²/day]**	**Δw∞ [%]**
CD13	0.003	1.79 ± 0.05
PD13	0.005	1.68 ± 0.10
PD30	0.014	2.35 ± 0.06
PD50	0.054	3.58 ± 0.05
PA13	0.007	1.86 ± 0.08
PA30	0.020	2.08 ± 0.03
PA50	0.040	3.66 ± 0.09

As expected, the water uptake increased with increasing temperature in all cases. The effect of alkalinity (PA specimens) was not clear during the uptake period, i.e. the weight increase was slightly lower at high temperature and slightly higher at low temperature compared to the demineralized water values (PD).

The diffusion coefficients (D) according to Fick's second law [29] were determined as follows:

$$D = \pi \cdot \left(\frac{e}{4 \cdot \Delta w_{\infty}} \right)^2 \cdot \left(\frac{\Delta w_{t1} - \Delta w_{t2}}{\sqrt{t_1} - \sqrt{t_2}} \right)^2 \tag{3.2}$$

where Δw_{t1}, Δw_{t2} and $\Delta w_{t\infty}$ represent the weight increase at immersion times t_1, t_2 and at saturation, and e is the specimen thickness (3 mm). The equation was applied for the initial linear stage, i.e. for $\Delta w_t/\Delta w_{t\infty}<0.6$ [29]. The obtained D values are summarized in Tab. 3.3 for all conditioning cases; similar values were reported in literature [5, 12]. They followed the same trend as discussed for the weight increase, i.e. higher values with higher temperature and exhibited the same small inconsistent differences between demineralized and alkaline exposure.

Effect of water uptake on glass transition temperature

The glass transition temperature dependence on the weight increase due to the uptake of demineralized and alkaline water is shown in Fig. 3.3. A significant decrease occurred with increasing water uptake, which leveled off, however, when saturation was approached, i.e. the values stabilized at around 58°C at above 2% of weight increase. The behavior was almost independent of the immersion temperature and alkalinity; only the PA13 values at the lowest temperature were slightly higher. This decrease could be attributed to the well-known plasticization mechanism [11, 30, 31], i.e. the absorbed water broke the interchain van der Waals forces and hydrogen bonds and thus increased the chain segmental mobility [32]. However, water absorbed above 2% did not cause any further T_g decrease.

The relationship between T_g and the immersion time for the post-cured specimens is shown in Fig. 3.4. The T_g decrease occurred more rapidly at higher immersion temperatures since the weight increase also occurred more rapidly (see Fig. 3.2). However, the values converged to the above-mentioned limit when saturation was approached; similar behavior is reported in [16, 24, 32, 33]. Again, the results were almost independent of the water alkalinity. A closer look at the responses showed that after the first rapid decrease a slight increase of the values occurred at the higher temperatures. This may be attributed to the formation of two H-bonds between the water molecules and the resin's polar sites, resulting in bridging between the chain segments and thus secondary pseudo-crosslinking, which slightly increases the T_g according to [32].

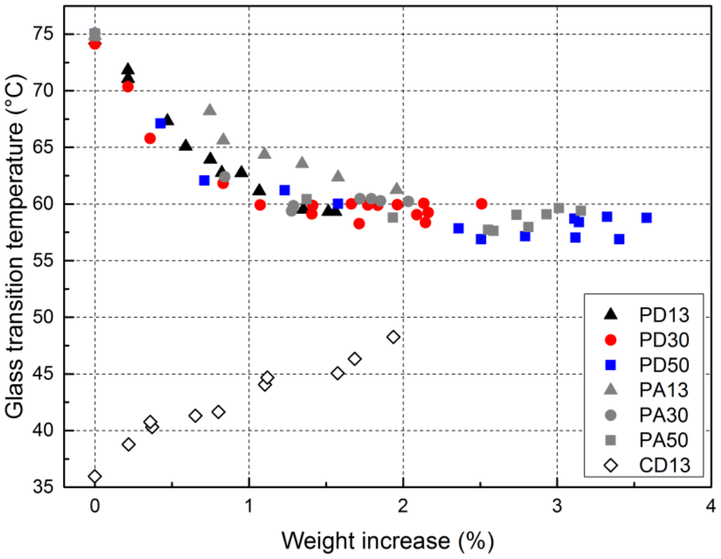

Fig. 3.3 *Glass transition temperature vs weight increase, all conditioning cases.*

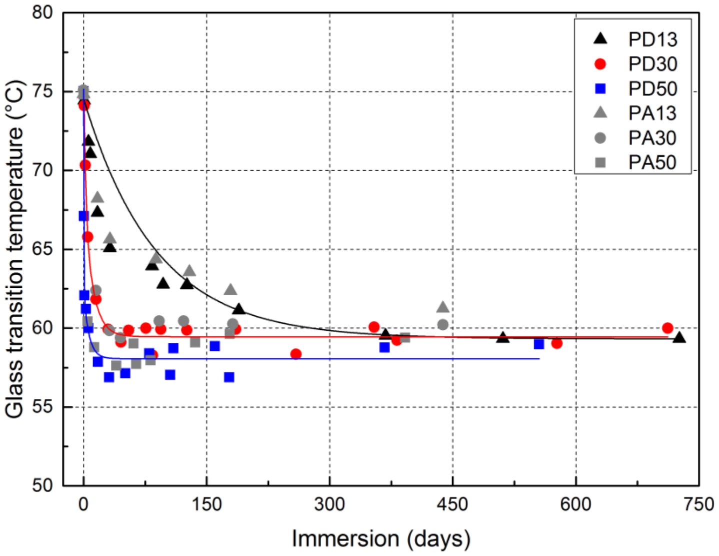

Fig. 3.4 *Glass transition temperature vs immersion time, post-cured specimens.*

Effect of water uptake on stiffness and strength

The effect of water uptake on the tensile E-modulus as a function of weight increase and immersion time is shown in Fig. 3.5 and Fig. 3.6 respectively; average values and standard deviations are indicated. After a short plateau up to 0.5% weight increase, the E-modulus decreased almost linearly with increasing weight, independently of immersion temperature and alkalinity. Similar observations were made in [5, 34] regarding immersion temperature.

The PD50 values seemed to stabilize after saturation, although the PA50 values continued to decrease. On the time axis, a similar immersion temperature-dependent decrease of the E-modulus, as observed for the glass transition temperature (Fig. 3.4), was noticed, again independent of the alkalinity. However, the initial drop did not occur until after approximately 100 days at the lowest temperature at which water absorption is much slower, while it started directly after immersion at the highest temperature. After 150 days, the slopes of all curves were significantly reduced, although they retained a decreasing tendency, and thus did not approach a plateau. The maximum E-modulus reduction at the end of the immersion period was 20% for the lowest and 47% for the highest temperature.

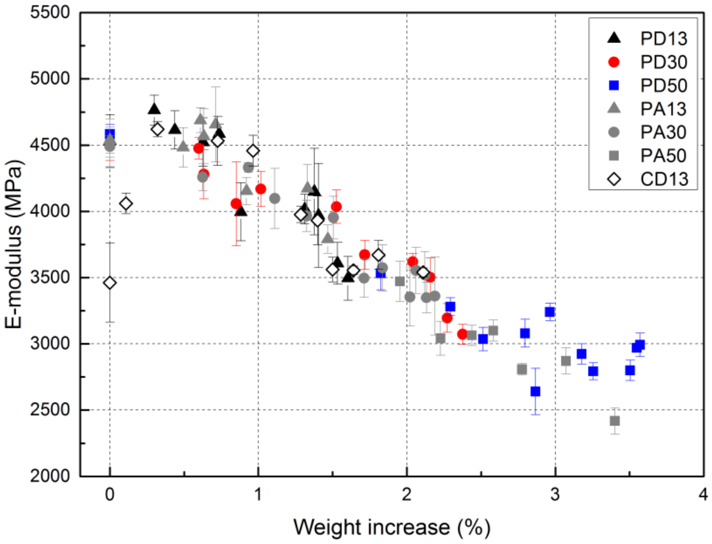

Fig. 3.5 *Tensile E-modulus vs weight increase, all conditioning cases.*

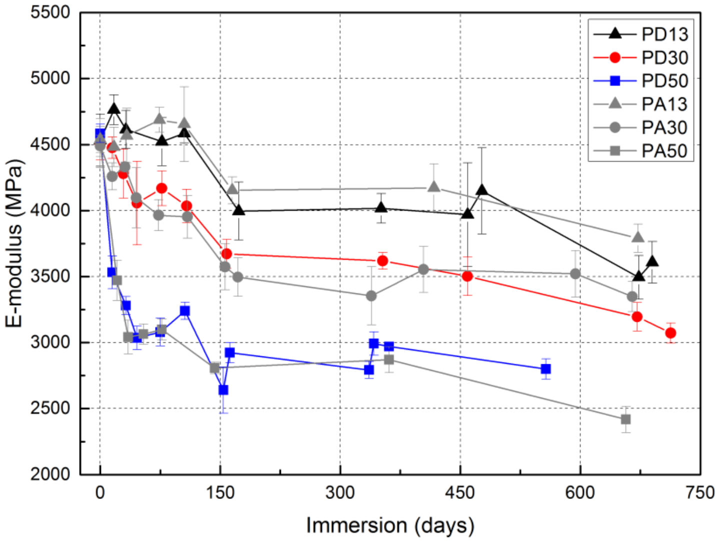

Fig. 3.6 *Tensile E-modulus vs immersion time, post-cured specimens.*

The tensile strength responses exhibited the same behavior as the E-modulus in relation to water uptake and immersion time, as shown in Fig. 3.7 and Fig. 3.8; again average values and standard deviations are indicated. The dependencies on temperature and alkalinity and the initial plateaus and decreasing tendencies were similar. The maximum strength reduction after the immersion period was 18% at the lowest and 37% at the highest temperature. Both E-modulus and strength decrease were attributed to the plasticization mechanism. Similar significant tensile property decreases during the first months of immersion were also reported in [16, 24, 35].

Plasticization induced by the water uptake also affected the stress-strain response of the specimens, as shown in Fig. 3.9 for the immersion in demineralized water at 13 and 50°C. The increasing water uptake changed the response from being initially almost linear to a significant non-linear behavior. Furthermore, stiffness and strength decreased while failure strain increased. Almost identical results were obtained for the alkaline water immersion. Similar responses of epoxies under moisture conditions are shown in [9, 33, 34].

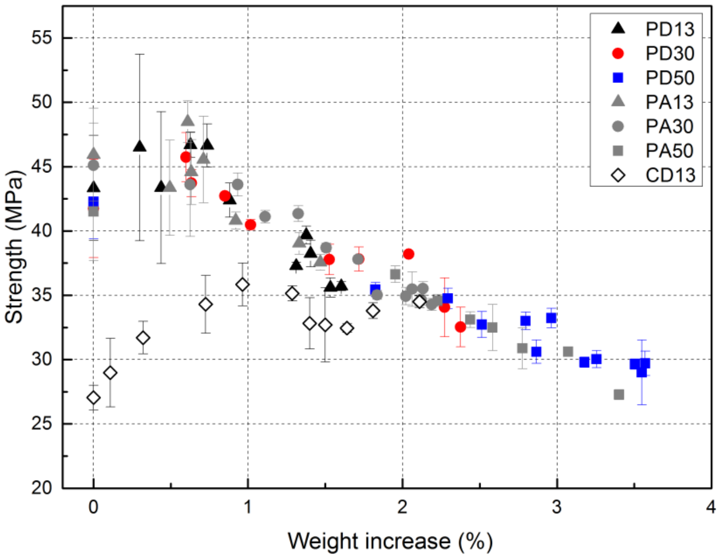

Fig. 3.7 *Tensile strength vs weight increase, all conditioning cases.*

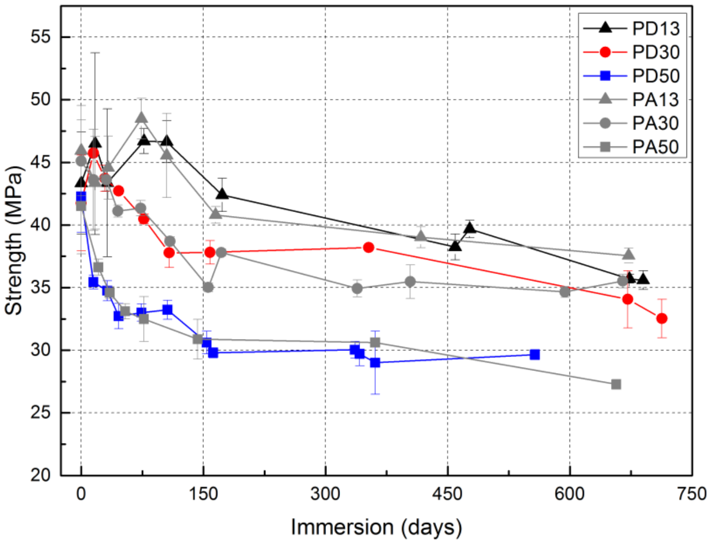

Fig. 3.8 *Tensile strength vs immersion time, post-cured specimens.*

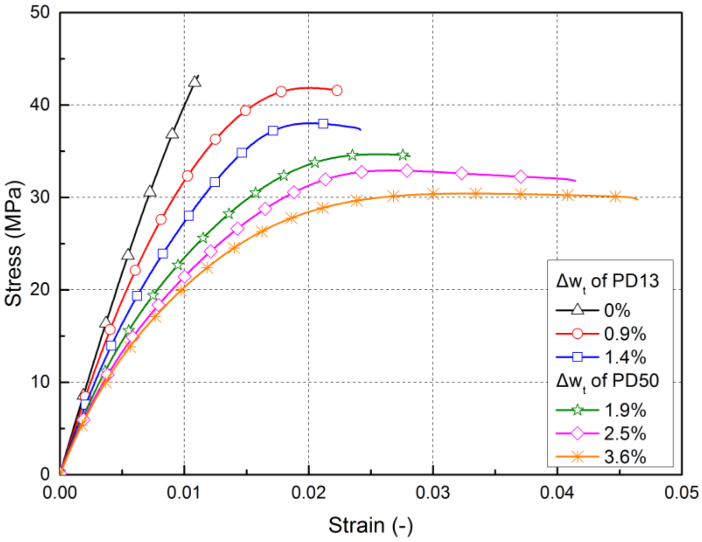

Fig. 3.9 *Stress-strain behavior at different water uptake, PD13 and PD50 specimens.*

The fracture surfaces of the dry reference specimens (P21) exhibited a flatter origin zone and a much rougher whitish propagation zone, as already described in [4] and shown in Fig. 3.10a). In the origin zone, fracture started from a small void or white dot, the latter being interpreted as a particle. In the immersed specimens (PD50) origin and propagation zones could no longer be clearly recognized, see Fig. 3.10b).

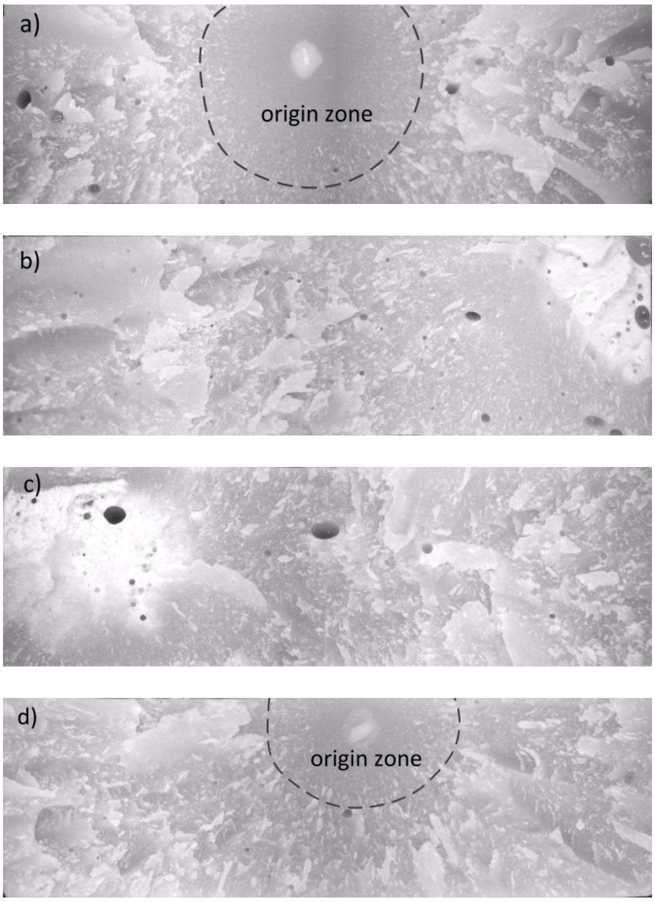

Fig. 3.10 *Typical fracture surfaces (13x4 mm^2) of specimens a) P21, reference, b) PD50 at $\Delta w=3\%$, c) CD13 at $\Delta w=1.6\%$, d) PD50 dried.*

3.3.3 Cold-curing specimens during immersion

Curing degree, water uptake and diffusion coefficients

As mentioned above, the cold-curing reference specimens already exhibited a high curing degree of 0.87 before immersion. Both the dry reference (C13) and immersed (CD13) specimens continued to cure. The curing degree of both conditioning cases reached values of 0.97-0.98 after 433 days, as shown in Tab. 3.4. The specimens were thus almost fully cured and the curing process did not seem to have been influenced by the water uptake.

No significant difference between the water uptake of the cold-curing CD13 and fully cured PD13 specimens could be observed, see Fig. 3.2, while the PA13 uptake was slightly higher. The cold-curing specimens exhibited lower diffusion coefficients than the fully cured ones, all the values were very small however due to the low immersion temperature, see Tab. 3.3.

Tab. 3.4 *Curing degree and residual heat of cold-curing immersed and dry specimens (average from two measurements)*

Conditioning	Time [days]	ΔH_{res} [J/g]	α [-]
C13	5	38.5	0.87
	433	7.5	0.98
CD13	6	35.0	0.88
	433	10.0	0.97
	564	5.0	0.98

Combined effect of water uptake and curing on glass transition temperature

The development of the glass transition temperature (Tg) of the specimens cold-curing at 13°C, immersed in demineralized water (CD13) and under dry conditions (C13, values from [4]) is compared in Fig. 3.11. Both T_g values increased with time while the values for the dry specimens were approximately 5°C higher than those for the immersed specimens. Since no obvious difference in the curing degree development of dry and immersed specimens was noticed, this T_g difference could be attributed to the plasticization of the immersed specimens. Both curves remained however clearly below the curve of the immersed fully cured PD13 specimens, which decreased significantly, although the cold-curing specimens were almost fully cured after 400 days (0.97-0.98, see Tab. 3.4). This result confirmed that T_g is very sensitive to the smallest changes in the curing degree when full cure is approached, a result that was already obtained in [4, 36]. Furthermore, it is not possible to conclude at this stage of the research, either from Fig. 3.3 or from Fig. 3.11, whether the CD13 curve would approach the PD13 curve in the mid-term or if a gap would always remain due to the exposure of the not yet fully cured material to humidity.

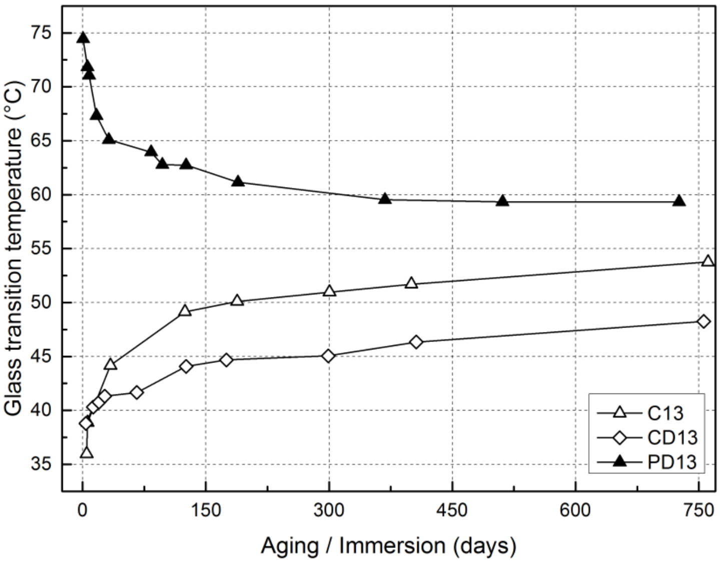

Fig. 3.11 *Glass transition temperature vs immersion/aging time at 13°C of cold-curing immersed/dry and post-cured immersed specimens.*

Combined effect of water uptake and curing on mechanical properties

The development of the E-modulus of the cold-curing immersed (CD13) and dry (C13, from [4]) specimens is shown and compared to the post-cured wet (PD13) specimens in Fig. 3.12. In Chapter 2 [4], the E-modulus of cold-curing dry specimens (C13) exhibited a peak after approximately 100 days, which was attributed to physical aging, i.e. a densification of the molecular network. This peak could not be observed for the immersed (CD13) specimens. After a rapid increase during the first days, the E-modulus reached the values of those of the PD13 specimens and both subsequently decreased at almost the same rate. Since the E-modulus of the C13 dry specimens did not decrease, this decrease could again be attributed to plasticization, which is confirmed in Fig. 3.5, where the E-modulus is only dependent on the water uptake (above 0.5% for CD13).

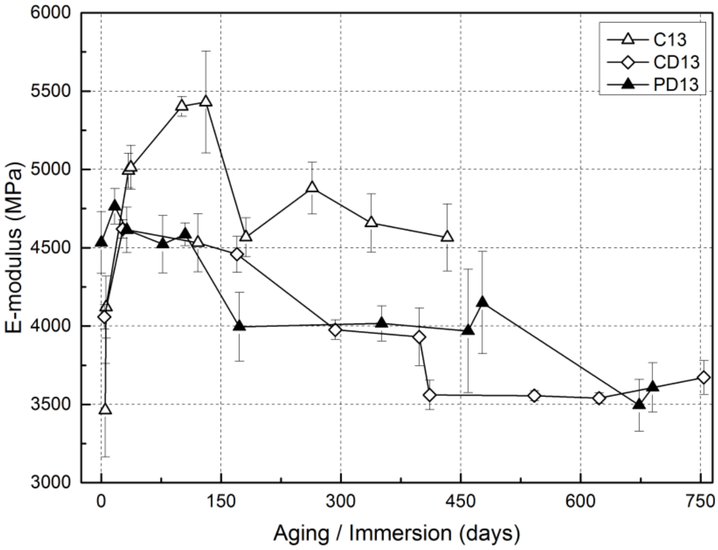

Fig. 3.12 *Tensile E-modulus vs immersion/aging time at 13°C of cold-curing immersed/dry and post-cured immersed specimens.*

Plasticization therefore also inhibited a densification of the molecular network, i.e. physical aging, as referred to in [8, 12]. This is confirmed by the DSC scans shown in Fig. 3.13. After five or six days, the dry and immersed specimens showed similar curves, both exhibiting a relaxation peak at around 50°C, indicating physical aging. After 433 days, however, the peak disappeared in the immersed CD13 specimen, while it is still visible in the dry C13 specimen. The immersed CD13 specimen also exhibited a slight endothermic peak just above 100°C, which could be attributed to water evaporation and was not yet visible after six days.

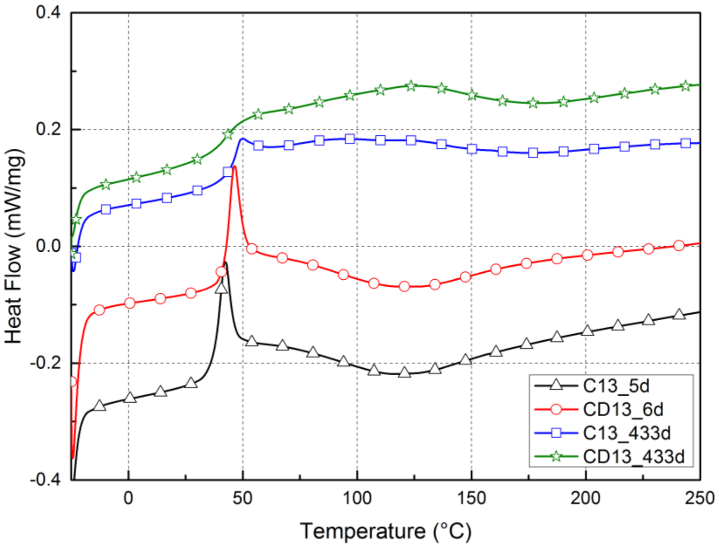

Fig. 3.13 *DSC scans of immersed and dry specimens after 5-6 and 433 days.*

The development of the tensile strength of the CD13 and C13 specimens is compared in Fig. 3.14. In the early age, strength developed at the same rate. In the later age, however, the strength of the dry specimens continued to increase while that of the immersed specimens started decreasing. In the early age, curing was thus the dominant mechanism in the immersed specimens while plasticization dominated in the later age. The strength of the CD13 specimens approached that of the post-cured specimens

(PD13) in the later age, as is also shown in Fig. 3.7, since the former were almost fully cured at that time. The fracture surface of the immersed CD13 specimens exhibited the same texture as the immersed post-cured specimens (PD50), as shown in Fig. 3.10c).

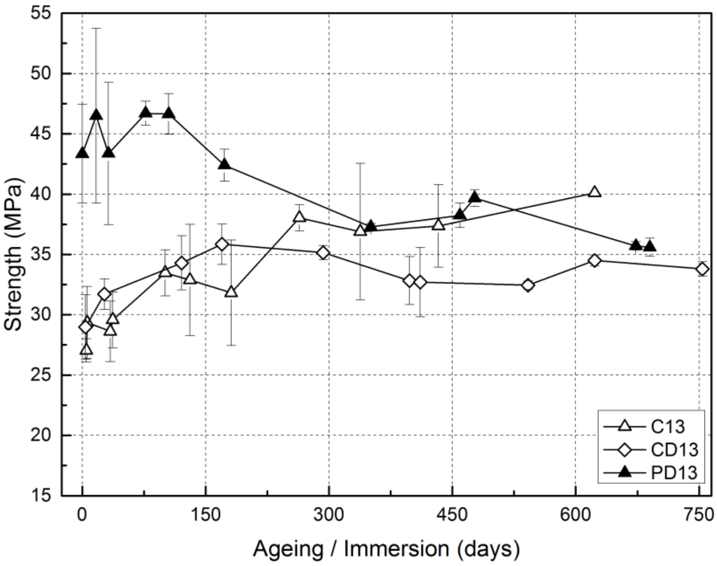

Fig. 3.14 *Tensile strength vs immersion/aging time at 13°C of cold-curing immersed/dry and post-cured immersed specimens.*

3.3.4 Post-cured specimens after drying

The weight loss of the PD50 prismatic (DMA) specimens during drying is shown in Fig. 3.15. After drying at 50°C, the loss was slightly higher than the gain during immersion, indicating that the specimens may not have been fully dried after the post-curing. However, leaching of solvents or compounds not forming part of the final cross-linked epoxy structure could also explain the additional weight loss [11]. Drying at 21°C could not completely remove the water, although the measurements leveled off. Furthermore, drying occurred much more rapidly than water uptake (compare Fig. 3.15 with Fig. 3.2); similar results were found in [11, 12].

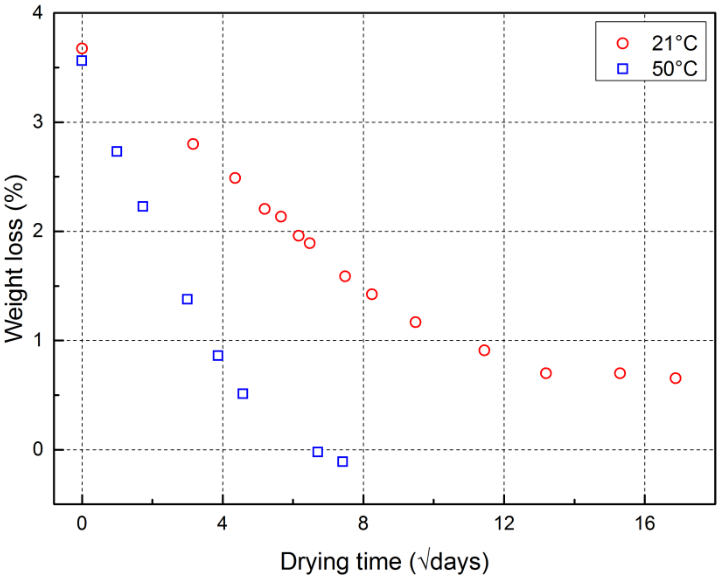

Fig. 3.15 *Weight loss during drying of PD50 prismatic specimens at 21 and 50°C.*

Selected values for the glass transition temperature and mechanical properties during and after drying are listed in Tab. 3.5 and Tab. 3.6 respectively and compared to the reference values of Tab. 3.2. The results show that all properties fully recovered after drying. The values correspond to the water uptake values at the same weight if compared to Fig. 3.3, Fig. 3.5 and Fig. 3.7. Values higher than 100% for the T_g and E-modulus may be explained by the leaching of solvents or compounds not forming part of the final cross-linked epoxy structure. The fracture surface after drying was similar to that before immersion, as shown in Fig. 3.10d).

Tab. 3.5 *Recovery of glass transition temperature of PD50 DMA specimens after drying*

Drying temperature [°C]	Remaining water [%]	Drying duration [days]	T_g [°C]	T_g [%] of reference
21	2.0	38	62.6	84
	0.6	285	68.9	92
50	2.2	3	62.4	84
	-0.2	55	79.7	107

Tab. 3.6 *Recovery of mechanical properties of PD50 tensile specimens after drying*

Drying temperature [°C]	Remaining water [%]	Drying duration [days]	E-modulus [MPa]	Strength [MPa]	E-modulus [%] of reference	Strength [%] of reference
21	3.1	5	3342 ± 217	33.0 ± 0.2	74	76
	2.7	15	3499 ± 103	34.0 ± 0.8	77	79
	2.0	46	3572 ± 54	35.3 ± 0.1	79	82
	0.8	258	4290 ± 200	44.2 ± 2.7	95	102
50	0	55	4932 ± 40	46.7 ± 0.7	109	108

3.4 Modeling and lifetime prediction

3.4.1 Arrhenius law application

The Arrhenius law was applied to predict the E-modulus and strength decrease of the specimens immersed in the alkaline baths up to a bridge service life of 100 years. Keeping the maximum temperature of 50°C clearly below the onset of the glass transition temperature assured that only one degradation mechanism was activated and accelerated, which is a precondition for the applicability of this method in its basic and simple form [37]. The Arrhenius principle can be expressed as follows [38]:

$$\log\left(\frac{1}{k}\right)=\frac{E_A}{2.3\cdot R}\cdot\frac{1}{T}-\log A \tag{3.3}$$

where k is the rate of the property decrease, E_A [J/mol] is the activation energy, R=8.314 [J/(K·mol)] is the universal gas constant, T [K] is the absolute temperature, and A is a constant. Eq. 3.3 represents an equation for a straight line, $y=mx+c$, that can be fitted to the experimental data if the Arrhenius law is obeyed, where m allows the determination of the activation energy E_A.

Based on Eq. 3.3 and the availability of sets of data at different temperatures, T, allows the determination of time shift factors, α_T, related to a reference temperature T_0, according to the following equation:

$$\log\alpha_T=\log\left(\frac{k}{k_0}\right)=\frac{E_A}{2.3\cdot R}\cdot\left(\frac{1}{T}-\frac{1}{T_0}\right) \tag{3.4}$$

These time shift factors can be used to shift the experimental data from different temperatures on the time axis to form a master curve at a selected reference temperature and thus predict properties over a much longer time period than experimentally covered, provided that the activation energy is the same, i.e. the slopes of the curves according to Eq. 3.3, at the different temperatures, are the same.

3.4.2 Lifetime prediction

The E-modulus and strength retention of the PA specimens (post-cured and immersed in alkaline water), i.e. the measured values normalized by the not-immersed average reference values according to Tab. 3.2, at the measured times and at the three different temperatures, are shown in Fig. 3.16 and Fig. 3.17 respectively. Setting the time axes on a logarithmic scale allowed the fitting of the data by straight lines, which are almost parallel; the correlation coefficients are higher than 0.9 for strength and approximately 0.8 for stiffness. These results already indicated that the Arrhenius process is applicable.

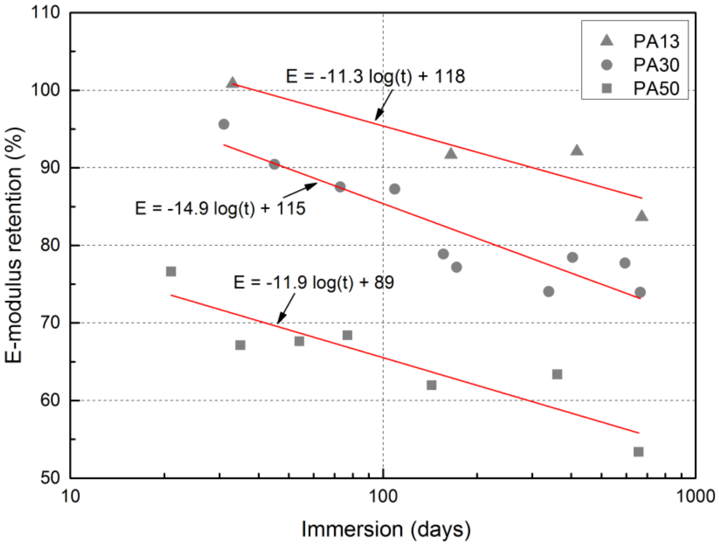

Fig. 3.16 *Retention of E-Modulus vs logarithm of immersion time of PA specimens at three immersion temperatures.*

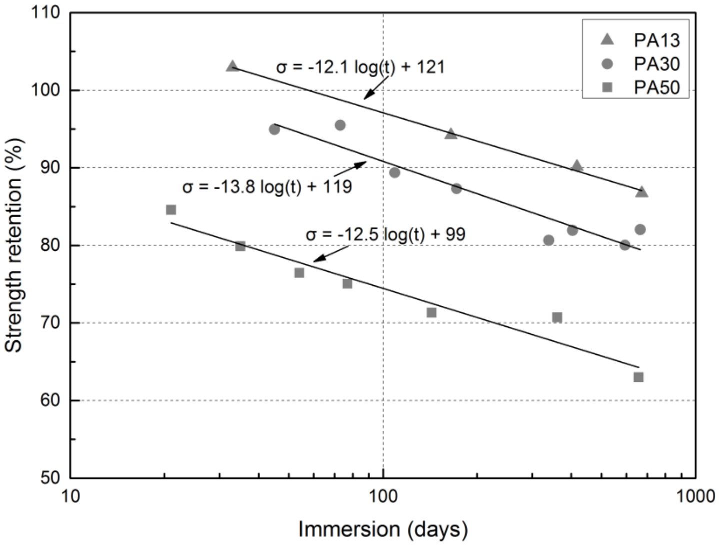

Fig. 3.17 *Retention of strength vs logarithm of immersion time of PA specimens at three immersion temperatures.*

The results shown in Fig. 3.16 and Fig. 3.17 were converted into the Arrhenius plot according to Eq. 3.3, i.e. time vs reciprocal of temperature, see Fig. 3.18. The time in days has been plotted on a logarithmic scale. The resulting fitted straight lines were again almost parallel and the activation energy, obtained from their slope, was E_A =15.4 ± 0.7 kJ/mol, for the E-modulus, and E_A =11.0 ± 0.3 kJ/mol, for the strength. Knowing the activation energies then allowed the determination of the time shift factors according to Eq. 3.4 for selected reference temperatures, e.g. 10°C and 20°C, as shown in Tab. 3.7. The experimental data shown in Fig. 3.16 and Fig. 3.17 was then multiplied by these shift factors and again straight lines were fitted to the shifted data to obtain the master curves at the two reference temperatures for E-modulus and strength, as shown in Fig. 3.19.

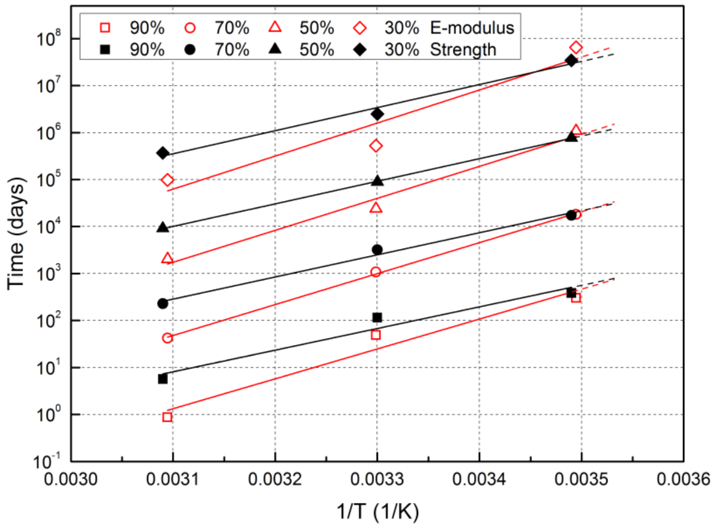

Fig. 3.18 *Arrhenius plots of time vs inverse of absolute temperature, at different tensile strength and E-modulus retention.*

Tab. 3.7 *Time shift factors at reference temperatures 10 and 20°C*

Experimental Temp. [°C]	**$\alpha_{T,10°C}$ [-]**		**$\alpha_{T,20°C}$ [-]**	
	E-modulus	**Strength**	**E-modulus**	**Strength**
13	1.8	1.5	0.3	0.4
30	36.3	12.8	5.7	3.4
50	846.0	120.0	132.0	32.1

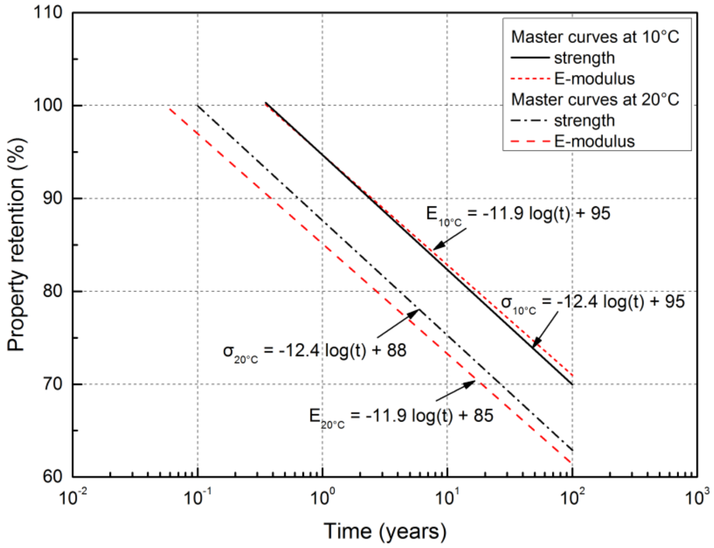

Fig. 3.19 *Predicted tensile strength and E-modulus retention vs time at reference temperatures 10°C and 20°C.*

The predictions in Fig. 3.19 show that the percentage of E-modulus and strength retention at a certain time is very similar. Retention at a lower temperature is higher and the main degradation occurs in the early age. After a bridge service life of 100 years, E-modulus and strength retentions are 72% and 70% at a 10°C reference temperature and 62% and 64% at 20°C. Since no significant differences between the results of immersion in demineralized and alkaline water could be observed, it can be assumed that these values are also valid for demineralized water. It should however be underlined that these values are based on fully immersed and saturated specimens. Adhesives exposed to a less harsh environment, i.e. not to stagnant water, are expected to retain higher E-modulus and strength values.

3.5 Conclusions

The effects of aging in a wet bridge environment on the physical and mechanical properties of a cold-curing structural epoxy adhesive were investigated. Since the study in Chapter 2 showed that the cold-curing adhesive was almost fully cured after one year in a dry bridge environment, cold-curing and fully cured materials were investigated. Furthermore, the effects of drying and alkalinity of the pore water solution in concrete-adhesive bridge joints on the physical and mechanical properties was evaluated. The following conclusions were drawn:

1) A significant decrease of the glass transition temperature, tensile E-modulus and tensile strength of the fully cured adhesive was observed during the two years of immersion at different temperatures. This decrease could be attributed to plasticization.
2) The decrease of the glass transition temperature leveled off after approximately one year and a reduction of 23% (from approximately 75°C to 58°C). The E-modulus and strength, however, continued to decrease. Predictions based on the Arrhenius law indicated a retention of at least 70% of E-modulus and strength at a 10°C reference temperature, after a 100-year bridge service life. These retentions, however, were obtained under full immersion and may thus be higher in real cases where only a defect in the sealing of an adhesive joint occurs.
3) Plasticization changed the stress-strain behavior from almost linear under dry conditions to highly nonlinear at full saturation.
4) Full recovery of glass transition temperature, E-modulus and strength was obtained after drying the immersed and fully saturated material.
5) The immersion in alkaline water of pH 13.0 resulted in reductions of physical and mechanical properties similar to those obtained after immersion in demineralized water. The alkalinity thus did not have a detrimental effect.
6) Concurring mechanisms were effective in the immersed cold-curing, not yet fully cured material, i.e. continuation of curing and plasticization. The former was dominant in the early age and led to an increase of the glass transition temperature, E-modulus and strength. The latter decelerated the increase of the glass transition temperature and led to a decrease of the E-modulus and strength in the later age. Both approached the values of those of the fully cured material, the E-modulus very rapidly, after less than one month, and the strength much later, after 20 months.
7) DSC residual heat measurements did not show any difference in the curing progression between dry and wet materials.
8) In contrast to a cold-curing dry material, no effects of physical aging, i.e. densification of the molecular network, could be observed in the cold-curing immersed material.

3.6 References

[1] H. Hänsch, W. Krämer, Versuche mit geklebten Verbundkonstruktionen, Strasse 3 (1968) 137–141.

[2] B. Täljsten, A. Hejll, G. James, Carbon Fiber-Reinforced Polymer Strengthening and Monitoring of the Gröndals Bridge in Sweden, J. Compos. Constr. 11 (2007) 227–235.

[3] T. Keller, J. Rothe, J. de Castro, M. Osei-Antwi, GFRP-Balsa Sandwich Bridge Deck: Concept, Design, and Experimental Validation, J. Compos. Constr. 18 (2013) 04013043 (1-10).

[4] M. Savvilotidou, A. P. Vassilopoulos, M. Frigione, T. Keller, Effects of aging in dry environment on physical and mechanical properties of a cold-curing structural epoxy adhesive for bridge construction, Constr. Build. Mater. 140 (2017) 552–561.

[5] M. Heshmati, R. Haghani, M. Al-Emrani, Effects of Moisture on the Long-term Performance of Adhesively Bonded FRP/steel Joints Used in Bridges, Compos. Part B 92 (2016) 447–462.

[6] M. Heng, K. Murata, Aging of concrete buildings and determining the pH value on the surface of concrete by using a handy semi-conductive pH meter, Anal. Sci. 20 (2004)1087–1090.

[7] E. Schaumann, T. Vallée, T. Keller, Direct load transmission in hybrid FRP and lightweight concrete sandwich bridge deck, Composites Part A 39 (2008) 478–487.

[8] M.S. Sciolti, M. Frigione, M.A. Aiello, Wet lay-up manufactured FRP's for concrete and masonry repair. Influence of water on the properties of composites and of their epoxy components, J. Compos. Constr. 14 (2010) 823–833.

[9] P. Silva, P. Fernandes, J. Sena-Cruz, J. Xavier, F. Castro, D. Soares, V. Carneiro, Effects of different environmental conditions on the mechanical characteristics of a structural epoxy, Composites Part B 88 (2016) 55–63.

[10] J.W. Shi, H. Zhu, G. Wu, Z.S. Wu, Tensile behavior of FRP and hybrid FRP sheets in freeze–thaw cycling environments, Composites Part B 60 (2014) 239–247.

[11] Y. Zhang, R.D. Adams, L.F.M. da Silva, Absorption and glass transition temperature of adhesives exposed to water and toluene, Int. J. Adh. Adh. 50 (2014) 85–92.

[12] M. Frigione, M. Lettieri, Procedures Conditioning the Absorption/Desorption Behavior of Cold-Cured Epoxy Resins, J. Polym. Sci., Part B: Polym. Phys. 46 (2008) 1320–1336.

[13] S. Kajorncheappunngam, R. Gupta, H. GangaRao, Effect of Aging Environment on Degradation of Glass-Reinforced Epoxy, J. Compos. Constr. 6 (2002) 61-69.

[14] S. Cabral-Fonseca, J.P. Nunes, M.P. Rodrigues, M.I. Eusébio, Durability of epoxy adhesives used to bond CFRP laminates to concrete structures, Proceedings of the17th International Conference on Composite Materials (ICCM 17) UK, 2009.

[15] G. Z. Xiao, M. E. R. Shanahan, Water absorption and desorption in an epoxy resin with degradation. J. Polym. Sci. B Polym. Phys. 35 (1997) 2659–2670.

[16] Q. Yang, G. Xian, V.M. Karbhari, Hygrothermal ageing of an epoxy adhesive used in FRP strengthening of concrete, J. Appl. Polym. Sci. 107 (2008) 2607–2617.

[17] L. Wolff, K. Hailu, M. Raupach, Mechanisms of Blistering of Coatings on Concrete, International Symposium Polymers in Concrete, Portugal, 2006.

[18] R.P. Brown, Predictive techniques and models for durability tests, Polym. Test. 14 (1995) 403–414.

[19] J. Zhou, X. Chen, S. Chen, Durability and service life prediction of GFRP bars embedded in concrete under acid environment, Nucl. Eng. Des. 241 (2011) 4095–4102.

[20] A. Eldridge, A. Fam, Environmental Aging Effect on Tensile Properties of GFRP Made of Furfuryl Alcohol Bioresin Compared to Epoxy, J. Compos. Constr., 18 (2014) 04014010 (1–10).

[21] ASTM D3045-92(2010), Standard Practice for Heat Aging of Plastics Without Load, ASTM International, West Conshohocken, PA, 2014.

[22] H.M. Smith, A.V. May, C.L. Long, Shelf Life Determination of an Epoxy Resin by Accelerated Aging., Final report, Bendix Corp., Kansas City Div., USA, 1981.

[23] Z.N. Sanjana, R.L. Selby, The use of dielectric analysis to study the cure of an epoxy casting compound, Proceedings of the 14th Electrical/Electronics Insulation Conference (EIC) USA, 1979.

[24] S. Popineau, C. Rondeau-Mouro, C. Sulpice-Gaillet, M.E.R. Shanahan, Free/bound water absorption in an epoxy adhesive, Polymer 46 (2005) 10733–10740.

[25] O. Moussa, A.P. Vassilopoulos, J. de Castro, T. Keller, Long-term development of thermophysical and mechanical properties of cold-curing structural adhesives due to post-curing, J. Appl. Polym. Sci. 127 (2013) 2490–2496.

[26] E.A. Turi, Thermal Characterization of Polymeric Materials, Volume I, second ed., Academic Press, New York, 1997

[27] ASTM D638-14, Standard test Method for tensile properties of plastics, ASTM International, West Conshohocken, PA, 2014.

[28] ASTM D570-98(2010)e1 Standard Test Method for Water Absorption of Plastics, ASTM International, West Conshohocken, PA, 2010.

[29] J. Crank, The mathematics of diffusion, second ed., Oxford: Clarendon Press, 1975

[30] M.Y.M. Chiang, M. Fernandez-Garcia, Relation of swelling and Tg depression to the apparent free volume of a particle-filled, epoxy-based adhesive, J. Appl. Polym. Sci. 87 (2003) 1436–1444.

[31] S.G. Prolongo, A. Ureña, Durability of Aluminium Adhesive Joints Bonded with a Homopolymerised Epoxy Resin, J. Adhes. 83 (2007) 1–14.

[32] J. Zhou, J.P. Lucas, Hygrothermal effects of epoxy resin. Part II: variation of glass transition temperature, Polymer 40 (1999) 5513–5522.

[33] S. Xu, D.A. Dillard, Environmental aging effects on thermal and mechanical properties of electrically conductive adhesives, J. Adhes. 79 (2003) 699–723.

[34] W.K. Loh, A.D. Crocombe, M.M. Abdel Wahab, I.A. Ashcroft, Modelling anomalous moisture uptake, swelling and thermal characteristics of a rubber toughened epoxy adhesive, Int. J. Adhes. Adhes. 25 (2005)1–12.

[35] G. Viana, M. Costa, M. D. Banea, and L. F. M. da Silva, Behaviour of environmentally degraded epoxy adhesives as a function of temperature, J. Adhes. 93 (2017) 95–112.

[36] O. Moussa, A.P. Vassilopoulos, T. Keller, Effects of low-temperature curing on physical behavior of cold-curing epoxy adhesives in bridge construction, Int. J. Adhes. Adhes. 32 (2012) 15–22.

[37] L.C. Bank, T.R. Gentry, B.P. Thompson, J.S. Russell, A model specification for FRP composites for civil engineering structures, Constr. Build. Mater.17 (2003) 405–437.

[38] W. Nelson, Accelerated testing- Sustained models, test plans, and data analyses, Wiley, New York, 1990.

4 Fatigue performance

4.1 Overview

Structural adhesives have been used in bridge construction since the 1960s [1, 2], but mainly for strengthening or upgrading purposes [3, 4]. Only lately have such materials been used for bonding critical structural components in bridge applications, such as the bonding of a glass fiber-reinforced polymer (GFRP) bridge deck onto steel girders presented in [5]. In contrast to mechanical connections, adhesives used in these applications allow the easy and rapid joining of different materials, without disturbing their integrity by drilling holes for bolted connections for example.

Due to the often large bonding surfaces and in most cases outdoor applications, cold-curing adhesives are employed for such joints. Bond lines of this type have to sustain millions of fatigue cycles [6], which however are of low cyclic stress level [7, 8], during their operational lifetime. Normally, such joints in bridge construction are sealed to prevent exposure to humidity and UV radiation. Nevertheless, in view of the long service life of bridges, up to 100 years, damage to the sealing cannot be excluded, and the adhesive may thus be exposed to moisture or even stagnant water during several decades [9].

The fatigue performance (with or without the presence of environmental effects) of adhesives has usually been examined through the investigation of the performance of adhesively-bonded joints, probably due to the fact that in aerospace applications thin adhesive layers are used and their behavior is always investigated in relation to the adjacent adherends. The experimental set-up for joints is simpler than that for adhesives, reproducibility is better, and scatter is less. However, the analysis of the results in terms of fatigue resistance may be complicated by the complex stress state achieved in such testing configurations [10].

When moisture is present, adhesive behavior is decisive for overall joint performance, since adhesives are the joint components more susceptible to water effects. Aggressive environments can adversely influence the bond strength; water molecules diffuse into adhesively-bonded joints and degrade both the interface and the adhesive itself [11-12], thus influencing the structural performance of the joints, especially when exposed to water environments over long periods [13-15]. Water effects on the adhesive's mechanical properties are diffusion-dependent and can be correlated to the extent of plasticization, as discussed in [9, 13, 16-18].

In civil engineering, as well as in wind energy, cold-curing adhesives are often used and thicker adhesive layers than those used in the aerospace industry are employed. Important characteristics of the bond lines found in these applications are large adhesive thicknesses and volumes, and multiaxial (fatigue) loading conditions. For example, the thickness of the bond lines in 70-m wind turbine blades can attain 30 mm [19], while that of the bond line between the sandwich bridge deck and the steel girders of a 12-m-long vehicular bridge can reach 8 mm [5]. In such cases, the fatigue behavior of the bulk adhesives, excluding the effects of any adherends, needs to be investigated in order to obtain valuable date for an appropriate structural design.

There is a scarcity of experimental data concerning the fatigue performance of bulk structural adhesives related to any engineering domain. As mentioned above, numerous studies exist on the fatigue behavior of adhesively-bonded joints with or without temperature and water effects. Less information exists regarding the investigation of the fatigue behavior of bulk adhesives [20-24], while very little exists on the fatigue behavior of bulk structural adhesives subjected to wet conditions [25].

Previous results show that the fatigue behavior of bulk adhesive specimens and resin specimens can be modeled by typical S-N equations, such as the exponential Basquin relationship [24]. S-N curves of epoxy specimens exhibit similar slopes to those of S-N curves of unidirectional glass fiber epoxy composite laminates, indicating that the fatigue behavior of the matrix is decisive for the behavior of unidirectional composite laminates.

Stress strain loops can be monitored during fatigue life to provide information about material stiffness fluctuations (usually derived from the slope of the loops), as well as the hysteretic fatigue behavior of the examined material, linked to structural changes, the development of cyclic creep, and self-heating (hysteretic heating) during fatigue loading [20, 22, 26-28].

During fatigue cycles, the material temperature increases due to self-heating. When the frequency is sufficiently low, and other conditions are fulfilled, e.g., thin specimens, cooled testing space, low damage accumulation, etc., the energy resulting from self-heating is usually released to the environment, causing no damage to the material's structural integrity. However, under certain conditions, self-heating can have detrimental effects on the material's lifetime [25]. Epoxy resins are sensitive to hysteretic heating effects as from the early life, while polyester seems more resistant to such effects up until the late stages, close to failure [25].

Cyclic creep strain is progressively accumulated under stress-controlled cyclic loading of polymer composites [26, 29-30], as well as of epoxy polymers [22, 27]. This strain is of a viscoelastic nature, as can be confirmed by its complete recovery after load removal [27]. The amount of the accumulated strain depends on the applied cyclic mean stress [22]; the former is diminished under inversed fatigue loading, $R=\sigma_{min}/\sigma_{max}=-1$, while it becomes significant for tension-tension ($0<R<1$) and compression-compression ($1<R<\infty$) fatigue loadings [29].

An estimation of the material fatigue stiffness can be obtained by fitting the cyclic stress-strain data over each cycle [26]. This process allows the estimation of the secant stiffness variations during fatigue life. The fluctuations of this property over the material's lifetime have been intensively investigated for composite laminates, and adhesively-bonded joints, as a function of different parameters, such as the laminate stacking sequence, loading patterns, as well as a function of temperature and humidity. Nevertheless, there is no information on the fatigue stiffness variations, self-induced temperature and damage area development during the fatigue life of bulk epoxy adhesives for bridge applications, neither wet, nor subjected to water environments.

The above comprehensive literature review shows that, although there is a limited number of reports on the durability of resins and adhesives, there is no study investigating the fatigue performance of cold-curing structural adhesives for civil engineering applications, especially when they are subjected to wet environmental conditions.

This work investigates the fatigue behavior of a cold-curing epoxy structural adhesive, subjected to aggressive environments encountered in typical bridge applications. A wide range of cyclic loads is applied to the specimens in order to cover all regions of fatigue life, from the low-cycle fatigue to the operational lifetime of up to 10^7 cycles, within the serviceability load ranges of a bridge. Dry, saturated wet, and dried specimens are examined to investigate the water effects on their long-term behavior. The effects of water content on fatigue life, the fatigue damage accumulation, and the fatigue stiffness are described and thoroughly discussed. Specimens' failure surfaces are presented in order to relate observed failure mechanisms to water and fatigue loading effects.

4.2 Experimental procedures

4.2.1 Material and specimen preparation

A commercial cold-curing epoxy adhesive (Sikadur-330, supplied by SIKA Schweiz AG), commonly used in structural civil engineering applications, was selected for this study. Typical applications of this adhesive include the bonding of carbon fiber-reinforced polymer plates or the impregnation of fabrics to strengthen existing structures.

The adhesive was produced under laboratory conditions (T=21±3°C and RH=40±10%) with 4:1 resin to hardener mixing ratio, and then was poured into aluminum molds to produce specimens with the dimensions shown in Fig. 4.1, according to ASTM D638-14 [31]. To represent adhesive applications under on-site bridge conditions, no vacuum was applied to remove entrapped air.

The molds were left under laboratory conditions for seven days to allow the specimens to cure. All specimens were then post-cured at 60ºC for three days in a climatic chamber with a precision of 0.5ºC. After this post-curing process, the T_g, defined at the peak of the loss modulus vs temperature curve obtained by DMA, was estimated at approximately 75°C [9]. The mechanical properties of these specimens correspond to properties obtained for the same adhesive if naturally aged for nine months at ambient temperature on a bridge as shown in [32].

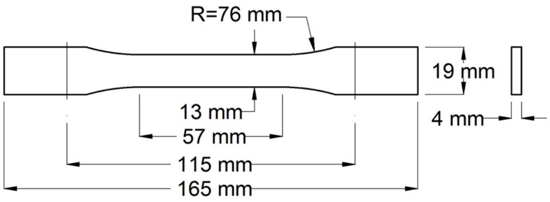

Fig. 4.1 *Bulk specimen geometry.*

4.2.2 Preconditioning

A first set of specimens (DRY) was used for the derivation of the reference quasi-static and fatigue data (designated as P21 in Tab. 2.1). Fatigue data for this set were collected after the aforementioned post-curing treatment over a period of nine months after the post-curing. During this time, the specimens were stored under laboratory conditions, and as previously proved [32] their quasi-static properties were not significantly affected by such time periods.

The second set (WET) comprises the wet specimens, those that, immediately after post-curing, were placed in a bath of demineralized water at 50ºC (designated as PD50 in Tab. 3.1). The temperature of the bath was 50°C to accelerate the diffusion process, but remained below the transition onset in storage modulus measured by DMA (at approximately 65°C) to avoid activating additional degradation mechanisms [9]. The specimens were left in the bath until saturation according to ASTM D570-98 [33]. In that case, saturation was achieved after approximately one year when the weight increase caused by the water uptake was 3.5-3.65%. According to [9], the saturated state reached after immersion at 50°C for a sufficient period of time, causes similar mechanical property deterioration to that occurring after approximately 100 years under ambient immersion conditions at 10°C. Such saturated conditions simulate very aggressive water exposures that can rarely occur in reality in the case of sealed adhesive joints; therefore, the obtained results should be considered as conservative material data. The wet specimens were subjected to fatigue loading immediately after being removed from the bath. During loading up to 2 million cycles, corresponding to a period of less than four days outside the bath, only limited weight loss, in the range of 0.3%, occurred [9].

The third set (DRIED) comprises the saturated specimens removed from the bath and left to dry under laboratory conditions for approximately eight months before loading. After this time, specimens had approached a plateau in the weight loss vs drying time curve and retained a percentage of water in their mass in the range of 0.75 to 0.90%. By drying the specimens, the cycles of meteorological seasons have been taken into consideration i.e. when wet periods, causing increase in the adhesive weight are followed by warm and dry seasons that enhance the evaporation of water and solvents, decreasing the adhesive's weight. The drying can also correspond to adhesive condition after repair of adhesive sealing damage.

The preconditioning program is summarized in Tab. 4.1, while the absorption/desorption curves for the adhesive are presented in Fig. 4.2.

***Tab. 4.1** Description of preconditioning program*

Specimen type	**Immersion medium**	**Temperature [°C]** **Humidity [%]** **Days of immersion**	**Drying [days] after immersion**
DRY	None	21±3 RH=40±10 0	0
WET	Demineralized water, pH≈7.0	50±1.5 Immersed 342-433	0
DRIED	Demineralized water, pH≈7.0	21±3 RH=40±10 437	231-288

The specimens were named according to the gravimetric condition and the loading they would undergo. For example, specimen DRY_F_01 is the first (01) dry specimen (DRY) subjected to fatigue loading (F). WET_ST_01 is the first (01) wet specimen (WET) subjected to quasi-static (ST) loads. DRIED_F_01 is the first (01) dried specimen (DRIED) subjected to fatigue (F) loading etc.

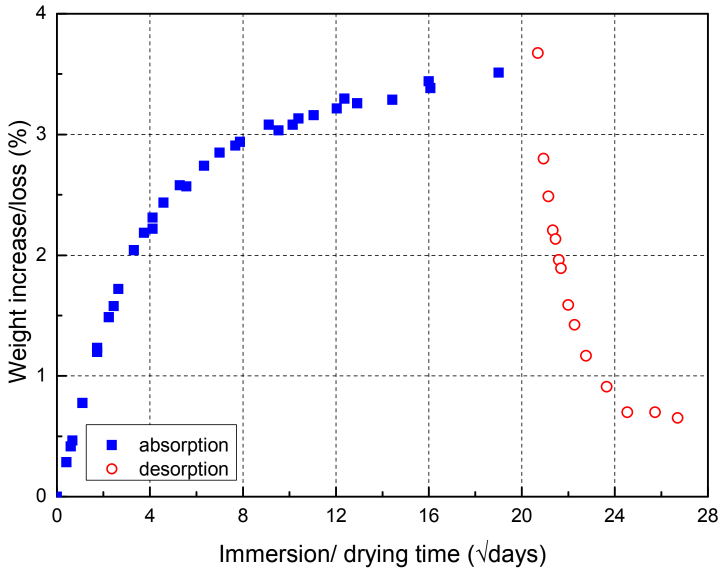

***Fig. 4.2** Absorption/desorption curves of specimens.*

4.2.3 Experimental set-up and instrumentation

Quasi-static experiments

Quasi-static tensile experiments were performed according to ASTM D638-14 [31], using an MTS Landmark servo-hydraulic loading machine, calibrated to a load capacity of 5 kN with ± 0.5% of applied force accuracy. All experiments were conducted under laboratory conditions (T=21±3°C and RH=40±10%). A constant displacement rate of 3.5 mm/min was applied to the dog-bone-shaped specimens. An MTS clip-on extensometer with a gage length of 25±0.05 mm and an accuracy of ±0.5% of the calculated strain was used for measuring the longitudinal strain. Nominal strength, i.e. based on the initial cross section of each specimen, was considered. The tensile elastic modulus was calculated as the slope of the stress-strain curve in the initial linear part, between 0.05% and 0.15% strain. At least three specimens were considered for the mechanical characterization in each condition. Specimens that presented tab failure were not taken into account in the analysis. Residual strength was also measured for those specimens that had not failed after the fatigue experiments.

Fatigue experiments

Fatigue experiments were conducted under laboratory conditions using the same servo-hydraulic MTS 810 testing rig. All experiments were carried out in accordance with ASTM D7791-12 [34] under load control, with a stress ratio, $R=\sigma_{min}/\sigma_{max}=0.1$, with sinusoidal waveform. This tension-tension loading profile was selected to avoid specimen buckling and be comparable to results from fatigue surveys concerning other materials, mainly tested with R=0.1. The frequency was kept at 5 Hz for all experiments except in some cases at low stress levels where 15 Hz was used to save time. The frequency was chosen based on preliminary investigations to reduce loading time without the risk of hysteretic heating that might affect results. Temperature was recorded for selected specimens with an infrared-thermal camera (thermoIMAGER TIM) with 0.1°C resolution to confirm that no temperature rise was caused by the frequency used. This camera calculates the surface temperature based on the emitted infrared energy of objects and provides thermographic images that describe temperature variations along the specimen surface.

Once the specimens were placed in the grips, the load was raised to the maximum of the cyclic load, and the fatigue experiment started. All specimens were loaded until ultimate failure, while a postmortem failure surface analysis was performed to monitor the failure surfaces. Four to five stress levels were chosen for each set of specimens to obtain fatigue results ranging in all regions between 10^2 and 10^7 fatigue cycles. Specimens that sustained more than $2\text{x}10^6$ fatigue cycles were considered as run-outs; in such cases, the fatigue experiment was interrupted, at random cycles, and a quasi-static loading was performed to estimate the remaining strength.

The machine's displacement, load, and number of cycles were recorded. Approximately twenty load and displacement measurements were recorded per cycle to estimate the strain fluctuations and hysteresis loops throughout the fatigue life of all the examined specimens. In parallel, a video extensometer (a camera Point Grey - Grasshopper3 with a resolution of 2.2 Mpixels and a Fujinon HF35SA-1 35mm F/1.4 lens) with a frequency of acquisition of 162 images/sec, within a gage length of 50 mm, was used for the acquisition of additional strain measurements. The cyclic strain derived by dividing the machine's displacement by the initial between-grip length of each specimen was then compared to the strain measured by the video extensometer. The comparison showed no significant difference between the machine's displacement and the video extensometer measurements.

Failure surface monitoring

Images of the fracture surfaces of the tensile specimens were captured using a digital handheld microscope Dino-Lite AD7013MZT. This microscope is equipped with a 5-megapixel sensor with an adjustable polarizer on an aluminum alloy body with an interchangeable nozzle feature. It provides up to 240x magnification and a resolution of 2592x1944 pixels.

4.3 Experimental results and discussion

4.3.1 Quasi-static behavior

Quasi-static experiments were performed on all types of specimens to monitor their response. All quasi-static and residual strength results are summarized in Tab. 4.2, while selected cases are presented in Fig. 4.3 for comparison. The dry specimens exhibited an almost linear elastic behavior up to failure. No particular differences in the stress-strain behaviors of the dry specimens aged for different time spans were noticed, this being in agreement with results shown in [32]. A representative curve is thus only shown in Fig. 4.3 for the dry specimens. The wet specimens showed significantly reduced strength and stiffness values, as well as much higher strain to failure, due to plasticization caused by the water uptake [9]. However, the plasticization effect seems to be reversible as can also be concluded by observation of the stress-strain behavior for the dried specimens shown in Fig. 4.3; strength and stiffness are almost completely recovered while the differences between the dried and the dry specimen responses can be attributed to the amount of water retained after the drying process.

***Tab. 4.2** Summary of quasi-static (ST) and residual (R) strength results*

Specimen ID	Storage time [months]	Strength [MPa]	E-modulus [MPa]	Strain to failure [%]	σ_{max} [MPa]	N	Reco-very [days]
DRY_R_01	3-6	44.47	4949	1.11	15.29	2031817	0
DRY_R_02	1-3	27.57	4553	0.64	9.60	3421240	0
DRY_R_03	1-3	33.49	4903	0.74	11.60	11967962	0
DRY_R_04	3-6	45.68	4764	1.17	11.41	4215118	17
WET_R_01	-	33.12	3132	2.01	9.55	2158242	0
DRIED_R_01	-	44.18	4541	1.83	11.82	2120000	0
DRY_ST_01	1-3	40.69	5106	0.94	-	-	-
DRY_ST_02	1-3	47.08	5142	1.14	-	-	-
DRY_ST_03	1-3	39.74	5121	0.93	-	-	-
DRY_ST_04	1-3	28.61	4601	0.67	-	-	-
DRY_ST_05	1-3	39.0	4759	0.95	-	-	-
DRY_ST_06	1-3	53.16	4695	1.53	-	-	-
DRY_ST_07	1-3	47.15	4875	1.23	-	-	-
DRY_ST_08	3-6	48.88	5441	1.19	-	-	-
DRY_ST_09	3-6	54.04	4913	1.52	-	-	-
DRY_ST_10	3-6	36.67	4722	0.87	-	-	-
DRY_ST_11	3-6	48.17	5061	1.24	-	-	-
DRY_ST_12	6-9	29.84	4895	0.77	-	-	-
DRY_ST_13	6-9	30.29	4386	0.76	-	-	-
DRY_ST_14	6-9	37.46	4520	1.07	-	-	-
DRY_ST_15	6-9	31.97	5310	0.76	-	-	-
WET_ ST_01	-	28.79	2905	3.09	-	-	-
WET_ ST_02	-	30.43	3015	4.64	-	-	-
WET_ ST_03	-	29.91	3056	3.94	-	-	-
DRIED_ ST_01	-	45.39	4207	1.95	-	-	-
DRIED_ ST_02	-	46.11	4145	2.28	-	-	-
DRIED_ ST_03	-	41.21	4518	1.27	-	-	-

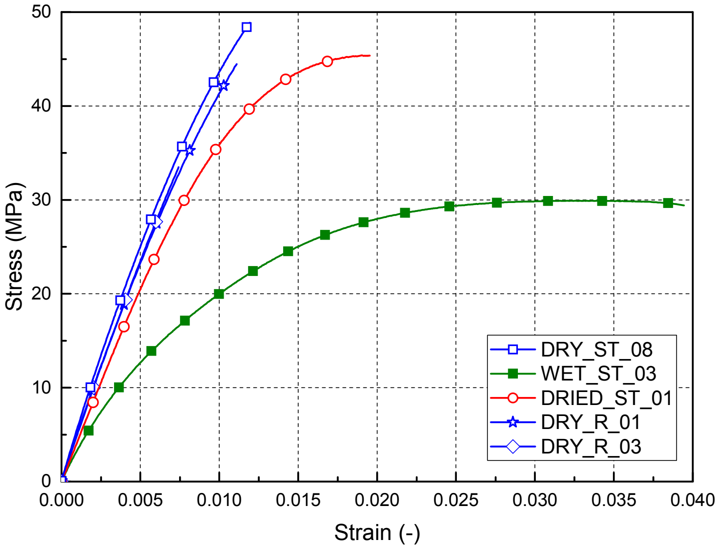

Fig. 4.3 *Typical quasi-static stress strain behavior of dry, wet, and dried specimens.*

4.3.2 Fatigue behavior

Fatigue life

The surface temperature variations were recorded during a preliminary phase to ensure that no significant temperature rises were caused by the fatigue loading. As shown in Fig. 4.4, where typical surface temperature measurements are presented, only a limited temperature increase, ~1°C, can be observed up to the lifetime of 1,077,000 cycles of a specimen loaded with σ_{max}=15.85 MPa at 15 Hz. As shown in Fig. 4.4(a), the temperature of the specimen is evenly distributed on its surface, while Fig. 4.4(b) shows that the temperature fluctuations are mainly due to environmental temperature variations and not internal heating caused by the fatigue loading itself.

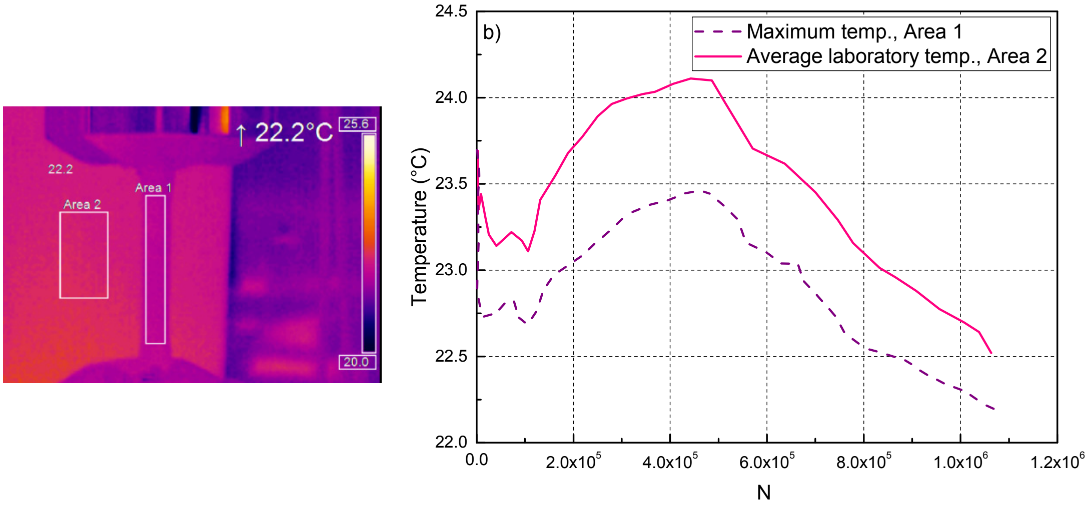

Fig. 4.4 *Thermal camera measurements (a) and temperature evolution with fatigue life (b).*

The experimental fatigue results are compared in Fig. 4.5 and are summarized in Tab. 4.3 for all the examined specimens. The stress-life fatigue behavior of the dry specimens is typical of that of adhesives and adhesively-bonded joints [11, 23]. Nevertheless, the dry specimens show a very brittle behavior, exhibiting higher scatter than what is usually exhibited by polymers and polymer composites, i.e. similar to or higher than a fraction of a log increment [35]. The water absorbed by the wet specimens disrupts the interchange bonds, causing material plasticization and therefore the wet specimens show inferior fatigue behavior to the dry ones. The material softening due to plasticization, however, reduces the stress concentrations allowing the wet specimens to exhibit more consistent behavior. The results show that the fatigue life of saturated specimens is affected more significantly in areas of low stresses.

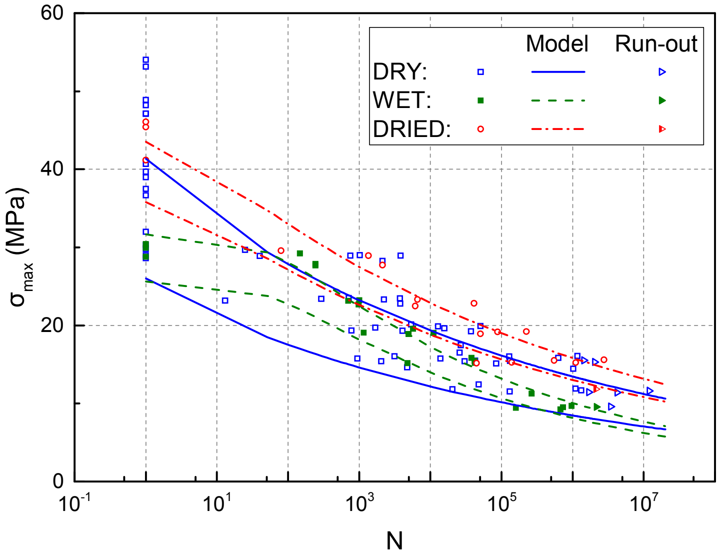

Fig. 4.5 *Fatigue behavior and modeling of all specimens.*

This behavior is reversible. Interchange bonds are reformed after water removal, and as described in [36] additional secondary crosslinking resulting from water-resin interaction can occur after long immersion periods, as was the case for the dried specimens. Nevertheless, the presence of a small amount of remaining water (ca. 1% in the case of the dried specimens), helps in retaining the stress concentrations reduction caused by the previous water uptake, and therefore the dried specimens also present consistent fatigue results. These arguments explain why the dried specimens not only show more consistent behavior, but also exhibit longer fatigue lives at all stress levels than the dry ones.

Residual strength was obtained for specimens that did not fail after the application of more than 2x10^{6} cycles. As shown in Fig. 4.3 and in detail for all specimens in Tab. 4.2, the residual strength, stiffness, and strain at failure of dry specimens after severe fatigue loading (run-outs between 2-12 million cycles) are, on average, only 7.5%, 2.3% and 11.8% respectively lower than the corresponding quasi-static values.

Different models exist for the simulation of the fatigue life of composite materials, adhesives and joints, see [37] for instance for a description of those most commonly used. In this case the wear-out method proposed by Sendeckyj [38, 39] was used in order to allow the implementation of the quasi-static, as well as the residual strength data obtained by run-out specimens, in the statistical analysis. The wear-out model assumes that the stronger specimen in fatigue should also be the stronger one under quasi-static loads and that therefore a relationship exists between the equivalent static strengths and cyclic stresses and number of cycles to failure.

***Tab. 4.3** Summary of experimental fatigue results for all specimens*

Dry			**Wet**			**Dried**		
Specimen ID	**σ_{max} [MPa]**	**N**	**Specimen ID**	**σ_{max} [MPa]**	**N**	**Specimen ID**	**σ_{max} [MPa]**	**N**
DRY_F_01	29.67	25	WET_F_01	27.86	243	DRIED_ F_01	29.56	80
DRY_F_02	28.96	1	WET_F_02	27.68	244	DRIED_ F_02	27.74	2132
DRY_F_03	28.90	40	WET_F_03	29.21	147	DRIED_ F_03	28.92	1349
DRY_F_04	23.47	3745	WET_F_04	22.67	981	DRIED_ F_04	23.31	6600
DRY_F_05	23.31	2220	WET _F_05	23.21	1001	DRIED_ F_05	22.48	6134
DRY_F_06	23.19	13	WET _F_06	23.14	699	DRIED_ F_06	22.82	41135
DRY_F_07	23.38	294	WET _F_07	18.88	4945	DRIED_ F_07	19.21	224485
DRY_F_08	22.79	3773	WET _F_08	19.02	11085	DRIED_ F_08	19.18	88086
DRY_F_09	19.33	4076	WET _F_09	19.57	5730	DRIED_ F_09	18.94	50678
DRY_F_10	19.25	37361	WET _F_10	19.06	1157	DRIED_ F_10	15.17	44696
DRY_F_11	19.35	780	WET _F_11	15.15	4791	DRIED_ F_11	15.27	139440
DRY_F_12	19.90	50659	WET _F_12	15.46	41831	DRIED_ F_12	15.50	550347
DRY_F_13	15.76	945	WET _F_13	15.20	42453	DRIED_ F_13	15.24	1104064
DRY_F_14	15.77	13937	WET _F_14	15.85	37816	DRIED_ F_14	15.60	2765615
DRY_F_15	15.14	84412	WET _F_15	11.27	264767			
DRY_F_16	16.01	128622	WET _F_16	9.43	160061			
DRY_F_17	14.64	4725	WET _F_17	9.25	674069			
DRY_F_18	14.45	1022327	WET _F_18	9.52	730606			
DRY_F_19	12.41	48102	WET _F_19	9.68	971300			
DRY_F_20	11.82	20398						
DRY_F_21	28.26	2130						
DRY_ F_22	28.92	3816						
DRY_ F_23	28.92	753						
DRY_ F_24	29.00	1019						
DRY_ F_25	23.49	711						
DRY_ F_26	17.46	26710						
DRY_ F_27	16.52	25799						
DRY_ F_28*	15.82	629530						
DRY_ F_29*	16.09	1163468						
DRY_ F_30	15.40	30239						
DRY_F_31	19.64	15784						
DRY_F_32	19.70	1689						
DRY_F_33	19.90	12816						
DRY_F_34	20.13	5357						
DRY_F_35	15.46	132377						
DRY_F_36	16.03	3121						
DRY_F_37	15.48	42603						
DRY_F_38	15.40	2042						
DRY_F_39	11.90	1101914						
DRY_F_40	11.55	130709						
DRY_F_41	11.68	1319389						

* Specimens tested at a frequency of 15 Hz

This relationship can be expressed mathematically by the following deterministic equation, Eq. 4.1:

$$\sigma_e = \sigma_{\max}\left[\left(\sigma_r/\sigma_{\max}\right)^{\frac{1}{S}} + \left(n-1\right)C\right]^S \tag{4.1}$$

where σ_e is the equivalent static strength, σ_{max} denotes the maximum cyclic stress level, σ_r, is the residual static strength, n is the number of loading cycles and S and C are the fatigue model parameters to be determined.

The initial values of *S* and *C* should be selected based on available fatigue data with *S* being the slope of the S-N curve and *C* a constant defining the shape of the S-N curve for a low-cycle fatigue region. By using the selected *S* and *C* values, all data is converted into equivalent static strengths, σ_e, using Eq. 4.1. A Weibull distribution is then fitted to the equivalent static strength data by using maximum likelihood estimators:

$$P(\sigma_e) = \exp\left[-\left(\frac{\sigma_e}{\beta}\right)^{\alpha_f}\right] \tag{4.2}$$

This process is performed iteratively for different values of *S* and *C*, until the maximum value of the shape parameter, α_f , is obtained [38].

Using the selected/estimated set of parameters *S*, *C* , β, α_f, the fatigue curve can be plotted for any desired reliability level *P(N)* (including 50%, which represents the mean value of the experimental data) by using the following equation:

$$\sigma_{\max} = \beta\left[-LnP(N)^{\frac{1}{\alpha_f}}\right]\left[(N-A)C\right]^{-S} \tag{4.3}$$

with *A=-(1-C)/C*.

As shown in Fig. 4.5 the behavior of all sets of specimens can be adequately simulated by power law S-N curve equations. The upper lines correspond to the median, while the lower lines correspond to 95% reliability curves. The *CCfatigue* software [40] was used for the S-N curve analysis and estimation of the parameters tabulated in Tab. 4.4, together with the average ultimate tensile stress (UTS) of each set.

Tab. 4.4. *Estimated statistical parameters for examined fatigue data and average static strengths*

Parameter	DRY	WET	DRIED
α_f	5.61	12.35	13.32
β [MPa]	44.15	32.61	44.73
S	0.079	0.117	0.080
C	1.495	0.018	0.310
UTS [MPa]	40.9±8.5	29.7±0.8	44.2±2.7

Irrespective of the gravimetric condition of the adhesive, typical slopes of the S-N curves, similar to those exhibited by other adhesives, [24, 28], composite laminates and adhesively-bonded joints [37] were estimated. The S-N curve corresponding to the wet specimens exhibits a higher slope than the S-N curve derived for both the other sets; the wet specimens are more susceptible to failure when loaded at low cyclic stresses for longer times. All derived S-N curves indicate that the cyclic stress that all material sets can sustain for ca. 10 million cycles (typical for a bridge lifetime) is above 5 MPa.

Stress-strain loops, stiffness degradation and dissipated energy

For materials with a purely elastic behavior, the elastic energy per loading cycle is equal to the total energy and no dissipation energy is measured. However, for the majority of materials, energy is dissipated at each load cycle, either due to additional structural changes, or due to hysteretic heating. Typical definitions regarding the hysteresis area and relevant measurements are shown in the schematic diagram in Fig. 4.6.

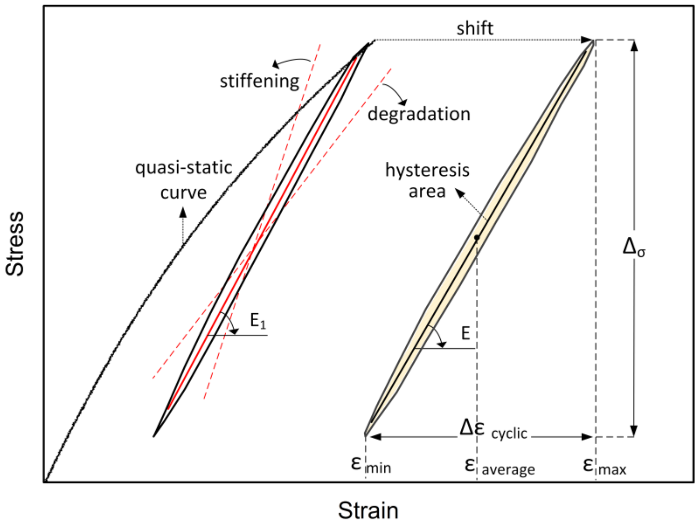

Fig. 4.6 *Schematic representation of stress-strain loops.*

During a load-controlled fatigue experiment, the hysteresis loops can shift during fatigue loading, indicating the presence of creep, and the evolution of the average strain per cycle can be monitored to describe the creep behavior [26, 41, 42]. Stiffness changes may also be recorded by estimating the slope of the loops showing stiffening, e.g. due to fiber alignment in FRP materials, or degradation of stiffness due to damage evolution. The internal energy dissipation can be investigated by monitoring the area of each stress-strain loop [42-44].

According to these definitions, the mechanical response of the examined material can be characterized by measuring several parameters of the hysteresis loops. The examined adhesives exhibited all the aforementioned behaviors.

Hysteresis loops were recorded for all examined specimens in order to obtain the cyclic strain fluctuations and calculate the dissipated energy, and the adhesive damping capacity as a function of stress level and gravimetric conditions. The fatigue stiffness for all specimens was calculated during the lifetime as the slope of each stress-strain loop by linear regression. Experimental results of selected specimens will be presented in the following due to space limitations. The discussion and conclusions however are representative of the exhibited behavior, since other specimens behaved in a consistent way.

Typical hysteresis loops for all three sets of specimens, under low and high cyclic stresses, are presented in Fig. 4.7-Fig. 4.8 respectively. For all specimen sets, the cyclic stress-cyclic strain loops show little hysteresis, and are linear, even in cases where the applied loads exceed the linear behavior of the material (see e.g. Fig. 4.8(b)). The wet specimens have larger hysteresis areas than the dry and dried ones; this difference becomes more apparent at higher stress levels as shown in Fig. 4.8 and even more so in Fig. 4.9 where it can also be observed that the hysteresis area does not seem to exhibit measureable increases with fatigue cycles. The creep strain, i.e., the average cyclic strain, $\varepsilon_{average}$, with cycles, increases for all specimens, but at different rates as shown in Fig. 4.10.

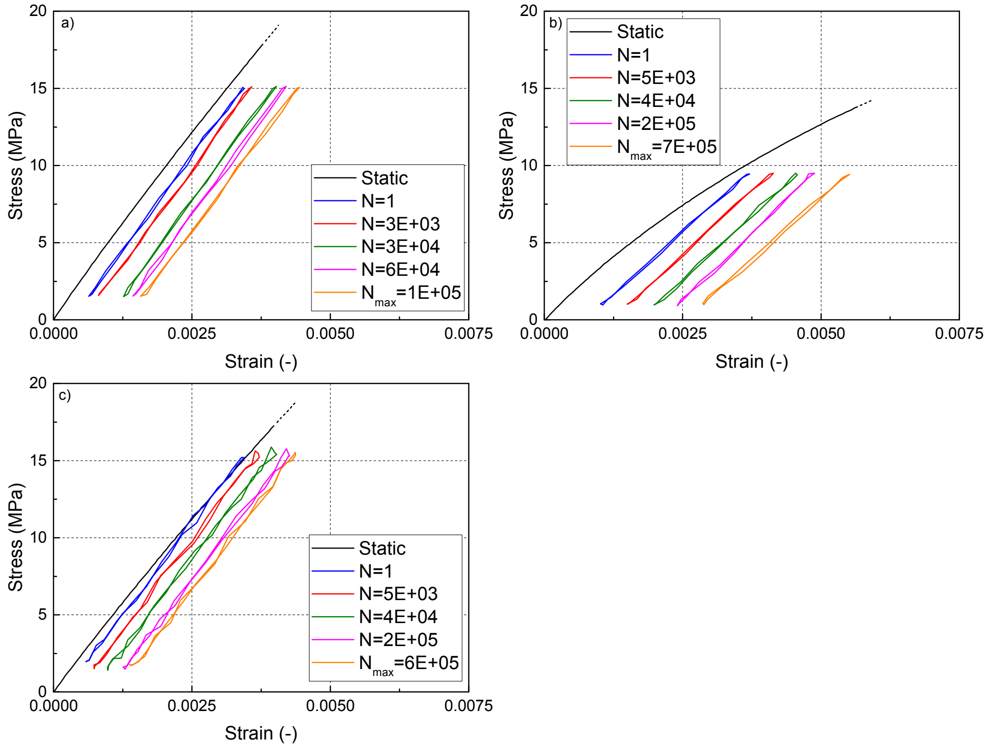

Fig. 4.7 *Hysteresis loops at low stress levels, (a) DRY_F_15, (b) WET_F_18, (c) DRIED_F_12.*

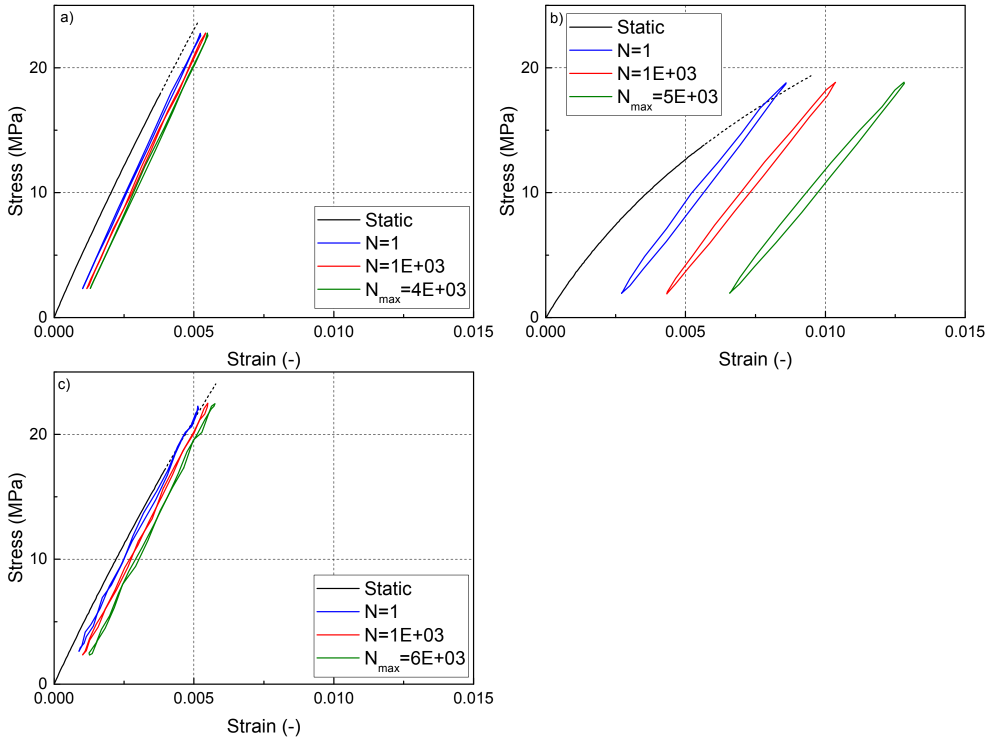

Fig. 4.8 *Hysteresis loops at high stress levels, (a) DRY_F_08, (b) WET_F_07, (c) DRIED_F_05.*

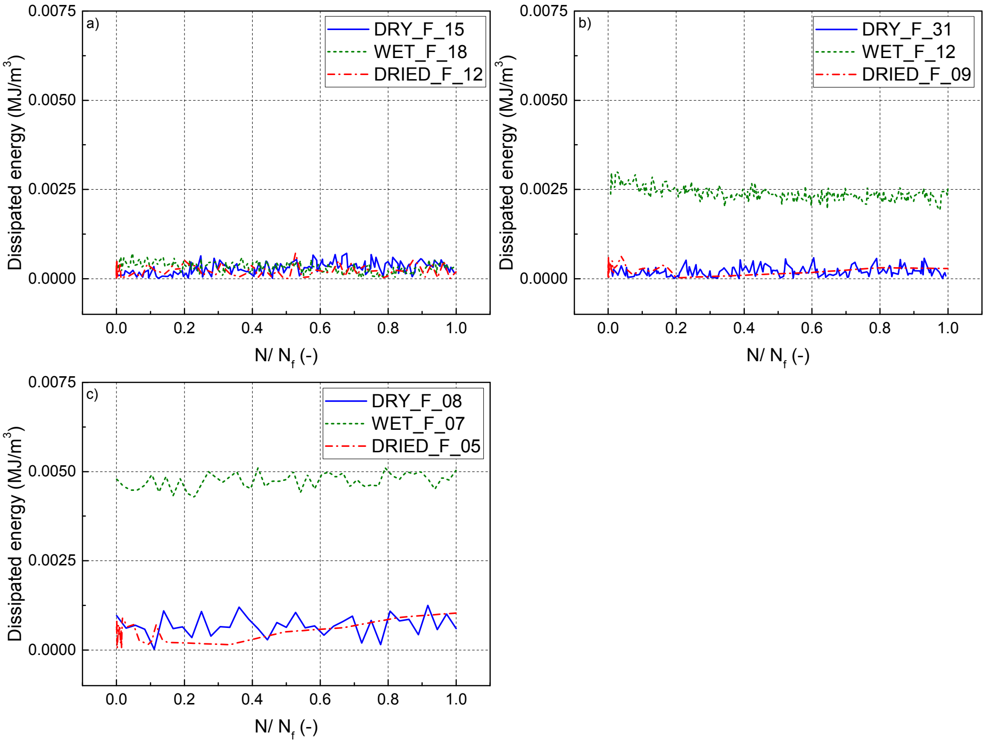

Fig. 4.9 *Dissipated energy during fatigue life for (a) low, (b) moderate, (c) high stress levels.*

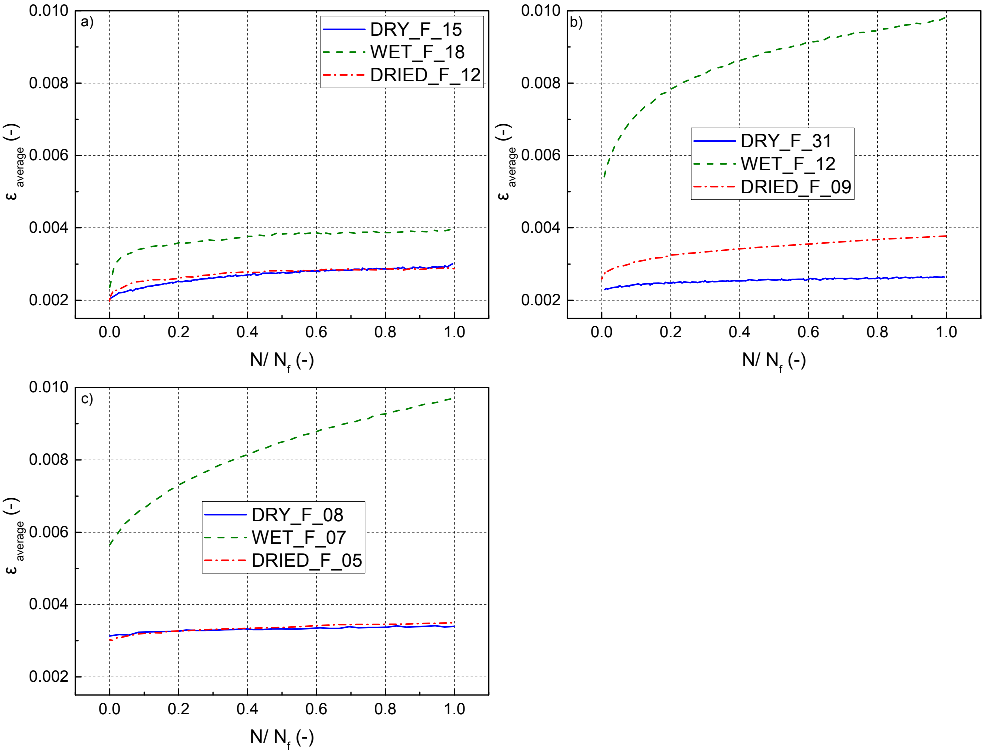

Fig. 4.10 *Creep strain during fatigue life for low (a), moderate (b) and high (c) stress levels.*

The wet specimens start creeping from higher strain values since they are less stiff than the dry and dried ones, in agreement with the quasi-static behavior presented in previous sections. The drifting of the hysteresis loops is more evident for the wet specimens, while it is minimal for the other two sets as shown in Fig. 4.10. The rate decreases with the increasing number of cycles and an asymptotic value of the creep strain is reached for the dry and dried specimens, while an increasing trend is observed at moderate and high stress levels for the wet specimens, as also reported in [27, 41].

However, this phenomenon is reversible; when the cyclic loads are removed, the specimen is able to attain the same tensile (residual) strength in the range of the quasi-static strength. The same behavior, proving the viscoelastic nature of the creep strain, has been noted in other publications [27, 41, 43] where it was observed that the creep strain, attributed to plasticization, could be fully recovered after load removal [27]. The plasticization phenomena are often related to an increase of the free volume of the polymer, and to the destruction of intramolecular hydrogen bonds, enhancing the molecular mobility and subsequently increasing the creep [9, 16].

The wet specimens show significantly higher strains at failure (calculated as the sum (ε_{min}+$\Delta_{\varepsilon,cyclic}$) of the last cycle) after the fatigue loading, see Fig. 4.11, in agreement with the comparison of strains to failure under quasi-static loading also shown in Tab. 4.2. The dried and dry specimens exhibit the same strain to failure for the same cyclic stress level, although their quasi-static values differ. However, the total strains reached at failure due to fatigue loading remain well below the strains to failure under quasi-static loading, and are dependent on the stress level. This fact does not allow the derivation of a common critical cyclic failure strain level for each set.

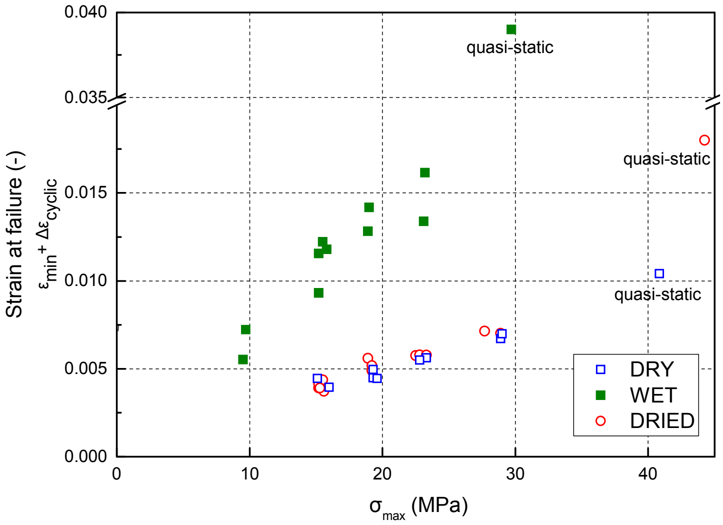

***Fig. 4.11** Strains at failure during fatigue life at different cyclic stress levels.*

The narrow range of the cyclic strain fluctuation reflects the limited fatigue stiffness fluctuations during fatigue life for all cases, as shown in Fig. 4.12, where normalized stiffness values regarding the stiffness of the first cycle are plotted against normalized fatigue life for low, moderate, and high cyclic stress levels. It can be observed in Fig. 4.12 that only the stiffness of the wet specimens is sensitive to the applied load level.

A slight increase in stiffness, and a corresponding decrease in cyclic strains, was observed in some of the examined cases, especially under low and moderate cyclic stresses for the wet specimens, while stiffness degradation is observed at higher cyclic stress levels for the wet specimens. This is a peculiar observation, showing a material stiffening during loading. Nevertheless, this has also been reported by other researchers for different materials [26, 45], and attributed either to experimental artifacts that can cause strain hardening [26] or micromechanical phenomena, e.g., wear that can cause flaw blunting and ameliorate the stress concentrations [45]. For fiber-reinforced composites, an initial decrease of the hysteresis area and increase of the fatigue stiffness [41, 44] can be attributed to fiber reorientation during loading, especially at low stress ratios. Nevertheless, no such observation regarding the fatigue behavior of cold-curing structural adhesives has been reported in the literature concerning structural adhesives.

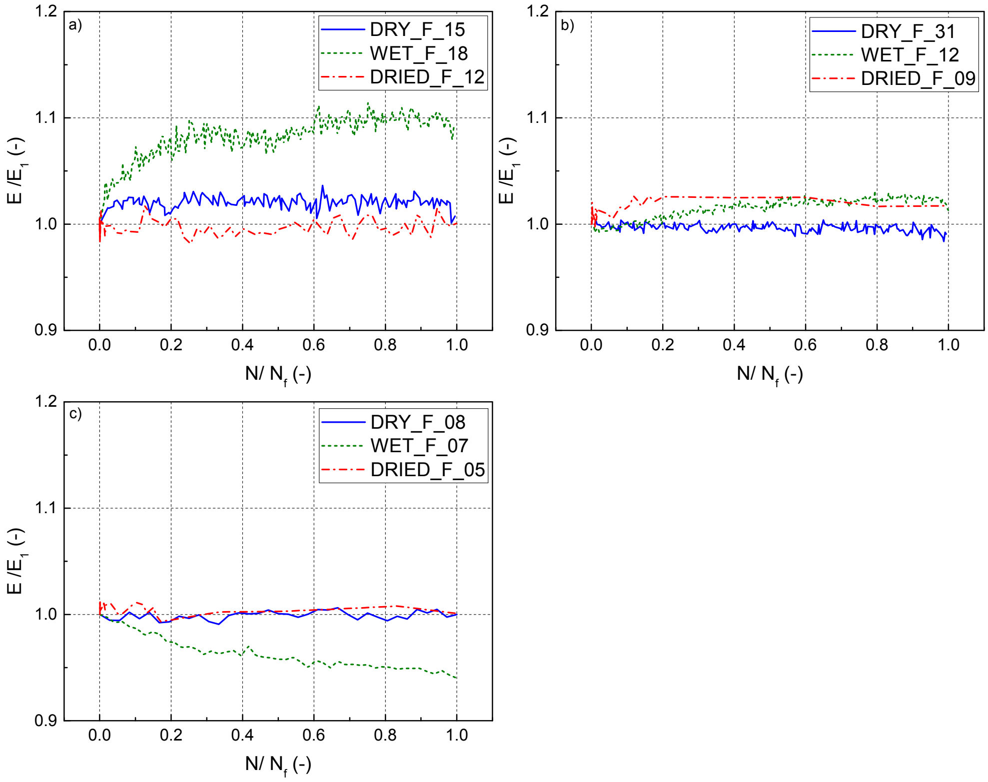

Fig. 4.12 *Stiffness fluctuation during fatigue life (a) low, (b) moderate and (c) high cyclic stress levels.*

Failure surfaces

Fracture surfaces of all sets of specimens show a brittle failure initiated by some kind of flaw near the edge of or inside the materials, in agreement with those reported for the failure surfaces for the same material examined under quasi-static loading [9, 32]. Typical fractographic photos are presented in Fig. 4.13-Fig. 4.14 for low-moderate and high cyclic stress levels respectively.

For all examined cases, two regions can be recognized; one shown by a light grey or white color and the other by a darker color but with some light scattering at high stresses due to the material’s layered texture. The light or white color area is the damage origin region, and is located close to flaws in the material and at the edges, at potential locations of stress concentrations [46]. Striations [25] were not observed in this area, but this can be due to the limited magnification capacity of the microscope used. The darker area corresponds to the unstable crack propagation area, the one that develops rapidly when the specimen, due to fatigue damage, no longer possesses an adequate cross section area to sustain the applied loads and breaks.

A difference between the surface of specimens loaded under low-moderate and those loaded under high cyclic stresses can be observed, with the surface of the latter being rougher independent of the water content, indicating an increase of the crack propagation zone as explained in [47]. More defects can be observed on the failure surfaces of the wet specimens (Fig. 4.13(b), Fig. 4.14(b)), showing that the softening by water may have permitted the stretching of the material and caused the enlargement of existing voids before failure. However, more concrete arguments are necessary to support these observations.

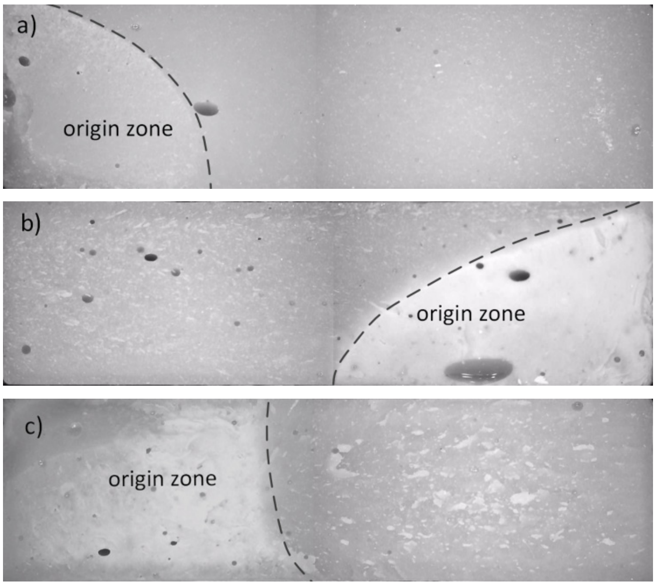

Fig. 4.13 *Typical failure surfaces (13x4 mm^2) at low-moderate cyclic stresses, (a) DRY_F_41, (b) WET_F_13, (c) DRIED_F_10*

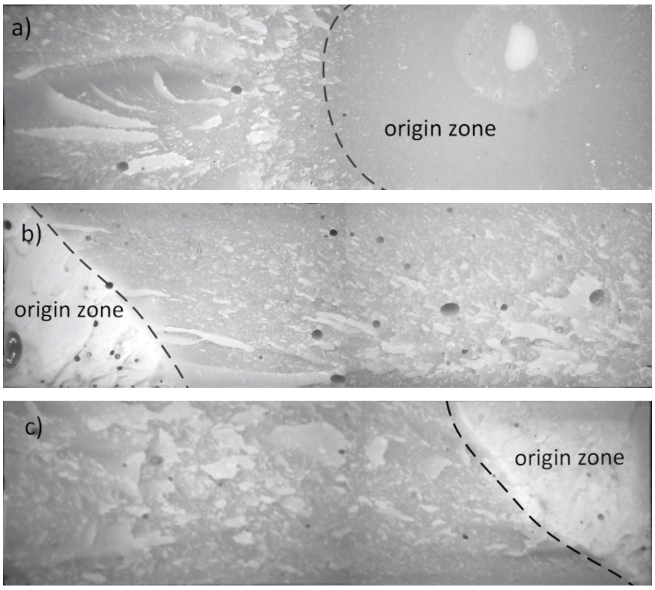

Fig. 4.14 *Typical failure surfaces (13x4 mm^2) at high cyclic stresses, (a) DRY_F_23, (b) WET_F_05, (c) DRIED_F_06*

4.4 Conclusions

An experimental program designed to study the effects of aging and wet environment on the fatigue behavior of epoxy resins used in bridge applications has been conducted over a period of two years and the results have been presented in this paper. The experimental matrix contains data from bulk adhesive specimens, fabricated and cured in the laboratory, as well as from specimens that have undergone a certain amount of aging, including immersion in demineralized water for up to over a year. The specimens of the latter set are representative of 100-year-immersed specimens at the lower temperature of 10°C, commonly encountered in bridge environments.

1) The experimental campaign showed that the examined structural adhesive, even if degraded due to water uptake, is capable of attaining fatigue lives of between 2 and 10 million cycles without failure at maximum stress levels of higher than 5 MPa (at R=0.1).

2) The examined sets of specimens showed a fatigue behavior similar to that exhibited by fiber-reinforced composite materials with smooth S-N curves with slopes (1/*S*) around 10-12.5. The steeper S-N curve corresponds to the wet specimens, while both the curves derived from the fatigue results of the dry and dried specimens had the same slope. The wet specimens, although they seemed to be more susceptible to low stresses than the dry and dried ones, exhibited more consistent fatigue behavior, with considerably less scatter estimated for their fatigue results.
3) The plasticization and consequently the softening due to water uptake are responsible for the main differences between the behavior of the wet and the other two specimen sets. The dried specimens exhibited a better fatigue life compared to the dry ones, being at the same time more consistent, showing a positive effect of the remaining water (<1%) on the fatigue performance of the investigated adhesive. Nevertheless, more sound experimental evidence is necessary for the investigation of this observation.
4) The plasticization also seems to affect the material structure; those specimens containing more water showed bigger defects and voids in the volume at both high and low cyclic stress levels. A clear difference between the failure surfaces at low and high cyclic stresses can be observed for all sets, with those under low stresses being smoother.
5) Analysis of the hysteresis loops revealed that the wet specimens deformed more due to creep, achieving a strain to failure after fatigue almost 100% higher than the other two sets of specimens. Nevertheless, for all specimens, the (fatigue) strains at failure are well below those attained under quasi-static loading and are dependent on the applied load level. No critical fatigue failure strain could be derived from this investigation.
6) The results presented in this paper provide sufficient information for the feasibility of using such adhesives for long-term engineering structures. Additional information regarding the effect of different loading conditions, such as under different stress ratios, the effect of remaining water content after drying, and different environments simulating real bridge applications more precisely would enhance the understanding of the behavior of this type of structural adhesive.

4.5 References

[1] F. Hugenschmidt, Epoxy adhesives in precast prestressed concrete construction, PCI J. 19 (1974) 112–124.

[2] F.A. Sims, Applications of resins in bridge and structural engineering, Int. J. Cem. Compos. Lightweight Concrete 7 (1985) 225–232.

[3] T. Keller, Strengthening of concrete bridges with carbon cables and strips, Proceedings of the 6th International Symposium on FRP Reinforcement for Concrete Structures (FRPRCS-6), Singapore, 2003.

[4] B. Täljsten, A. Hejll, G. James, Carbon Fiber-Reinforced Polymer Strengthening and Monitoring of the Gröndals Bridge in Sweden, J. Compos. Constr. 11 (2007) 227–235.

[5] T. Keller, J. Rothe, J. de Castro, M. Osei-Antwi, GFRP-Balsa Sandwich Bridge Deck: Concept, Design, and Experimental Validation, J. Compos. Constr. 18 (2013) 04013043 (1-10).

[6] EN 1991-2 Eurocode 1. Actions on structures - Part 2: Traffic loads on bridges

[7] O. Moussa, Thermophysical and Thermomechanical Behavior of Cold-Curing Structural Adhesives in Bridge Construction PhD #5244, EPFL, 2011

[8] A. R. Hutchinson, Durability of structural adhesive joints, PhD thesis, University of Dundee, 1986

[9] M. Savvilotidou, A. P. Vassilopoulos, M. Frigione, T. Keller, Development of physical and mechanical properties of a cold-curing structural adhesive in a wet bridge environment, Constr. Build. Mater. 144 (2017) 115–124.

[10] R. D. Adams, J. Coppendale, The Stress-Strain Behaviour of Axially-Loaded Butt Joints, J. Adhes. 10 (1979) 49–62.

[11] G. Doyle, R. A. Pethrick, Environmental effects on the ageing of epoxy adhesive joints, Int. J. Adhes. Adhes. 29 (2009) 77–90.

[12] R. A. Dickie, L. P. Haack, J. K. Jethwa, A. J. Kinloch, J. F. Watts, The fatigue and durability behavior of automotive adhesives, Part II: Failure mechanisms, J. Adhes. 66 (1998) 1–37.

[13] K. B. Katnam, A. D. Crocombe, H. Sugiman, H. Khoramishad, I. A. Ashcroft, Static and fatigue failures of adhesively bonded laminate joints in moist environments, Int. J. Damage Mech. 20 (2011) 1217–1242.

[14] A.J. Kinloch, Adhesion and Adhesives, Chapman and Hall, London, 1987.

[15] F. Rodriguez, Principle of Polymer Systems, forth ed., Taylor & Francis, Washington DC, 1996.

[16] A. Chateauminois, B. Chabert, J. P. Soulier, L. Vincent, Hygrothermal ageing effects on the static fatigue of glass/epoxy composites, Composites, 24 (1993) 547–555.

[17] B. Dewimille, A.R. Bunsell, The modelling of hydrothermal ageing in glass fibre reinforced epoxy composites, J. Phys D Appl. Phys. 15 (1982) 2079–2091.

[18] C.C. Chamis, J.H. Sinclair, Durability/life of fiber composites in hygrothermomechanical environments, Composite Materials: Testing and Design, STP284927S, I. Daniel, Ed., ASTM International, West Conshohocken, PA (1982) 498–512.

[19] D. Zarouchas, R. Nijssen, Mechanical behaviour of thick structural adhesives in wind turbine blades under multi-axial loading, J. Adhes. Sci. Technol. 30 (2016) 1413–1429.

[20] G. Tao, Z. Xia, Biaxial fatigue behavior of an epoxy polymer with mean stress effect, Int. J. Fatigue 31 (2009) 678–685.

[21] G. Tao, Z. Xia, Fatigue behavior of an epoxy polymer subjected to cyclic shear loading, Mater. Sci. Eng. A, 486 (2008) 38–44.

[22] G. Tao, Z. Xia, Ratcheting behavior of an epoxy polymer and its effect on fatigue life, Polym. Test. 26 (2007) 451–460.

[23] N. Su, R.I. Mackie, W.J. Harvey, The Effects of Ageing and Environment on the Fatigue Life of Adhesive Joints, Int. J. Adhes. Adhes.12 (1992) 85–93.

[24] E. Stammes, R. P. L. Nijssen, T. Westphal, Static and fatigue tests on resin for wind turbine rotor blades, 14th ECCM, Budapest, 2014.

[25] L. J. Broutman S. K. Gaggar 1972, Fatigue behavior of epoxy and polyester resins, Int. J. Polym. Mater. Po. 1 (1972) 295–316.

[26] M.C. Sobieraj, J.E. Murphy, J.G. Brinkman, S.M. Kurtz, C.M. Rimnac, Notched fatigue behavior of PEEK, Biomaterials, 31 (2010) 9156–9162.

[27] X. Shen, Z. Xia, F. Ellyin, Cyclic deformation behavior of an epoxy polymer. Part I: Experimental investigation, Polym. Eng. Sci. 44 (2004) 2240–2246.

[28] G-T. Wang, H-Y Liu, N. Saintier, Y-W. Mai, Cyclic fatigue of polymer nanocomposites, Eng. Fail. Anal. 16 (2009) 2635–2645.

[29] D. Samborsky, J. F. Mandell, D. A. Miller, Creep/Fatigue behavior of resin infused biaxial glass fabric laminates, AIAA SDM Wind energy Session, 2013.

[30] A. D. Drozdov, Cyclic viscoelastoplasticity and low-cycle fatigue of polymer composites, Int. J. Solids Struct. 48 (2011) 2026–2040.

[31] ASTM D638-14, Standard test Method for tensile properties of plastics, ASTM International, West Conshohocken, PA, 2014.

[32] M. Savvilotidou, A. P. Vassilopoulos, M. Frigione, T. Keller, Effects of aging in dry environment on physical and mechanical properties of a cold-curing structural epoxy adhesive for bridge construction, Constr. Build. Mater. 140 (2017) 552–561.

[33] ASTM D570-98(2010)e1, Standard Test Method for Water Absorption of Plastics, ASTM International, West Conshohocken, PA, 2010.

[34] ASTM D7791-12, Standard Test Method for Uniaxial Fatigue Properties of Plastics, ASTM International, West Conshohocken, PA, 2010.

[35] K. H. Boller, Fatigue fundamentals for composite materials, Composite materials: Testing and Design, STP49819S, S. Yurenka, Ed., ASTM International, West Conshohocken, PA (1969) 217–235.

[36] J. Zhou, J. P. Lucas, Hygrothermal effects of epoxy resin. Part II: Varaition of glass transition temperature, Polymer 40 (1999) 5513–5522.

[37] R. Sarfaraz, A. P. Vassilopoulos, T. Keller., Experimental investigation of the fatigue behavior of adhesively-bonded pultruded GFRP joints under different load ratios, Int. J. Fatigue, 33 (2011) 1451–1460.

[38] R. Sarfaraz, A. P. Vassilopoulos, T. Keller., Modeling the constant amplitude fatigue behavior of adhesively bonded pultruded GFRP joints, J. Adhes. Sci. Technol. 27 (2013) 855–878.

[39] G. Sendeckyj, Fitting Models to Composite Materials Fatigue Data, Test Methods and Design Allowables for Fibrous Composites, STP29314S, C. Chamis, Ed., ASTM International, West Conshohocken, PA (1981) 245–260.

[40] A. P. Vassilopoulos, R. Sarfaraz, B.D. Manshadi, T. Keller., A computational tool for the life prediction of GFRP laminates under irregular complex stress states: Influence of the fatigue failure criterion, Comp. Mater. Sci. 49 (2010) 483–491.

[41] A. Benaarbia, A. Chrysochoos, G. Robert, Thermomechanical behavior of PA6.6 composites subjected to low cycle fatigue, Compos. Part B Eng. 76 (2015) 52–64.

[42] S. Fouvry, Ph. Kapsa, L. Vincent, Analysis of sliding behavior for fretting loadings: Determination of transition criteria, Wear 185 (1995) 35–46.

[43] C. Blanchard, A. Chateauminois, L. Vincent, A new testing methodology for assessment of fatigue properties of structural adhesives, Int. J. Adhes. Adhes. 16 (1996) 289–299.

[44] J. Petermann, K. Schulte, The effects of creep and fatigue stress ratio on the long-term behaviour of angle-ply CFRP, Compos. Struct. 57 (2002) 205–210.

[45] M. R. Kharrazi, S. Sarkani, Frequency-dependent fatigue damage accumulation in fiber-reinforced plastics, J. Compos. Mater. 35 (2001) 1924–1953.

[46] M. Hayes, D. Edwards, A. Shah, Fractography in Failure Analysis of Polymers, Elsevier, Oxford, 2015.

[47] J. R. M. d'Almeida, G. W. Menezes, S. N. de Monteiro, Ageing of the DGEBA/TETA epoxy system with off-stoichiometric compositions, Mater. Res. 6 (2003) 415–420.

5 Adhesive applications in bridge construction

Based on the results of the scientific studies performed in Chapters 2-4, further investigations with regard to potential epoxy adhesive applications in bridge construction were carried out and conclusions are drawn in the following. It should be remembered that the results of this project concern only the adhesive, and not the interfaces with the adherend materials of adhesively-bonded joints, and therefore the interfaces may behave differently.

In Section 5.1, two typical joint cases were selected and investigated with regard to the effects of moisture ingress into the adhesive layer on the mechanical properties of the latter. The first case concerns the adhesive bonding of a concrete bridge deck onto the top flange of a steel I-girder while the second concerns CFRP strips bonded onto the bottom flange of the same steel I-girder in order to strengthen the latter. Moisture diffusion into the adhesive layers for a period of up to 100 years was numerically modeled and, based on the results obtained in Chapter 3, corresponding degradations of the mechanical properties were derived.

Section 5.2 provides sets of resistance factors applicable for adhesives, selected from current recommendations, and comparisons were made to the results obtained in Chapter 3 regarding environmental conditions. Furthermore, the fatigue behavior of the adhesive studied in Chapter 4 was compared to that of CFRP and steel materials.

Section 5.3 finally suggests which preconditioning should be selected for adhesive material tests in order to cover the time-dependent variations obtained in Chapter 2. The different developments of mechanical properties and the glass transition temperature were further addressed.

5.1 Effect of water ingress on adhesive performance

The diffusion of moisture or water into a) fiber-reinforced polymer (FRP) composite laminates [1-5], b) the adhesive layer of bonded FRP composite or hybrid joints [1-3, 5] and c) the entire joint (CFRP-to-CFRP [2], CFRP-to-concrete [6]) has been successfully predicted using finite element (FE) models. FE mass-diffusion analyses can simulate the moisture concentration distribution inside the large surfaces of the adhesive layers, such as those in the case of bridge joints. Full-scale experimental campaigns to investigate such cases are complicated, time-consuming and costly and moreover, only the average moisture uptake can be obtained from such investigations.

In some of the aforementioned works, the studies concerned the FRP laminates and adhesives composing FRP composite bridges [1, 3, 5]. A segment of a GFRP deck bonded to a steel girder was simulated in [3] and the moisture concentration distribution was predicted for the whole service life. The interface between the steel plate and the polyurethane adhesive layer of dimensions 600x250x6-mm was considered to be impermeable, but the diffusion from the adhesive edges was permitted. After a 26-year immersion in water, the polyurethane adhesive layer was completely saturated. At the point equal to a time period of 100 years, moisture had diffused into almost the whole FRP deck section, without full saturation being attained however. No link to mechanical property degradation was established.

The influence of the adherend permeability on the moisture concentration distribution in the epoxy adhesive layer of adhesively-bonded CFRP joints was numerically studied in [1, 2]. The diffusion coefficient of the epoxy-CFRP adherend varied according to the number of plies in the matrix [2], but remained low and delayed the diffusion through the epoxy adhesive layer [1]. Polyester-based GFRP laminates, however, presented a diffusivity four orders of magnitude higher than that of epoxy-based CFRPs.

From these studies it can be concluded that diffusion through epoxy materials is significantly smaller than through other polymers such as polyester or polyurethanes.

In this section, numerical models were developed to predict the moisture uptake in the epoxy layer of two typical joints in bridges that are adhesively bonded. The first model simulates the water ingress in a relatively thick adhesive layer between a bridge deck and a steel girder, while the second model simulates the moisture diffusion process in the thin adhesive layer through an externally bonded CFRP strip used to reinforce a steel girder. The diffusion-controlling parameter is the diffusion coefficient of the epoxy adhesive, which was obtained in Chapter 3 from the experimental results on the Sikadur 330 adhesive. The FE analysis software Abaqus 6.14 was used for the mass-diffusion analyses.

Finally, the distribution of the material properties, i.e. the tensile stiffness and strength, corresponding to the predicted moisture distribution in the adhesive layer, was estimated based on the relationship between property development and water uptake derived from the experimental investigations in Chapter 3.

5.1.1 Introduction to the FE analysis

In order to validate the subsequent numerical analyses, a simple FE model was developed to simulate the immersion conditions of the adhesive specimens Sikadur 330 with dimensions 35x10x3-mm, see Fig. 5.1, as used in Chapter 3 to perform weight measurements and derive the adhesive's diffusion coefficients at different immersion temperatures (see Chapter 3, Fig. 3.2 and Tab. 3.3).

As shown in Fig. 5.1, the weighed specimen was longer in the *x*- and *y*- directions than in the z-direction and thus the diffusion can be considered as one-dimensional (1D) in the z-direction. Accordingly, in the FE analysis a representative bar along the z-direction of the bulk adhesive with dimensions 0.15x0.15x3-mm was modeled, see Fig. 5.1.

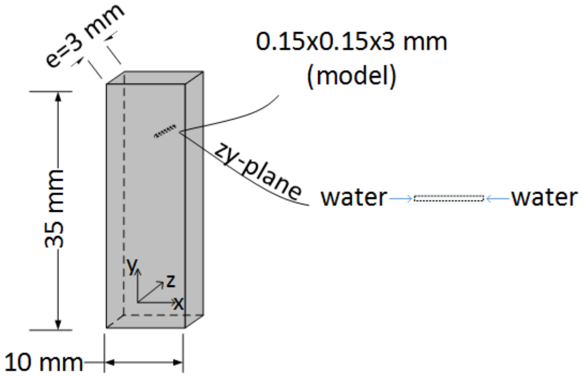

Fig. 5.1 *Geometry of gravimetric specimen for FE 1D diffusion validation.*

Water molecules move into the polymer because of a concentration gradient. Any diffusion process that is governed by such concentration gradients can be expressed by Fick's laws of diffusion [7]. Accordingly, Fickian modeling is proposed for FRPs exposed to moisture in ASTM D5229 [8].

For the FE model geometry in Fig. 5.1, Fick's second law can predict how diffusion causes the moisture concentration (c) to change with time (t) in the z-direction with the following equation [7]:

$$\frac{\partial c}{\partial t} = D_z \frac{\partial^2 c}{\partial z^2} \tag{5.1}$$

where D_z is the diffusion coefficient in the z-direction, normal to the specimen surface, derived by the weight measurements at different immersion temperatures in Chapter 3 (see Tab. 3.3).

As both specimen surfaces in Fig. 5.1 are simultaneously exposed to constant maximum moisture concentration, c_∞ (full immersion conditions), the boundary conditions can be described as:

$$t \geq 0: \quad z = 0,\ c = c_\infty \quad and \quad z = e,\ c = c_\infty \tag{5.2}$$

where *e* is the representative bar length.

The analytical solution of Eq. 5.1 is used by the FE software for the calculation of the moisture concentration, *c*, as a function of time, *t*, and distance, *z*, by [7, 9]:

$$\frac{c_{t,z}}{c_\infty} = 1 - \frac{4}{\pi}\sum_{n=0}^{\infty}\frac{(-1)^n}{2n+1}\exp\left[-\frac{D_z\ (2n+1)^2\pi^2 t}{e^2}\right]\cdot\cos\frac{(2n+1)\pi z}{e} \tag{5.3}$$

Integration of Eq. 5.3 with respect to the spatial variable *z* results in the analytical expression for the calculation of the average moisture concentration, corresponding to the amount of absorbed water in the specimen at time *t*:

$$\Delta \mathrm{w}_t = \Delta \mathrm{w}_\infty \left\{1 - \frac{8}{\pi^2}\sum_{n=0}^{\infty}\frac{1}{(2n+1)^2}\exp[-\frac{D_z\ (2n+1)^2\pi^2 t}{e^2}]\right\} \tag{5.4}$$

where Δw_∞ is the maximum amount of water absorbed during the diffusion process. When both *c* and Δw are expressed as a percentage of the dry specimen mass, then $c_\infty(\%)=\Delta w_\infty(\%)$. The average moisture concentration was experimentally obtained by the weight measurements of specimens using Eq. 3.1 in Chapter 3, and is compared in the following with the simulated average moisture concentration to verify the modeling procedure.

5.1.2 Verification of the FE modeling procedure

The experimentally derived diffusion coefficients for two immersion temperatures, 13°C and 30°C, studied in Chapter 3, have been introduced into the FE model in Fig. 5.1. Their values were $D_{z,13°C}$ = 0.005 mm^2/day and $D_{z,30°C}$ = 0.014 mm^2/day (see Chapter 3, Tab. 3.3). The exposed yx-planes shown in Fig. 5.1 were set to reach full saturation instantaneously at the boundary conditions, i.e. the maximum moisture concentration. As moisture concentration changed with time (in the z-direction), a transient mass-diffusion analysis was performed. A 3D mesh with only one element in the *yx*-plane was used. The heat transfer element DC3D8, which is an 8-node linear brick element, was chosen from the Abaqus library.

Because the rate of change of concentration varies widely during the transient analysis, the integration time increments were set to be automatically controlled between a minimum and maximum value. This enables time increments to change in order to maintain accuracy in the time integration.

A parametric study was also performed to investigate the effects of several model parameters, namely, a) the user-defined maximum concentration change allowed at any node during an increment (DCMAX), b) the number of time steps, and c) the mesh density. The study showed a certain sensitivity of the model only to the mesh density; a finer mesh with 60 elements along the 3-mm bar provided more accurate results. The use of one time step, and thus input of a single minimum-maximum range for the time increment during the whole analysis, was adequate. Decrease of the DCMAX from 0.1 to 0.001 increased the frequency of the time increments but not the accuracy of the model.

The transient diffusion process was modeled for two years (730 days) to represent the experimental duration and reach saturation states at both immersion temperatures. The predicted contour plots of the normalized moisture concentration (divided by the maximum at each temperature, designated as NNC11 in Abaqus) at the integration points in the modeled epoxy bar are shown in Fig. 5.2 for the two temperatures after 213 days of exposure.

As expected, the higher temperature accelerated the diffusion process, according to the Arrhenius principle as explained in detail in Chapter 3. Consequently, after 213 days at 13°C only the surfaces closer to the boundary had approached saturation (c>0.9), while the in-between-surfaces were 60% saturated (see Fig. 5.2a). At 30°C, however, the whole epoxy bar was more than 90% saturated at 213 days (see Fig. 5.2b).

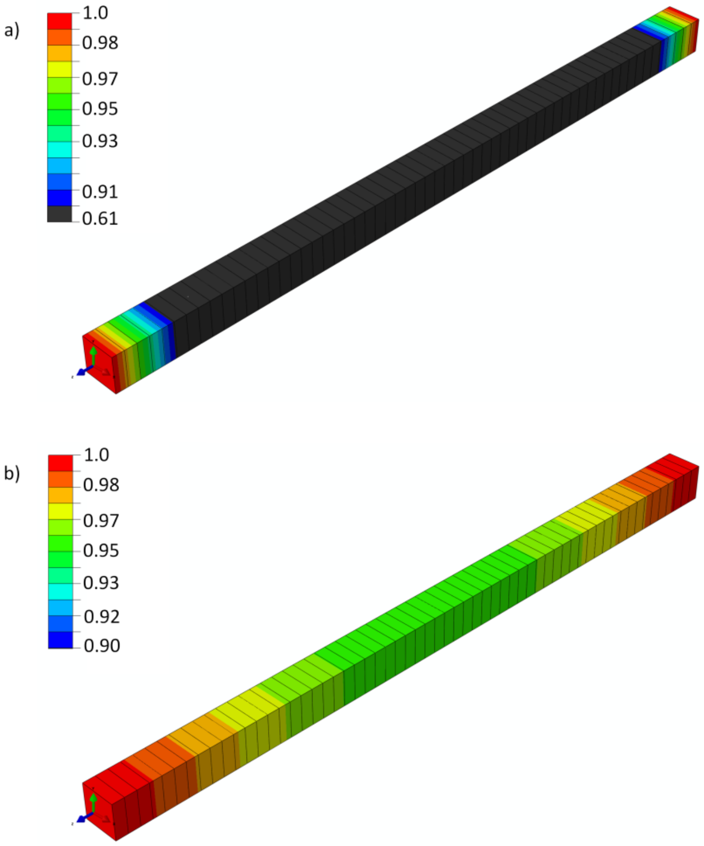

Fig. 5.2 *Predicted moisture profiles in epoxy bar at immersion times 213 days at a) 13°C; b) 30°C.*

The average moisture concentration (see Eq. 5.4) was calculated at each time increment and is plotted with the root of time in Fig. 5.3. The experimental data collected from immersed specimens at 13°C and 30°C (see Fig. 3.2, Chapter 3) is also shown. The simulated average moisture concentration was corroborated well by the experimental data, especially for the lower temperature (see Fig. 5.3a) for which the material diffusion shows a Fickian behavior.

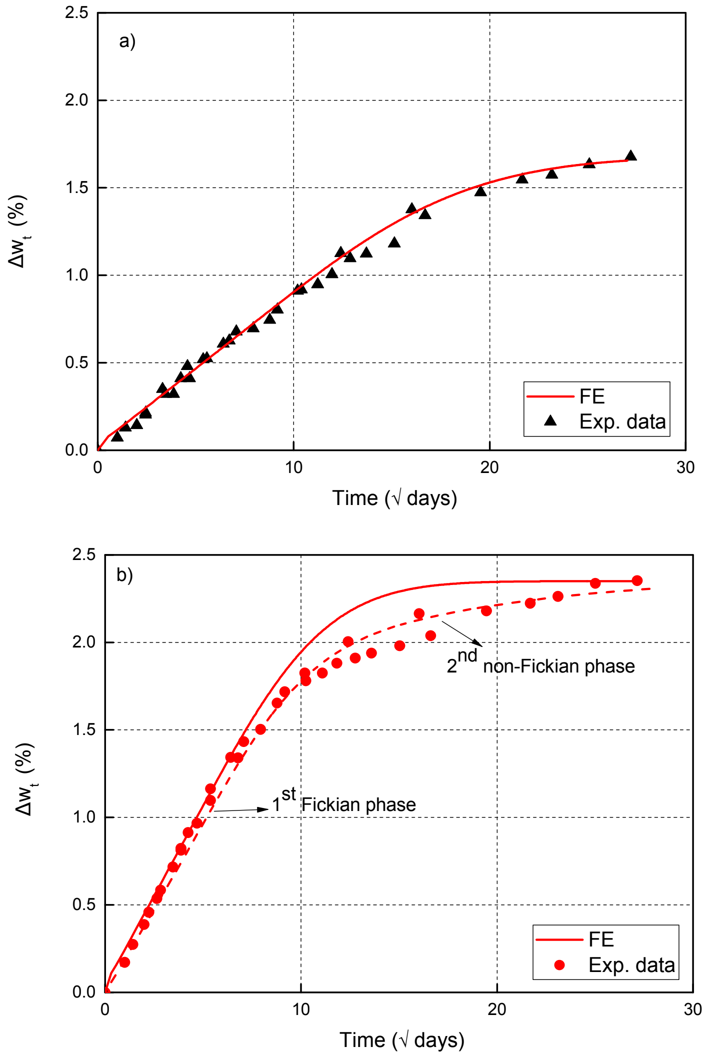

Fig. 5.3 *FE mass-diffusion analysis results vs experimental data for Sikadur 330 at immersion temperatures a) 13°C; b) 30°C.*

However, the Fickian model overestimated the response after the initial linear phase at 30°C (see Fig. 5.3b) when the specimens underwent a second relaxation phase, as described in [10]. During this phase, a rearrangement of polymer chains slowly takes place resulting in an additional increase of the water absorption, although at a lower rate than that of the initial phase. Swelling may occur, resulting in an enlargement of voids and redistribution of free volumes [11]. Deviations from Fickian behavior in polymers, e.g. in the case of a time-dependent diffusion coefficient or moisture concentration at the exposed surfaces, were also observed elsewhere and attributed to viscoelastic effects [9]. Accordingly, various non-Fickian models were proposed in [1, 9, 10].

The FE model and analysis used in the following for the modeling of moisture diffusion in the adhesive layers of bridge joints at lower temperatures were thus considered as validated, representing the ambient diffusion conditions commonly met in a wet bridge environment due to stagnant water.

5.1.3 Bridge-adhesive joints in wet environment – selection of case studies

Adhesively-bonded joints in bridges may have thick adhesive layers in the range of 5-10 mm between bridge deck and steel girders [12] or much thinner ones of 1-2 mm, as for example in cases of strengthening with bonded CFRP strips. Normally, in such joints the adhesive is sealed at the edges and thus protected from direct exposure to the environment. However, imperfections in the adhesive sealing during construction or caused by incidents during the long operation life cannot be excluded, and the adhesive may thus be exposed to moisture or even stagnant water during several decades, see Chapter 3. In the case of external reinforcement with bonded epoxy-CFRP strips, in spite of the low diffusion rate through the CFRP [1, 2], moisture could penetrate the thin CFRP adherends through the fiber-matrix interfaces and attack the also thin adhesive layer. Plasticization effects occur after such occurrences and result in the deterioration of both the physical and mechanical properties of the adhesive, as described in Chapter 3.

In this study, three different cases, based on two typical adhesively-bonded joints in bridges, have been numerically investigated. The three cases are schematically shown in Fig. 5.4 and correspond to moisture attack due to damage to the adhesive sealing in a bridge deck-to-girder joint (Case 1), moisture ingress along the interface in the same deck-to-girder joint (Case 2) and moisture penetration through the permeable adherend in a CFRP-to-girder (strengthening) joint (Case 3).

The distribution of the moisture concentration in the adhesive layer was predicted for all three cases. The FE analyses simulated a period of immersion of up to 100 years. The distribution of the tensile properties as a function of moisture concentration was subsequently estimated by use of the tensile experimental results from immersed specimens, see Chapter 3.

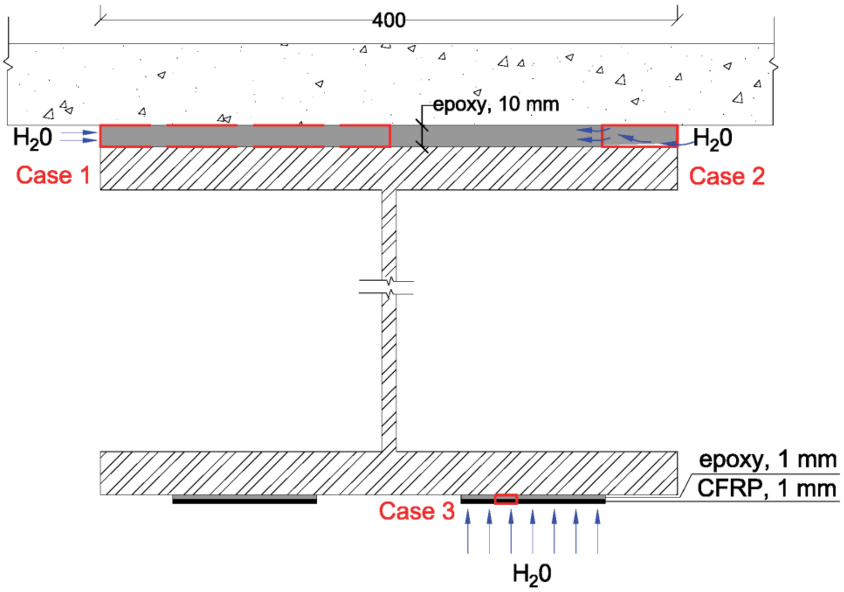

Fig. 5.4 *Case studies; 1) Deck-girder joint (sealant defect); 2) Deck-girder joint (interface defect); 3) CFRP-girder joint (adherend permeability).*

The diffusion parameters (D and c_∞ or Δw_∞) experimentally obtained for the epoxy Sikadur 330 at 13°C were used in all simulations, see Tab. 5.1. Diffusion parameters through the thickness of an epoxy-CFRP strip were selected from literature [1] under ambient fully immersed conditions. For the epoxy adhesive layer, simple Fickian models were able to describe the diffusion process through the CFRP material in [1]. One-dimensional diffusion was thus assumed in all cases. Furthermore it was assumed that the concrete deck is sealed and thus no moisture penetrates from the concrete into the adhesive.

Tab. 5.1 *Diffusion parameters (experimentally obtained) of materials used in FE*

Material	**D [mm^2/day]**	**Δw_∞ [%]**
Epoxy Adhesive (Chapter 3)	0.005	1.68
CFRP-strip [1]	0.00051	0.33

5.1.4 Diffusion into deck-girder joint (sealant defect)

Only half of the cross section was modeled due to symmetry and the mesh was refined near the edge of the adhesive where high concentration gradients were expected. The variation of the normalized moisture concentration inside the epoxy layer is shown in Fig. 5.5 in contour plots at different times. Only the part near to the edge is shown (first 50 mm). Full saturation has been reached in the red regions where the normalized moisture concentration is equal to 1. After 100 years, moisture had penetrated only about 40 mm into the 400-mm-wide joint between the deck and the top steel girder flange, i.e. only about 10% of the joint was affected by moisture.

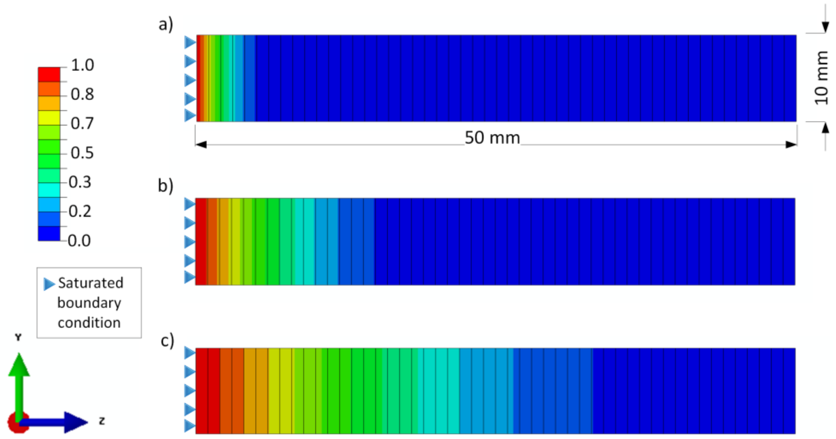

Fig. 5.5 *2D Contour plots of moisture concentration in adhesive layer of deck-girder joint (Case 1), after: a) 2 years; b) 20 years; c) 100 years.*

5.1.5 Diffusion into deck-girder joint (interface defect)

The case of interfacial debonding along a distance of 50 mm at the adhesive-steel interface was studied (see Fig. 5.4). As can be seen in Fig. 5.6, the variation of moisture concentration with time inside the epoxy layer varies also in the thickness direction, in contrast to Case 1. The adhesive became fully saturated above the debonding, however progression in the joint width direction was reduced and lower than in Case 1.

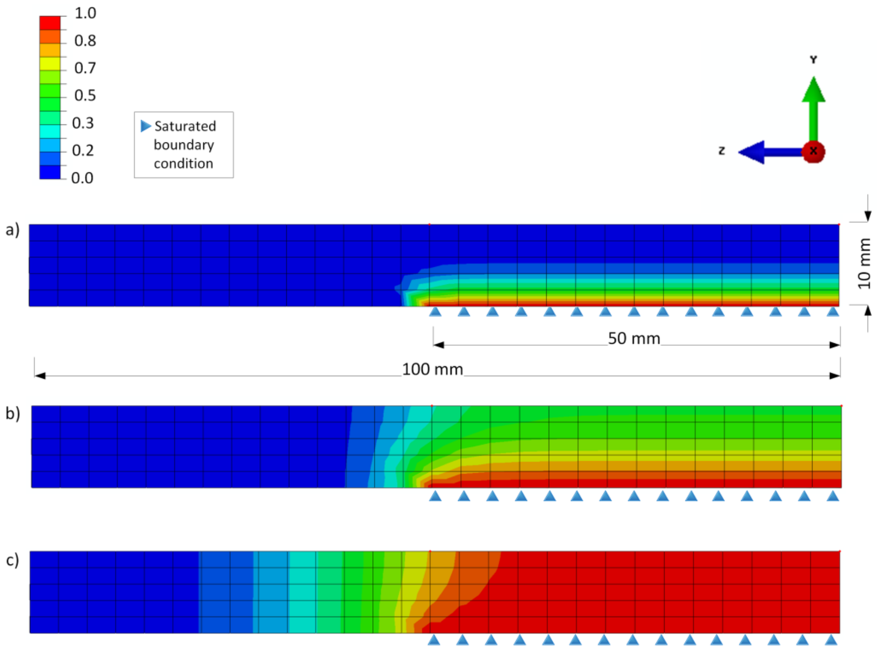

Fig. 5.6 *2D Contour plots of moisture concentration in adhesive layer of deck-girder joint (Case 2), after: a) 2 years; b) 20 years; c) 100 years.*

5.1.6 Diffusion into CFRP-girder joint (adherend permeability)

The variations of the normalized moisture concentration with time inside the CFRP and epoxy layers are shown in Fig. 5.7. Due to the only 1-mm thickness of the CFRP and adhesive layers in the diffusion direction, the whole adhesive layer became saturated within the investigated time period and this proved to be the most critical case of the three.

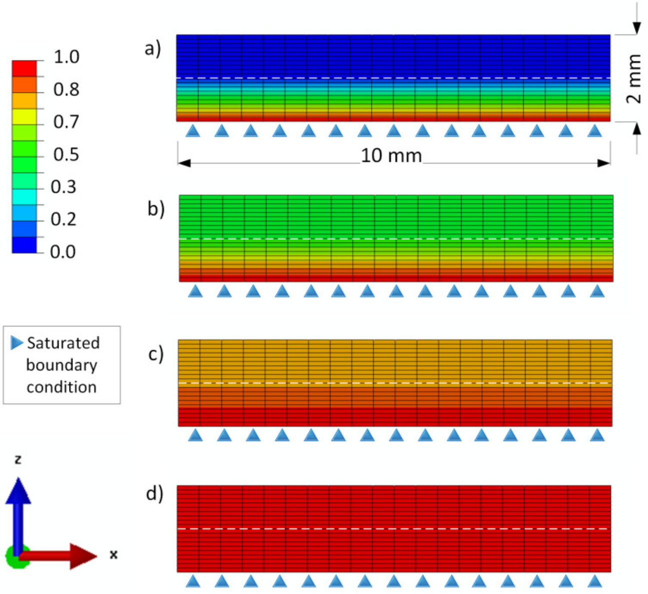

Fig. 5.7 *2D Contour plots of moisture concentration in adhesive layer of CFRP-girder joint (Case 3), after: a) 2 years; b) 20 years; c) 50 years; d) 100 years.*

5.1.7 Time-dependent retention of adhesive properties

Based on the moisture profiles shown above, graphs indicating the tensile property retention during progressive moisture ingress in the investigated epoxy layer were derived and are shown in Fig. 5.8 and Fig. 5.9 for Cases 1 and 3 respectively. Equations that relate the tensile strength and E-modulus to the water uptake predicted by FE were fitted to the experimental data presented in Fig. 3.5 and Fig. 3.7 of Chapter 3. Furthermore, the property retention after 100 years predicted by the 10°C master curves in Fig. 3.19 was adopted (i.e. approximately 70% after 100 years). A small inconsistency resulted from this procedure, since for 70% tensile property retention the Δw_∞ is roughly 2.3 % according to Fig. 3.5 and Fig. 3.7, while the experimental saturation level after two years was assumed as Δw_∞ =1.68% at 13°C (Tab. 3.3).

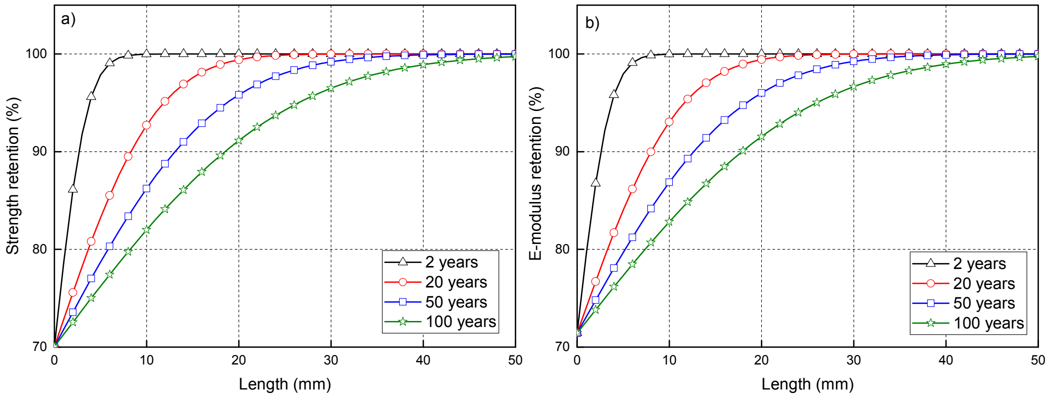

Fig. 5.8 *Retention of adhesive tensile properties along length in years, deck-girder joint (Case 1) in wet environment; a) strength; b) E-modulus.*

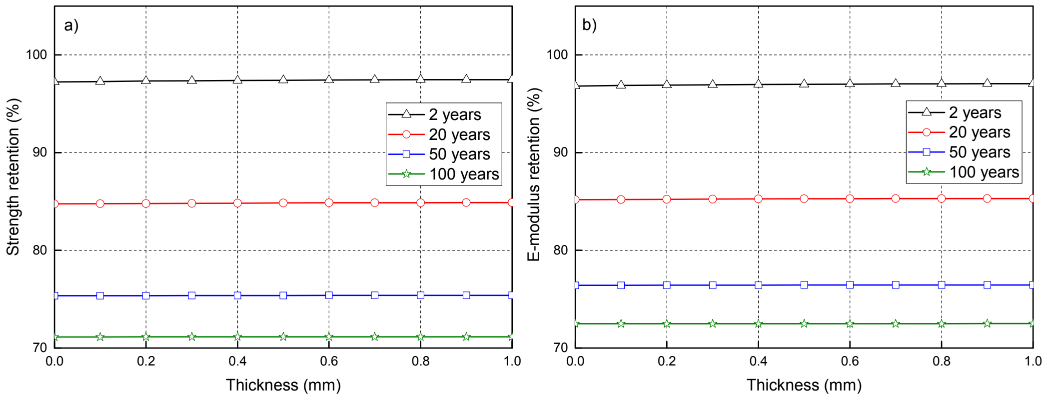

Fig. 5.9 *Retention of adhesive tensile properties along thickness in years, CFRP-girder joint (Case 3) in wet environment; a) strength; b) E-modulus.*

The results for Case 1 show that property degradation in the adhesive occurred only in the first 40 mm of the joint, as expected, and was limited to 30% of the dry values (i.e. 70% retention) after 100 years, see Fig. 5.8. The very short path for moisture ingress in Case 3 yielded a uniform distribution of moisture concentration along the thickness and consequently almost constant mechanical properties through the epoxy layer each time. At 100 years, the epoxy layer in Case 3 became uniformly saturated and is characterized by an average strength and E-modulus retention of 71% and 73% respectively (see Fig. 5.9).

5.2 Adhesive resistance factors

Since resistance factors for adhesive materials and joints are not defined in either in the Swiss standards or the Eurocodes, resistance factors from the Eurocomp Design Code and Handbook [14] can be adopted. This publication concerns fiber-reinforced polymer (FRP) materials and structures, but also comprises values for adhesives and joints and is conceptually similar and in accordance with the Eurocode design philosophy.

In this publication, the resistance factor (denominated partial safety factor) is split into sub-factors (coefficients) to take into account different effects on material properties, as described below.

5.2.1 Ultimate limit state (ULS)

At ULS, the Eurocomp design value of resistance, R_d, for adhesives is defined as follows (5.1.10 [14]):

$$R_d = \frac{R_k}{\gamma_m} = \frac{R_k}{\gamma_{m,1} \cdot \gamma_{m,2} \cdot \gamma_{m,3} \cdot \gamma_{m,4}} \qquad (5.5)$$

with R_k = characteristic value of resistance (5% fractile value), γ_m = partial safety factor, which is a product of four partial safety coefficients, shown in Tab. 5.2.

For brittle adhesives (shear strain to failure < 3%), $\gamma_m \geq 1.5$ applies. The factor $\gamma_{m,4}$=2.0 is thus larger than the experimental long-term reduction factor obtained in Chapter 3 of 1/0.7=1.43 (Fig. 3.19, reference temperature of 10°C). In the two joint cases discussed in Section 5.1, typical partial safety factors may thus be in the range of 3.1 to 5.6:

γ_m =1.25 (testing)·1.25 (spacers)·1.0 (traffic)·2.0 (laboratory) = 3.1

γ_m =1.5 (datasheet)·1.25 (spacers)·1.5 (dead load)·2.0 (laboratory) = 5.6

***Tab. 5.2** Partial safety coefficients according to Eurocomp [14]*

Source of the adhesive properties, $\gamma_{m,1}$	
Typical or textbook values (for appropriate adherends)	1.5
Values obtained by testing	1.25
Method of adhesive application, $\gamma_{m,2}$	
Manual application, no adhesive thickness control	1.5
Manual application, adhesive thickness controlled	1.25
Established application procedure with repeatable and controlled process parameters	1.0
Type of loading, $\gamma_{m,3}$	
Long-term loading	1.5
Short-term loading	1.0
Environmental conditions, $\gamma_{m,4}$	
Service conditions outside the adhesive test conditions	2.0
Adhesive properties determined for the service conditions	1.0

5.2.2 Serviceability limit state (SLS)

At SLS, the average values of the stiffness properties from the Eurocomp code are reduced by γ_m=1.30 and creep is considered by a further stiffness reduction factor, χ (see Fig. 4.13 in [14], the UD-in-shear curve may be applied).

Based on the experimental results obtained in Chapter 3, an increase of the 1.30 value to γ_m=1.50 is thus suggested.

5.2.3 Fatigue

In the case of fatigue, a further partial safety coefficient may be taken into account, applied to $\Delta\sigma_R$ or $\Delta\tau_R$ (normal or shear fatigue strength, 4.13 in [14]), here denominated $\gamma_{m,5}$, as shown in Tab. 5.3.

***Tab. 5.3** Partial safety coefficient for fatigue according to Eurocomp [14]*

Inspection and access	***"Fail-safe" components***	***Non "fail-safe" components***
Component subject to periodic inspection and maintenance. Detail accessible.	1.5	2.0
Component subject to inspection and maintenance. Poor accessibility.	2.0	2.5
Component not subject to periodic inspection and maintenance.	2.5	3.0

Note: "Fail-safe" structural components are such that local failure of one component does not result in failure of the structure or large sections of the structure.
Non "fail-safe" structural components are such that local failure of one component could lead to failure of the structure or large sections of the structure.

Schematic representative curves of $\Delta\sigma_R$ as a function of N (number of cycles) for the investigated epoxy adhesive Sikadur 330 (Chapter 4) and steel (according to SIA 263 or Eurocode 3 [15, 16]) are compared in Fig. 5.10 (normalized curves are shown). The slope of the adhesive curve is much lower than that of steel and the fatigue strength of the former is thus significantly higher than that of the latter. However, the adhesive does not exhibit a fatigue limit as steel does. Also shown is the behavior of a typical UD CFRP laminate (UD 55% [17]), as used in Section 5.1. The CFRP laminate has higher fatigue strength than the adhesive and also does not exhibit a fatigue limit.

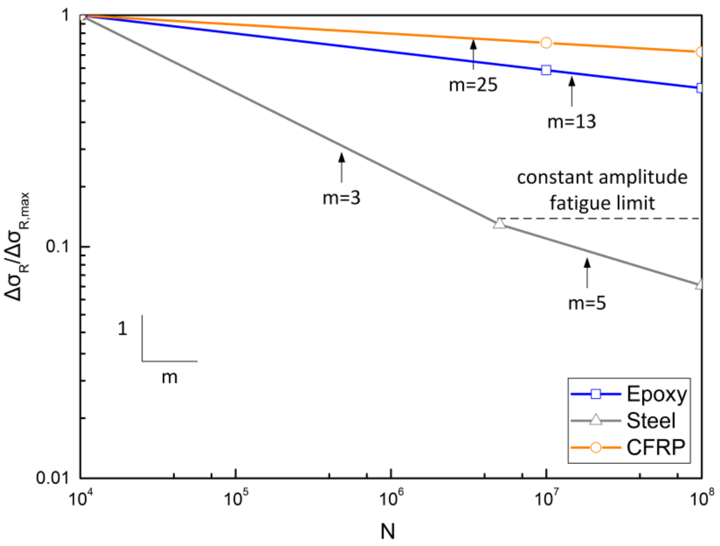

***Fig. 5.10** Normalized S/N curves, comparison of epoxy adhesive material with steel and CFRP ($\Delta\sigma_{R,max}$=$\Delta\sigma_R$ at 10^4 cycles).*

5.3 Mechanical and physical property determination

5.3.1 Tensile strength and E-Modulus

Specifications regarding the required preconditioning of adhesive specimens for mechanical tests that need to be performed for the ULS and SLS verifications in the designing of an adhesive bridge joint are given in the following.

Cold-curing epoxies exposed to low temperatures are characterized by low extents of cure in the early age and thus exhibit slow strength and stiffness development. The tensile properties during the first week of cure were extensively investigated in the previous work [18]. Practical examples proved that a period of three to seven days is sufficient in many cases for the development of an adequate tensile strength in the adhesive layer, even during wintertime (i.e. aging at $T_a < 10°C$). This time period may be further decreased if the reaction heat is trapped in the joint.

According to the results obtained in Chapter 2 (Fig. 2.14) of this study, the development of the tensile strength of a cold-curing epoxy adhesive during the first year in service develops in two stages, as shown in Fig. 5.11a, due to the combined physical aging and curing effects. Thus, for the short-term strength characterization, tensile experiments according to ASTM D638 [19] are recommended on specimens cured at laboratory temperature for seven days. The long-term strength, attained by a cold-curing epoxy after one year in service, is equivalent to that obtained by experiments on specimens cured for seven days under laboratory conditions and post-cured at 60°C for three more days.

Regarding stiffness, the E-modulus evolution of cold-curing epoxies is shown schematically in Fig. 5.11b. A maximum stiffness develops after the first week in service as a consequence of the main epoxy network densification (physical aging, see Fig. 2.13), but for longer aging times the E-modulus is reduced to values reached by the end of the first week of cure. For the SLS verification, stiffness can thus be estimated by tensile experiments carried out on specimens cured at laboratory temperature for seven days, according to ASTM D638 [19].

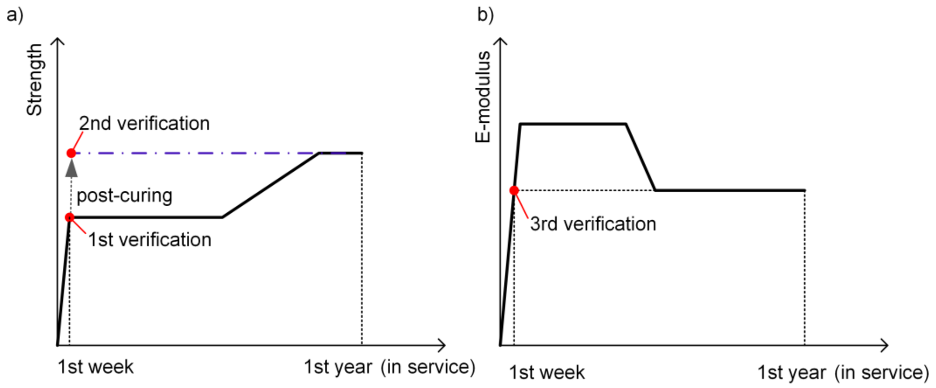

Fig. 5.11 *Recommended tensile experiments for a) ultimate limit state and b) serviceability limit state verifications.*

5.3.2 Long-term prediction of strength and E-modulus

A model that predicts the long-term variations in strength and stiffness of structural epoxy adhesives has been proposed in the previous work [18] and was based on a model for concrete strength development [20]. According to this model, the mechanical property (i.e. strength or stiffness) as a function of time, *P(t),* is given by the following equation:

$$P(t) = \beta_P(t)P_7 \tag{5.6}$$

where P_7 is the value of the mechanical property of an adhesive cured during seven days at 23°C (laboratory conditions), and $\beta_p(t)$ is a function describing the development of the adhesive mechanical property, governed by its chemical state or curing reaction state, i.e. by the change in the glass transition temperature, T_g, with time, equal to:

$$\beta_p(t) = \exp\left\{\left(1-\frac{7}{t}\right)^{0.5}\left[\frac{T_g(t)-T_{g,7}}{T_{g,7}}\right]^n\right\} \tag{5.7}$$

where $T_g(t)$ is the glass transition temperature of the adhesive at time *t* measured as the midpoint of the T_g step in DSC; $T_{g,7}$ is the glass transition temperature of the adhesive after seven days curing at 23°C (laboratory conditions); and *n* is a property-dependent parameter describing the rate of the mechanical property change with respect to the T_g change. The model was fitted to the experimental results in [18] for the same epoxy adhesive as studied here, i.e. Sikadur 330, and the values of *n* for the tensile strength and stiffness were found to be 1.06 and 2.62 respectively. The fact that the estimated *n* for strength was found to be close to 1.0 indicated that the rates of change of strength and T_g with time were somewhat similar. The higher value of the parameter for the E-modulus confirmed the lower rate of change of this property. The differences in the relationships of the E-modulus and strength with T_g is shown in Chapter 2, Fig. 2.22 and Fig. 2.23. On average, the E-modulus was constant and independent of T_g, whereas there was an exponential increase of strength in relation to T_g.

The aforementioned model was used to fit the tensile strength and stiffness development of the C21 specimens of this study during one year of aging at 21°C. The T_g development with time during the first year was obtained from the physical characterization (by DSC) in Chapter 2. The prediction and experimental data for strength and stiffness from Chapter 2 are shown in Fig. 5.12 and Fig. 5.13. It seems that the model predicts behavior over long aging times well, but it cannot capture the early age lower strength (Fig. 5.12) and higher stiffness (Fig. 5.13) caused by the physical aging. This is because Eq. 5.7 does not include any terms for the dependence of the mechanical properties on physical changes e.g. the relaxation enthalpy variation. The model takes into account only the effect of changes on the crosslinking level based on the T_g development. It is, however, in good agreement with the experimental results in Fig. 5.12 and Fig. 5.13 at the longer aging times, since cure becomes the predominant aging mechanism at those times, as discussed in detail in Chapter 2.

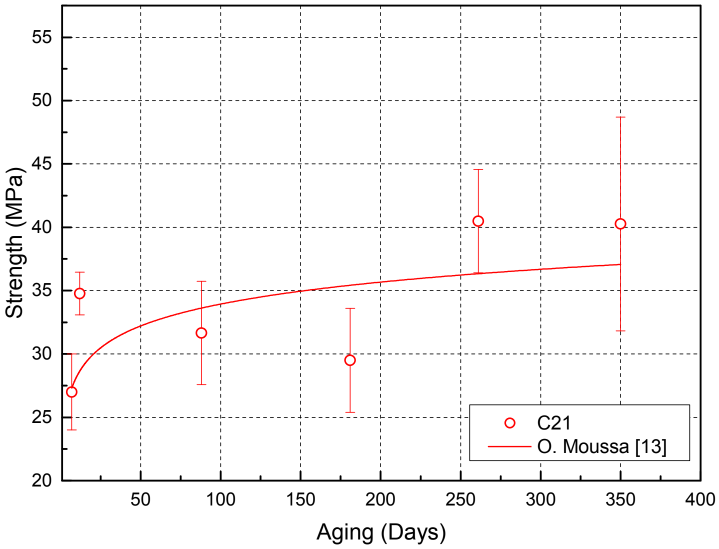

***Fig. 5.12** Tensile strength vs aging time relationship (experimental data and model predictions).*

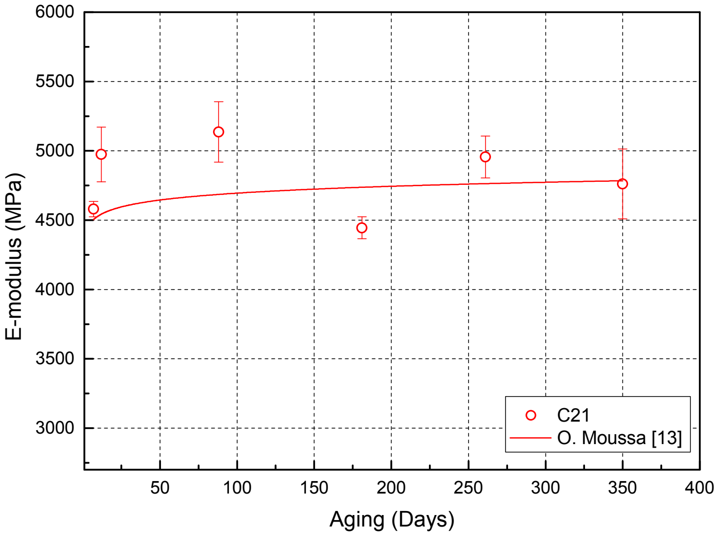

***Fig. 5.13** Tensile E-modulus vs aging time relationship (experimental data and model predictions).*

5.3.3 Glass transition temperature

Comparison of different methods for T_g acquisition

Values for the glass transition temperature, T_g, can be obtained in different ways, as shown in Chapter 2:

a) From Differential Scanning Calorimetry (DSC), at the transition midpoint ($T_{g,DSC}$), according to ASTM E1356 [21].

b) From Dynamic Mechanical Analysis (DMA) (see Fig. 5.14) [22, 23]:

- at the tangent intersection at the onset of the storage modulus drop ($T_{g,DMA,onset}$),
- at the maximum loss modulus ($T_{g,DMA,LM}$),

- at the maximum *tanδ* (loss factor) ($T_{g,DMA,tan\delta}$).

Differences of up to 15°C may exist depending on the method. The DSC provides additional information, such as the heat of endothermic and exothermic reactions. Estimation of the relaxation enthalpy and related physical aging effects and of the curing degree in order to assess the ultimate T_g can thus be obtained. The relevant value for adhesive joints in bridge construction is the $T_{g,DMA,onset}$ from the storage modulus in DMA, which occurs at the lowest temperature, before significant reductions of the mechanical properties occur. The $T_{g,DMA,onset}$ is used in guidelines for structural FRP design and is taken into account by ASTM E1640 [24, 25].

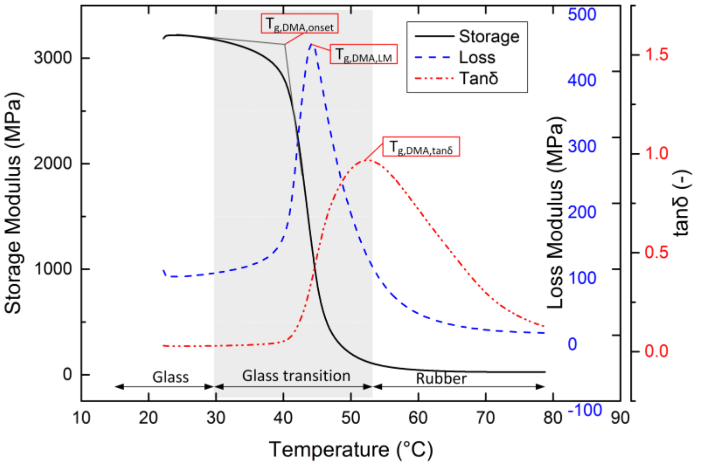

Fig. 5.14 *T_g determined by DMA.*

Strength and stiffness vs T_g development

The experimental investigations of the development of the adhesive properties in Chapters 2 and 3 have shown that when for similar mechanical properties are reached by different curing and/or immersion conditions, the T_g can still be very different. This is because the T_g is very sensitive to small differences in the curing degree, as already observed in the previous study [18], and is further reduced in a wet environment when the adhesive is plasticized [26]. Taking into account the fact that cold-curing epoxy adhesives are usually characterized by a T_g lower than 65°C [26], attention should be paid to the difference between the $T_{g,DMA,onset}$ and the exposure temperatures during service life. As the temperature approaches $T_{g,DMA,onset}$, the epoxy material starts changing from the glassy to the rubbery state and the mechanical properties accordingly start decreasing significantly. This is shown in Fig. 5.14 by the example of the steep slope of the storage modulus curve in the narrow glass transition region of around 20°C.

In a dry environment, at low temperature (i.e. 13°C), although strength and stiffness can be fully developed during the first year, T_g may remain below 50°C depending on the curing temperature, see Fig. 2.11 in Chapter 2. This is further illustrated in Fig. 5.15, i.e. the drop of the DMA storage modulus curve at 13°C occurs at a lower temperature than that which occurs at 21°C.

Similarly, in a wet environment, although the strength and stiffness of the adhesive immersed at low temperature (i.e. 13°C, CD13) may approach the values of the post-cured immersed material (PD13) within the first two years (Fig. 3.12 and Fig. 3.14 in Chapter 3), the T_g of the former still remains below 50°C whereas that of the latter is above 60°C (Fig. 3.11 in Chapter 3). A minimum value of around 58°C was found for long-term immersion in Fig. 3.4. The effect of the curing conditions is also shown in Fig. 5.16, where the drop of a cold-curing DMA storage modulus curve occurs at a lower temperature and higher rate compared to the post-cured one, both for immersion at 13°C. The results obtained in Chapter 3 however have also shown that the T_g values may fully recover after drying.

In the designing of adhesively-bonded joints, not only the mechanical property development, but also that of the T_g has thus to be taken into account. During the early bridge life or in a wet environment, the T_g may remain relatively low, in the range of 50°C. Depending on the exposure of the joint, e.g. for a CFRP strip to strengthen against negative moments below the asphalt, this may be critical, while other joints less exposed, e.g. below the bridge deck, such as a deck-to-girder joint, may be much less sensitive to this effect. On the other hand, exposing the adhesive at elevated temperature, even if only for a short period, may significantly increase the T_g [18].

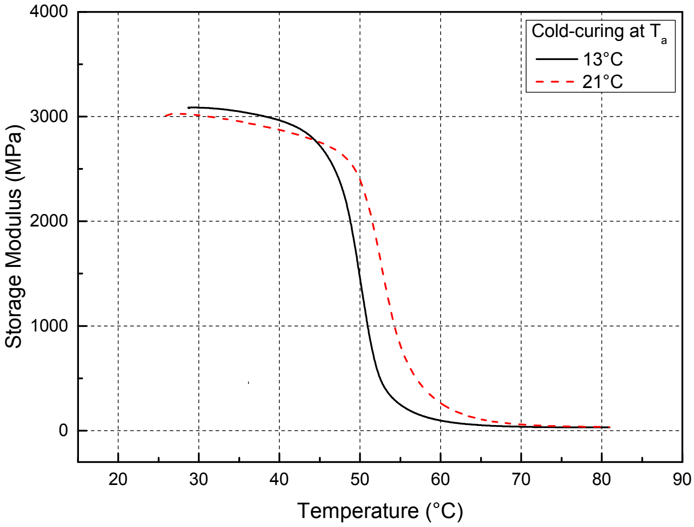

Fig. 5.15 *Storage modulus variations with temperature for epoxy adhesive curing at 13°C and 21°C in dry environment, after approximately 290 days.*

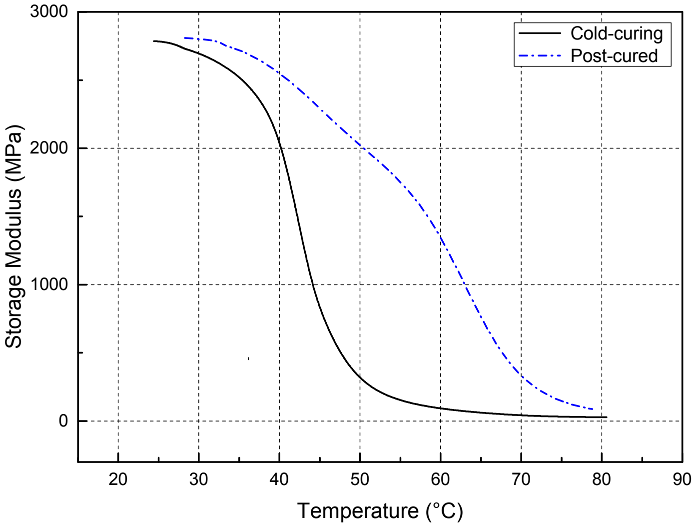

Fig. 5.16 *Storage modulus variations with temperature for cold- and post-cured epoxy adhesive at 125 days, both immersed in water at 13°C.*

5.4 Conclusions

Three typical cases of potential moisture ingress into the epoxy adhesive layer of bonded joints were analyzed. In the case of one-dimensional diffusion, moisture ingress and the associated degradation of mechanical properties are limited to a depth of approximately 40 mm after 100 years. Depending on the joint type, this effect may be critical. In the case of a typical 300-500-mm-long adhesive joint between a bridge deck and a top steel girder flange, the effect is marginal, while in the case of an only 1-mm-thick adhesive joint between a CFRP layer and the steel flange (or concrete) the effect may become critical. However, even in this case, the maximal loss of mechanical properties is roughly 30%, i.e. 70% of strength and stiffness is retained.

Exposure to lower levels of humidity, i.e. to not fully immersed conditions, would further postpone the degradation. Furthermore, after drying, the mechanical properties may fully recover, as shown in Chapter 3.

The above results are valid for the two-component epoxy adhesive Sikadur 330. In the previous work, the short-term mechanical behavior of similar epoxy adhesive products was compared and found to be similar [13]. The results obtained here may thus also apply to those products, however this requires further validation.

5.5 References

[1] M. Heshmati, R. Haghani, M. Al-Emrani, Effects of moisture on the long-term performance of adhesively bonded FRP/steel joints used in bridges, Compos. Part B Eng. 92 (2016) 447–462.

[2] L. P. Canal, V. Michaud, Micro-scale modeling of water diffusion in adhesive composite joints, Compos. Struct. 111 (2014) 340–348.

[3] X. Jiang, H. Kolstein, F. S.K. Bijlaard, Moisture diffusion in glass–fiber-reinforced polymer composite bridge under hot/wet environment, Compos. Part B Eng., 45 (2013) 407–416.

[4] Y. Joliff, L. Belec, M.B. Heman, J.F. Chailan, Experimental, analytical and numerical study of water diffusion in unidirectional composite materials – interphase impact, Comput. Mater. Sci. 64 (2012) 141–145.

[5] X. Jiang, H. Kolstein, F. Bijlaard, X. Qiang, Effects of hygrothermal aging on glass-fibre reinforced polymer laminates and adhesive of FRP composite bridge: Moisture diffusion characteristics, Compos. Part A Appl. Sci. Manuf. 57 (2014) 49–58.

[6] S. Amidi, J. Wang, Deterioration of the FRP-to-concrete interface subject to moisture ingress: Effects of conditioning methods and silane treatment, Compos. Struct. 153 (2016) 380–39.

[7] J. Crank, The Mathematics of Diffusion, second ed., Clarendon Press, Oxford, 1975.

[8] ASTM D5229/D5229M-14, Standard Test Method for Moisture Absorption Properties and Equilibrium Conditioning of Polymer Matrix Composite Materials, ASTM International, West Conshohocken, PA, 2014.

[9] G. LaPlante, A.V. Ouriadov, P. Lee-Sullivan, B.J. Balcom, , Anomalous moisture diffusion in an epoxy adhesive detected by magnetic resonance imaging, J. Appl. Polym. Sci. 109 (2008) 1350–1359.

[10] A.R Berens, H.B Hopfenberg, Diffusion and relaxation in glassy polymer powders: 2. Separation of diffusion and relaxation parameters, Polymer, 19 (1978) 489–496.

[11] W. K. Loh, A. D. Crocombe, M. M. Abdel Wahab, I. A. Ashcroft, Modelling anomalous moisture uptake, swelling and thermal characteristics of a rubber toughened epoxy adhesive, Int. J. Adhes. Adhes. 25 (2005) 1–12.

[12] T. Keller, J. Rothe, J. de Castro, M. Osei-Antwi, GFRP-Balsa Sandwich Bridge Deck: Concept, Design, and Experimental Validation, J. Compos. Constr. 18 (2014) 04013043/1–10.

[13] O. Moussa, T. Keller, Thermophysical and Thermomechanical Behavior of Cold-Curing Structural Adhesives in Bridge Construction, Rapport OFROU 654, Switzerland, 2013.

[14] J. L Clarke, Structural design of polymer composites - Eurocomp Design Code and Handbook, E & FN Spon, London, 1996.

[15] SIA 263, Steel Structures, SIA Swiss society of engineering and architects, Zurich 2003

[16] EN 1993 Eurocode 3: Design of steel structures.

[17] J. Brunbauer, H. Stadler, G. Pinter, Mechanical properties, fatigue damage and microstructure of carbon/epoxy laminates depending on fibre volume content, Int. J. Fatigue 70 (2015) 85-92.

[18] O. Moussa, T. Keller, Thermophysical and thermomechanical behavior of cold-curing structural adhesives in bridge construction, Rapport OFROU 654, Switzerland, 2013.

[19] ASTM D638-14, Standard test Method for tensile properties of plastics, ASTM International, West Conshohocken, PA, 2014.

[20] H. Müller, M. Haist, Effects of time upon strength deformation, fib Bulletin 51: structural concrete – Text book on behaviour, design and performance, 1 (2009) 53–71.

[21] ASTM E1356-08(2014) Standard Test Method for Assignment of the Glass Transition Temperatures by Differential Scanning Calorimetry, ASTM International, West Conshohocken, PA, 2014.

[22] Julien Michels, Robert Widmann, Christoph Czaderski, Reza Allahvirdizadeh, Masoud Motavalli, Glass transition evaluation of commercially available epoxy resins used for civil engineering applications, Composites Part B: Engineering, Volume 77, 2015, Pages 484–493.

[23] TA Instruments Brochure Library.

[24] CUR commission C124, Recommendation 96: Fibre-Reinforced Polymers in Civil Load-bearing Structures, CUR Gouda, The Netherlands, 2003.

[25] ASTM-E1640-13 Standard test method for the glass transition temperature by dynamic mechanical analysis ASTM International (2013).

[26] M. Frigione, M. Lettieri, A.M. Mecchi, Environmental effects on epoxy adhesives employed for restoration of historical buildings, J. Mater. Civ. Eng. 18 (2006) 715–72

6 Conclusions and future work

6.1 Main conclusions and contributions

This section presents a summary of the conclusions of this report, highlighting the key contributions with particular focus on the implementation of the results in bridge design.

6.1.1 Adhesive aging in dry bridge environment

Adhesives in sealed bridge joints are subjected to physical aging and curing effects in dry environments. An investigation of these effects that control the physical and mechanical behavior of the adhesive during the first year in service yielded the following main conclusions for an epoxy adhesive:

- Due to predominant physical aging in the earlier age (first three months), the mass density and tensile E-modulus exhibited a maximum, followed by a decrease in the later age when curing developed further and added volume to the epoxy network. Overall, the E-modulus development was independent of the adhesive curing conditions, i.e. cold- or post-cured.
- Tensile strength and failure strain development were delayed in the earlier age due to physical aging. Being dependent mainly on the cross-link density, their development was different under different curing conditions for the first nine months.
- Similar tensile properties, i.e. maximum strength and failure strain and a reduced E-modulus after a maximum, were reached for all curing conditions after nine months of aging. However, the glass transition temperature, T_g, was not yet fully developed after one year at low curing temperature (close to 10°C), being in the range of 50°C.

6.1.2 Adhesive aging in wet bridge environment

In practice, in view of the long service life of bridges of up to 100 years, bridge joints may be exposed to moisture, either due to damage to the initial sealing, or the porosity (e.g. concrete) or diffusivity (e.g. the matrix of thin CFRP strengthening materials) of the adherends. In order to investigate the moisture effects on the physical and mechanical properties of an epoxy adhesive exposed to a wet and alkaline bridge environment, a two-year experimental program was conducted. Both cold-curing and post-cured specimens were subjected to full immersion in distilled water and in an alkaline solution until saturation states were reached. In addition to a low immersion temperature (13°C), accelerated conditioning (i.e. high immersion temperatures) was applied and allowed long-term property predictions. The following conclusions were drawn from this investigation:

<u>In the earlier age (first two years):</u>

- For an immersed not yet fully cured material i.e. cold-curing at around 10°C, the continuation of curing and plasticization concurred, while physical aging effects were diminished.
- The E-modulus and strength approached the values of those of the post-cured material, the E-modulus after one month and strength after 20 months. However, the T_g still remained below 50°C after two years.
- DSC residual heat measurements did not show any difference in the curing progression between dry and wet cold-curing materials aging at around 10°C.

<u>In the later age (prediction up to 100 years):</u>

- Plasticization effects were induced by the water-alkaline attack causing a significant decrease of the glass transition temperature down to 58°C, and of the tensile E-modulus and tensile strength.

- The retention of 70% of the E-modulus and strength at an average 10°C reference temperature was predicted using the Arrhenius law after a 100-year bridge service life of the investigated adhesive.
- Full recovery of the mechanical and physical properties was obtained after drying the immersed and fully saturated material.
- In the case of concrete-adhesive joints, the immersion in alkaline water of pH≈13.0 had no noticeable detrimental effect on the mechanical and physical properties.

6.1.3 Fatigue performance under environmental effects

The effects of long-term aging and a wet environment on the fatigue behavior (life, damage accumulation and stiffness) were investigated. Post-cured bulk adhesive specimens (DRY), after immersion in 50°C demineralized water for over a year (WET) and others after drying (DRIED), were examined. The wet specimens were representative of specimens immersed for roughly 100 years at the low temperature of 10°C, commonly encountered in bridge environments. The main conclusions are as follows:

- The experimental campaign showed that the examined structural adhesive, even under wet conditions, characterized by 30% lower quasi-static strength, is capable of attaining fatigue lives of up 10 million cycles without failure at cyclic stress levels with σ_{max} of higher than 5 MPa (at R=0.1).
- Smooth power S-N curves with slopes between 10-12.5 were found to fit the experimental results well. The steepest corresponds to the wet specimens due to plasticization effects. When compared to the fatigue behavior of steel, a better fatigue performance was presented by the examined adhesive, with less steep S-N curves (a sloped at least four times lower), while no fatigue limit was observed however.
- The dried specimens exhibited a better and more consistent fatigue life compared to the dry ones, showing a positive effect of the retained water (<1%) on the fatigue performance and the reversal of the effects caused by plasticization even after representative long-term exposures.
- The wet specimens deformed more due to creep, attaining a strain to failure after fatigue almost 100% higher than the dry and dried specimens. The fatigue strains at failure are well below those attained under quasi-static loading for all specimens, and no critical fatigue failure strain could be derived.

6.1.4 Adhesive applications in bridge construction

On the basis of the above conclusions drawn from the scientific studies, the obtained results were implemented in practical examples and recommendations for bridge design as follows:

- Numerical modeling of the moisture ingress into the adhesive layer of typical bridge joints and associated predictions of the loss of mechanical properties revealed that moisture ingress through one-dimensional diffusion is limited to approximately 40 mm after 100 years. Depending on the joint type, this effect may be a) critical, i.e. if it concerns the entire adhesive layer thickness, e.g. in the case of thin bond lines of CFRP strengthening elements, or b) marginal, e.g. in the case of diffusion from the edges into wide deck-girder joints. However, even in the worst case, the maximum loss of mechanical properties is limited to roughly 30%, i.e. 70% of strength and stiffness are retained after 100 years of exposure. Furthermore, after drying, the mechanical properties may fully recover.
- In the case of joints exposed to humidity exhibiting a damaged sealing, the adhesive should be completely dried before repairing the sealing.
- A partial safety or resistance factor of 1.50 has been suggested to cover the effects of moisture on this material, applicable at the ULS and SLS. It has to be taken into account that the specimens were not stressed during the conditioning. Long-term subjection to high stresses during moisture exposure may increase the damage significantly.

- A preconditioning program comprising adhesive test specimens for the ULS and SLS verification has been proposed for this material in order to obtain the strength and stiffness properties relevant to the design.
- The different development of mechanical and physical properties, the T_g in the latter case, has been addressed. During the first year and in a wet environment, T_g may remain relatively low, in the range of 50°C, although the mechanical properties may have fully developed. Depending on the exposure of the joint, e.g. below or above the bridge deck (e.g. below the asphalt in the latter case), this may be critical for the mechanical performance of the adhesive and the overall integrity of the joint.

6.1.5 Impact on standardization

SIA 269/2 refers to SN EN 1504-4 and -6 for the determination of the glass transition temperature, T_g (articles 7.3.2.6 and 7.3.3.3). In these two EN standards, T_g is based on EN 12614, which determines this value through DSC or DTA. The results of this project demonstrated that the mechanical properties might already have significantly decreased at the DSC-based T_g-value. It is thus recommended to revise these standards and select T_g as the onset value of the storage modulus curve obtained through DMA, according to ISO 6721-11. Furthermore, it should be verified that the storage modulus curve in the glassy state, i.e. below $T_{g,onset}$, does not already decrease significantly, e.g. more than 5%.

The verification of $T_{g,onset}$ according to DMA should also be added in SIA 166, article 5.3.2.1. It should further be added that adhesive joints should be sealed.

6.2 Future work

This section outlines research topics that were beyond the scope of this work and should be addressed in the future to complement the present study.

6.2.1 Investigation of joint performance

This project focused on the investigation of the behavior of bulk adhesives and did not consider the performance of adhesively-bonded joints, e.g. between concrete, steel or CFRP strengthening elements. The development of the joint properties in the early age, when the adhesive has only attained a low degree of curing, as well as under environmental hygrothermal effects in the long term should be further investigated. The joints may not only exhibit a cohesive fracture in the adhesive, but also an interface fracture, when debonding between the adhesive and the adherend occurs, usually in the case of steel adherends [1, 2], or fracture in the concrete adherend [3].

Typical bridge joints, such as shear joints between concrete, steel and CFRP elements, or tensile joints of steel bars embedded in concrete, should be further investigated. The numerical simulation performed in this report can be extended to investigate the coupled structural-hygrothermal analysis of such joints.

6.2.2 Bulk adhesives under multiaxial stress states

This project focused on the adhesive tensile behavior. However, as also indicated in this report, multiaxial stress fields develop in the relatively thick layers of cold-curing adhesives like those often used in bridge applications. The comprehensive durability study conducted in this work should thus be complemented by additional investigations of the adhesive behavior under compressive, shear, multiaxial, i.e. tensile-shear, compressive-shear and/or tensile-compressive, loads.

Analytical and numerical models should be developed for the simulation of adhesive behavior under quasi-static multiaxial stress states, considering the effects of aging and water uptake identified by the current study.

6.2.3 Validation of aging processes for other structural adhesive

A great variety of structural adhesives are available on the market in response to the variety of joint parameters, e.g. type of adherend, load and environmental ranges. Together with other epoxy products on the market, flexible adhesives, such as polyurethanes and acrylics (often used in FRP composite applications), may be of interest since they may reduce stress concentrations and allow certain differential deformations and can provide ductility to the structure. The physical and mechanical behaviors as observed in this work under different curing conditions and environments should be investigated however. Various works for instance report much higher diffusion coefficients for polyurethane adhesives [4]. A consistent and comprehensive adhesive characterization under short- and long-term bridge conditions is still lacking however.

6.2.4 Fatigue in realistic/characteristic loading cases for bridges

The fatigue investigation in this report was limited to the constant amplitude tensile loading under an *R*-ratio of 0.1 in order to obtain results comparable to the majority of existing fatigue studies. The fatigue loading spectra in bridges however are far from being of constant amplitude. Irregular loading spectra, including overloads, are usually applied; their comprehensive investigation should complement the first results presented in this report. Analytical models, used for other types of materials, e.g., [5] can be adopted, and appropriately adapted to simulate the material's fatigue behavior under realistic loading conditions.

Such fatigue studies should also address topics related to the creep-fatigue interaction in the bulk adhesive under different loading patterns and gravimetric conditions. The reversibility of the viscoelastic effects caused to the materials during fatigue loading should also be thoroughly investigated.

Furthermore, this description of the future research required to complement the fatigue investigations is not limited to the bulk adhesive, but should also be applied to adhesively-bonded bridge joints.

6.3 References

[1] J. W. Shi, H. Zhu, G. Wu, Z. S. Wu, Tensile behavior of FRP and hybrid FRP sheets in freeze–thaw cycling, Composites Part B 60 (2014) 239–247.

[2] M. Chevalier, E. Dantras, C. Tonon, P. Guigue, C. Lacabanne, C. Puig, C. Durin, Correlation between sub-Tg relaxation processes and mechanical behavior for different hydrothermal ageing conditions in epoxy assemblies, J. Appl. Polym. Sci. 115 (2010) 1208–1214.

[3] M. A. Aiello, M. Frigione and D. Acierno, Effects of Environmental Conditions on Performance of Polymeric Adhesives for Restoration of Concrete Structures, J. Mater. Civil Eng. 14 (2002) 185–189.

[4] X. Jiang, H. Kolstein, F. S.K. Bijlaard, Moisture diffusion in glass–fiber-reinforced polymer composite bridge under hot/wet environment, Compos. Part B Eng. 45 (2013) 407–416.

[5] A. P. Vassilopoulos, B. D. Manshadi, T. Keller, Influence of the constant life diagram formulation on the fatigue life prediction of composite materials, Int. J. Fatigue 32 (2010) 659–669.

Terminology

In the present report the abbreviations and specific technical terms defined below are used:

Arrhenius principle: expresses the temperature dependence of reaction rates and assumes that the time to reach a given property retention at different experimental temperatures can be expressed by linear equations with common slope depending on the activation energy.

CFRP strips: are externally bonded carbon fiber-reinforced polymer strips used for structural strengthening purposes.

Cold-curing: is the continuation of the curing process at ambient service temperatures clearly below T_g. In the case of structural epoxy adhesives, aliphatic amines or polyamines curing agents are able to induce cross-linking reactions even at low temperatures.

Curing degree: is the degree of cross-linking of the polymer chains. Mechanical and physical properties increase with increasing curing.

De-aging: is the recovery of the enthalpy loss during the aging process by reheating the aged material to above T_g.

Differential Scanning Calorimetry (DSC): Heat-flux DSC records in function of time or temperature the difference of heat-flux diffusing between the sample holder, the reference holder and the testing unit of the equipment. This allows the detection of transitions such as melts, glass transitions, phase changes, and curing, see EN 12614.

Diffusion coefficient: is the proportionality factor D in *Fick's law* by which the mass of a substance dM diffusing in time dt through the surface dF normal to the diffusion direction is proportional to the concentration gradient grad-c of this substance: $dM=-D\cdot grad\text{-}c\cdot dF\cdot dt$.

Dynamic mechanical analysis (DMA): is used to determine the variation of the storage modulus, loss modulus and tan-delta as a function of temperature and frequency. From these data, a value for the glass transition can be determined, see ISO 6721-11.

Glass transition temperature (T_g): is the temperature that marks the transition from the glassy to the rubbery state. It can be determined by different methods which measure different property changes, i.e. the change in heat capacity through DSC or changes in the storage and loss modulus curves of DMA. Accordingly, the values may vary up to 25°C.

Loss modulus: is a measure of the energy dissipated as heat, representing the viscous portion, in viscoelastic materials.

Moisture concentration: is the quantity of water per unit volume or in percent contained in a material.

Physical aging: is the decrease of the specific enthalpy of the epoxy system, which can be attributed to a decrease of the specific volume (volumetric relaxation) and / or decrease in the molecular conformational energy by volume-independent rearrangements of molecular segments (enthalpy relaxation). Physical aging results in a denser network of higher stiffness.

Plasticization: is the decrease of mechanical and physical (T_g) properties due to absorption of moisture/water. The process is reversible during drying.

Post-curing: is the acceleration of the curing process by heating, usually (slightly) above T_g, in order to reach an almost complete curing.

Relaxation enthalpy: is the endothermic peak in the glass transition region of a DSC curve whose magnitude increases during physical aging.

Residual enthalpy: is the exothermic peak presented after the T_g on a DSC curve, which is used as a measure of the curing degree of the polymer.

Residual strength: is the quasi-static strength of a specimen previously subjected to e.g. fatigue cycles without failure or environmental conditioning.

Storage modulus: is a measure of the stored energy, representing the elastic portion, in viscoelastic materials.

Strength retention: is the remaining strength after aging, expressed as percentage of the reference strength of the unaged material.

Time shift factor: is the factor by which experimental data from different temperatures can be shifted on the time axis to form a master curve at a selected reference temperature, in order to predict properties over a much longer time period than that experimentally covered.

Viscoelastic material: exhibits both viscous and elastic characteristics when undergoing deformation. The relationship between stress and strain depends on time.

Project closure

Schweizerische Eidgenossenschaft
Confédération suisse
Confederazione Svizzera
Confederaziun svizra

Eidgenössisches Departement für
Umwelt, Verkehr, Energie und Kommunikation UVEK
Bundesamt für Strassen ASTRA

FORSCHUNG IM STRASSENWESEN DES UVEK

Formular Nr. 3: Projektabschluss

Version vom 09.10.2013

erstellt / geändert am: 3. Oktober 2017

Grunddaten

Projekt-Nr.: AGB 2012-012

Projekttitel: Dauerhaftigkeit und Ermüdungsbeständigkeit von kalthärtenden strukturellen Klebstoffen im Brückenbau

Enddatum: 31.07.2017

Texte

Zusammenfassung der Projektresultate:

Strukturelle Klebstoffe werden im Brückenbau seit den 1960er-Jahren verwendet. Heute gebräuchliche Anwendungen sind das Aufkleben von Stahl- oder Kohlefaserverbund- (CFK) Lamellen auf bestehende Tragwerke oder das Einkleben von Anschlussbewehrung in Bohrungen von Stahlbetonbauteilen. Im Brückenbau werden Klebeverbindungen meist auf der Baustelle vorgenommen, deswegen können in der Regel nur kalthärtende Klebstoffe, meist auf Epoxidharzbasis, eingesetzt werden. Bei Klebeverbindungen sind die freien Ränder normalerweise abgedichtet um eine Exposition gegenüber Feuchtigkeit und UV-Strahlung zu verhindern. Angesichts der langen Nutzungsdauer von Brücken, bis zu 100 Jahren, ist es jedoch denkbar, dass die Abdichtung früher oder später unwirksam wird und der Klebstoff somit Feuchtigkeit ausgesetzt wird. In Abhängigkeit der Art der Klebeverbindung kann diese auch einer wesentlichen Ermüdungsbeanspruchung unterliegen.

Im Rahmen dieses Projektes wurden sich in Aushärtung befindende und bereits ausgehärtete Prüfkörper des Epoxidklebstoffes Sikadur 330 während bis zu zwei Jahren unterschiedlichen Expositionen ausgesetzt. Das Alterungsverhalten unter feuchter Exposition wurde gemäss der Arrhenius-Methode beschleunigt, um das Verhalten bis auf 100 Jahre extrapolieren zu können. Mechanisch wurde das Zugverhalten unter statischer und Ermüdungsbeanspruchung untersucht, physikalische Untersuchungen betrafen hauptsächlich die Glasübergangstemperatur. Für diese sollte der Onset-Wert des DMA Speicher-Moduls verwendet werden, da nur dieser Wert den Beginn des signifikanten Abfalls der mechanischen Eigenschaften kennzeichnet. Ein Set von Widerstandsbeiwerten wird für die Klebstoffbemessung vorgeschlagen, welches die Quelle der mechanischen Eigenschaften, Applikationsmethode, Beanspruchungsart sowie Exposition und Ermüdungsbeanspruchung berücksichtigt.

Im Falle einer trockenen Exposition unter einer abgedichteten Verbindung überwiegen in der Anfangsphase die Auswirkungen der physikalischen Alterung jene der fortschreitenden Aushärtung. Nach weniger als neun Monaten wurden unter allen Aushärtungsbedingungen ähnliche Eigenschaften erreicht, d.h. maximale Zugfestigkeit und Bruchdehnung und ein gegenüber der Anfangsphase etwas reduzierter E-Modul. Die Glasübergangstemperatur hingegen war nach einem Jahr noch nicht voll entwickelt und immer noch von den Aushärtungsbedingungen abhängig. Basierend auf diesen Resultaten wurden Spezifikationen hinsichtlich den notwendigen Aushärtungsbedingungen von Prüfkörpern für mechanische Prüfungen definiert, um die für den Nachweis der Tragsicherheit und Gebrauchstauglichkeit erforderlichen Klebstoff-Materialkennwerte zu bestimmen.

In einer feuchten Umgebung wurde aufgrund einer Plastifizierung eine erhebliche Abnahme von Glasübergangstemperatur, E-Modul und Zugfestigkeit festgestellt. Nach einer vollständig eingetauchten Wasserexposition unter einer 10°C Referenztemperatur, während einer hundertjährigen Nutzungsdauer, wurden verbleibende E-Modul- und Festigkeitswerte von 70% der Anfangswerte extrapoliert. Die Alkalität des Wassers hatte keinen signifikanten Einfluss auf diese Resultate. Im Falle einer eindimensionalen Diffusion ist die Feuchtigkeitseindringtiefe in den Klebstoff und die damit verbundene Länge der Abnahme der mechanischen Eigenschaften auf ca. 40 mm nach 100 Jahren begrenzt. In Abhängigkeit der Art der Klebeverbindung kann diese Länge kritisch sein oder nicht. Im Falle einer 300-500 mm langen Klebeverbindung zwischen einer Brückenplatte und dem oberen Flansch eines Stahlträgers beispielsweise sind die Auswirkungen gering, während im Falle einer nur 1 mm dicken Klebeverbindung zwischen CFK Lamellen und Brückenkonstruktion die Auswirkungen erheblich sein können. Die Glasübergangstemperatur unter feuchten Bedingungen verblieb im Bereich von 50-60°C. Abhängig von der Exposition der Klebeverbindung können diese Werte kritisch werden, z.B. im Falle einer CFK Lamellenverstärkung der Brückenplatte unter dem Asphalt, wo die Temperaturen bis 80°C ansteigen können. Nach der Trocknung des Klebstoffs erholten sich jedoch die physikalischen und mechanischen Eigenschaften vollständig.

Die experimentellen Resultate haben gezeigt, dass der untersuchte Klebstoff auch während 100 Jahren Wasserlagerung in der Lage ist, typischen Ermüdungseinwirkungen zu widerstehen. Die Plastifizierung und damit verbundene Steifigkeitsabnahme war der Hauptgrund für das unterschiedliche Verhalten von untersuchten trockenen, gesättigten und (nach Sättigung) getrockneten Proben. Während die vollständig gesättigten Proben die geringste Ermüdungslebensdauer aufwiesen, erreichten die getrockneten Proben die längste Dauer, was durch einen positiven Effekt einer kleinen verbleibenden Restfeuchtigkeit in den getrockneten Proben erklärt wurde.

Das vorliegende Projekt fokussierte auf die Untersuchung des reinen Klebstoffs und beinhaltete nicht das Verhalten von gesamten Klebeverbindungen. Experimentelle Resultate von Klebeverbindungen haben gezeigt, dass vielfach das Verhalten der Verbundflächen (Interfaces) kritischer sein kann als jenes des Klebstoffs. Im weiteren sind die Resultate in erster Linie für den Zweikomponenten-Epoxidklebstoff Sikadur 330 gültig und bedürfen einer weiteren Validierung für andere Klebstoffprodukte.

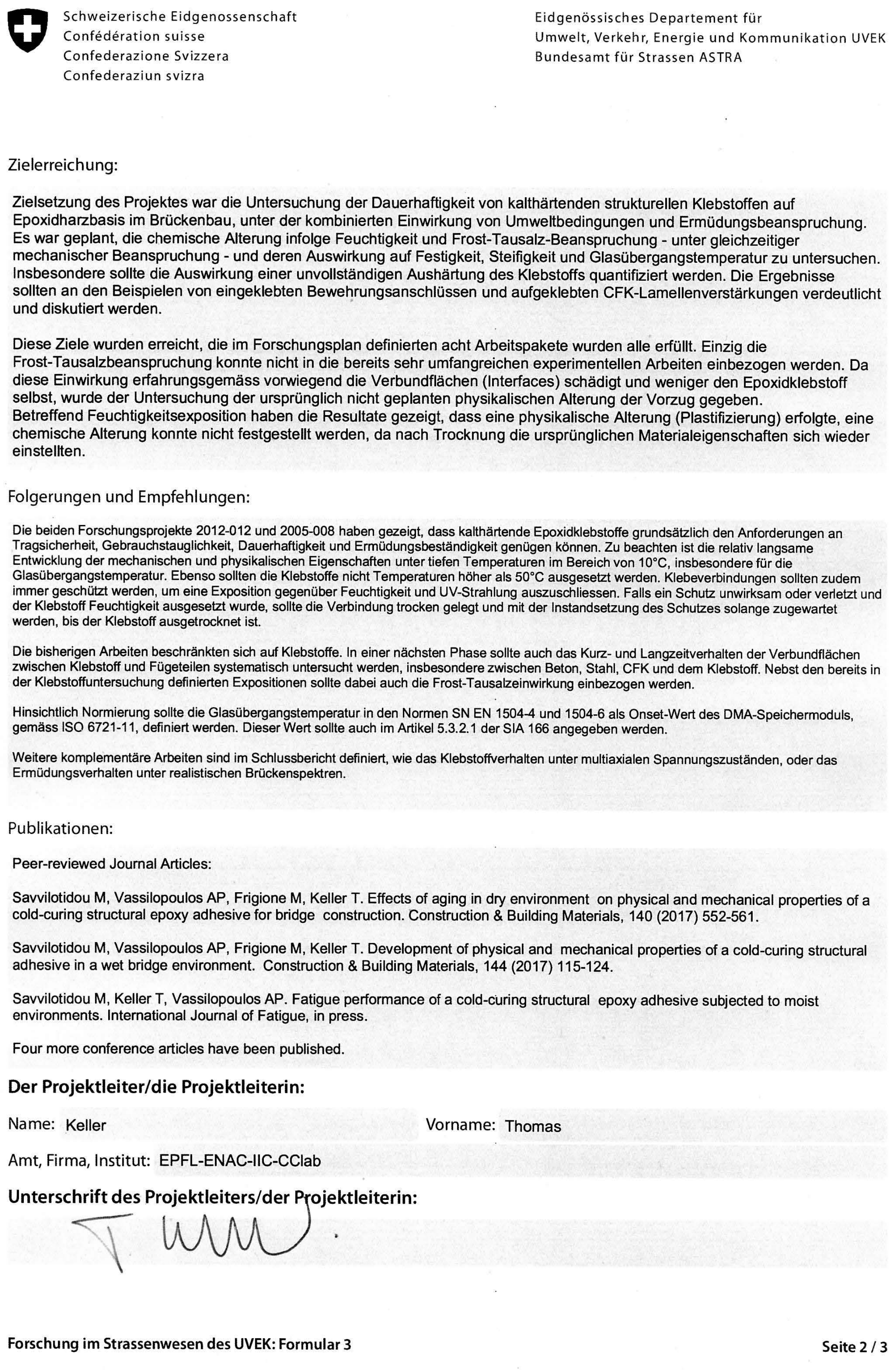

Zielerreichung:

Zielsetzung des Projektes war die Untersuchung der Dauerhaftigkeit von kalthärtenden strukturellen Klebstoffen auf Epoxidharzbasis im Brückenbau, unter der kombinierten Einwirkung von Umweltbedingungen und Ermüdungsbeanspruchung. Es war geplant, die chemische Alterung infolge Feuchtigkeit und Frost-Tausalz-Beanspruchung - unter gleichzeitiger mechanischer Beanspruchung - und deren Auswirkung auf Festigkeit, Steifigkeit und Glasübergangstemperatur zu untersuchen. Insbesondere sollte die Auswirkung einer unvollständigen Aushärtung des Klebstoffs quantifiziert werden. Die Ergebnisse sollten an den Beispielen von eingeklebten Bewehrungsanschlüssen und aufgeklebten CFK-Lamellenverstärkungen verdeutlicht und diskutiert werden.

Diese Ziele wurden erreicht, die im Forschungsplan definierten acht Arbeitspakete wurden alle erfüllt. Einzig die Frost-Tausalzbeanspruchung konnte nicht in die bereits sehr umfangreichen experimentellen Arbeiten einbezogen werden. Da diese Einwirkung erfahrungsgemäss vorwiegend die Verbundflächen (Interfaces) schädigt und weniger den Epoxidklebstoff selbst, wurde der Untersuchung der ursprünglich nicht geplanten physikalischen Alterung der Vorzug gegeben.
Betreffend Feuchtigkeitsexposition haben die Resultate gezeigt, dass eine physikalische Alterung (Plastifizierung) erfolgte, eine chemische Alterung konnte nicht festgestellt werden, da nach Trocknung die ursprünglichen Materialeigenschaften sich wieder einstellten.

Folgerungen und Empfehlungen:

Die beiden Forschungsprojekte 2012-012 und 2005-008 haben gezeigt, dass kalthärtende Epoxidklebstoffe grundsätzlich den Anforderungen an Tragsicherheit, Gebrauchstauglichkeit, Dauerhaftigkeit und Ermüdungsbeständigkeit genügen können. Zu beachten ist die relativ langsame Entwicklung der mechanischen und physikalischen Eigenschaften unter tiefen Temperaturen im Bereich von 10°C, insbesondere für die Glasübergangstemperatur. Ebenso sollten die Klebstoffe nicht Temperaturen höher als 50°C ausgesetzt werden. Klebeverbindungen sollten zudem immer geschützt werden, um eine Exposition gegenüber Feuchtigkeit und UV-Strahlung auszuschliessen. Falls ein Schutz unwirksam oder verletzt und der Klebstoff Feuchtigkeit ausgesetzt wurde, sollte die Verbindung trocken gelegt und mit der Instandsetzung des Schutzes solange zugewartet werden, bis der Klebstoff ausgetrocknet ist.

Die bisherigen Arbeiten beschränkten sich auf Klebstoffe. In einer nächsten Phase sollte auch das Kurz- und Langzeitverhalten der Verbundflächen zwischen Klebstoff und Fügeteilen systematisch untersucht werden, insbesondere zwischen Beton, Stahl, CFK und dem Klebstoff. Nebst den bereits in der Klebstoffuntersuchung definierten Expositionen sollte dabei auch die Frost-Tausalzeinwirkung einbezogen werden.

Hinsichtlich Normierung sollte die Glasübergangstemperatur in den Normen SN EN 1504-4 und 1504-6 als Onset-Wert des DMA-Speichermoduls, gemäss ISO 6721-11, definiert werden. Dieser Wert sollte auch im Artikel 5.3.2.1 der SIA 166 angegeben werden.

Weitere komplementäre Arbeiten sind im Schlussbericht definiert, wie das Klebstoffverhalten unter multiaxialen Spannungszuständen, oder das Ermüdungsverhalten unter realistischen Brückenspektren.

Publikationen:

Peer-reviewed Journal Articles:

Savvilotidou M, Vassilopoulos AP, Frigione M, Keller T. Effects of aging in dry environment on physical and mechanical properties of a cold-curing structural epoxy adhesive for bridge construction. Construction & Building Materials, 140 (2017) 552-561.

Savvilotidou M, Vassilopoulos AP, Frigione M, Keller T. Development of physical and mechanical properties of a cold-curing structural adhesive in a wet bridge environment. Construction & Building Materials, 144 (2017) 115-124.

Savvilotidou M, Keller T, Vassilopoulos AP. Fatigue performance of a cold-curing structural epoxy adhesive subjected to moist environments. International Journal of Fatigue, in press.

Four more conference articles have been published.

Der Projektleiter/die Projektleiterin:

Name: Keller

Vorname: Thomas

Amt, Firma, Institut: EPFL-ENAC-IIC-CClab

Unterschrift des Projektleiters/der Projektleiterin:

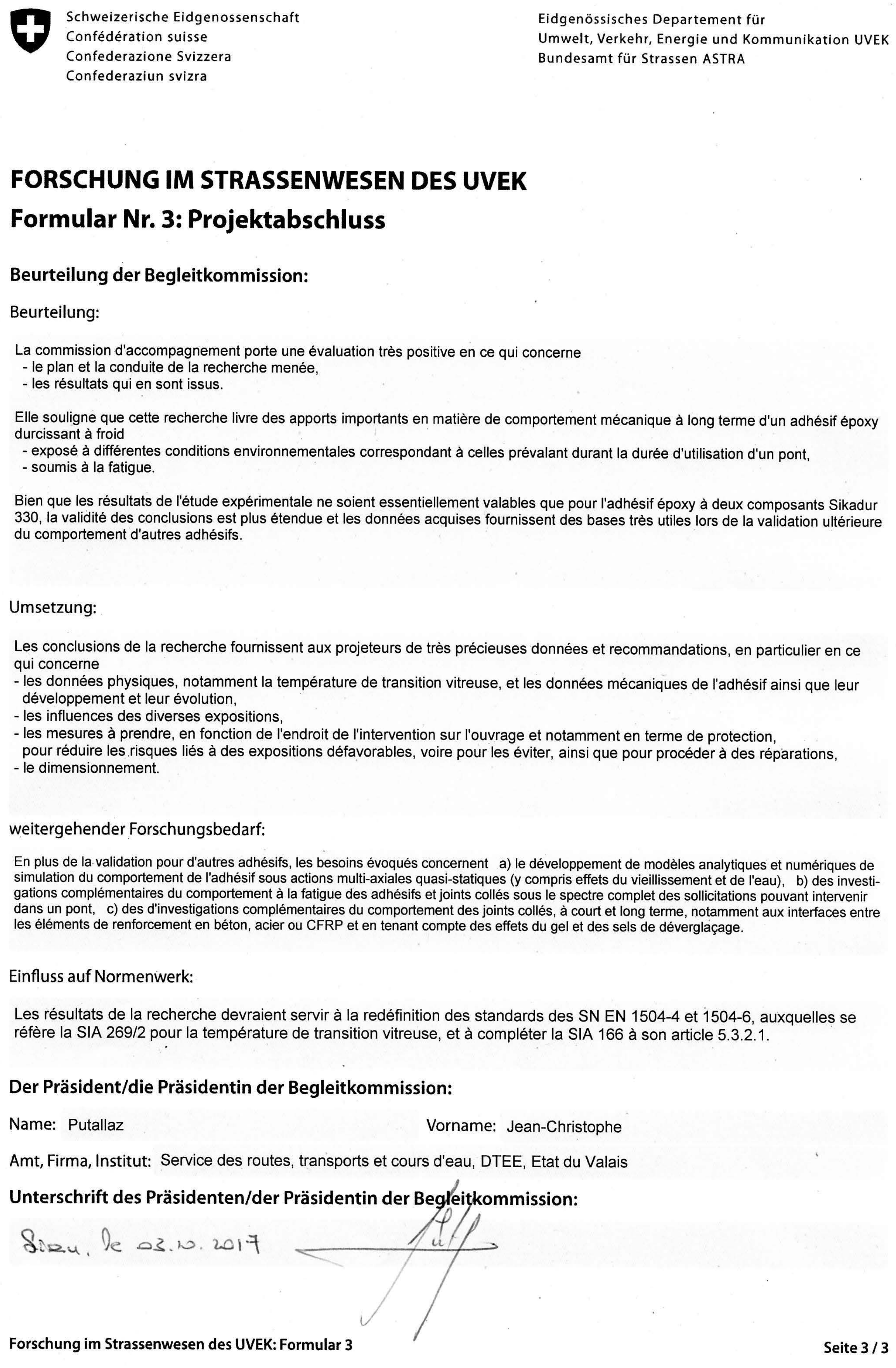

Schweizerische Eidgenossenschaft
Confédération suisse
Confederazione Svizzera
Confederaziun svizra

Eidgenössisches Departement für
Umwelt, Verkehr, Energie und Kommunikation UVEK
Bundesamt für Strassen ASTRA

FORSCHUNG IM STRASSENWESEN DES UVEK

Formular Nr. 3: Projektabschluss

Beurteilung der Begleitkommission:

Beurteilung:

La commission d'accompagnement porte une évaluation très positive en ce qui concerne
- le plan et la conduite de la recherche menée,
- les résultats qui en sont issus.

Elle souligne que cette recherche livre des apports importants en matière de comportement mécanique à long terme d'un adhésif époxy durcissant à froid
- exposé à différentes conditions environnementales correspondant à celles prévalant durant la durée d'utilisation d'un pont,
- soumis à la fatigue.

Bien que les résultats de l'étude expérimentale ne soient essentiellement valables que pour l'adhésif époxy à deux composants Sikadur 330, la validité des conclusions est plus étendue et les données acquises fournissent des bases très utiles lors de la validation ultérieure du comportement d'autres adhésifs.

Umsetzung:

Les conclusions de la recherche fournissent aux projeteurs de très précieuses données et recommandations, en particulier en ce qui concerne
- les données physiques, notamment la température de transition vitreuse, et les données mécaniques de l'adhésif ainsi que leur développement et leur évolution,
- les influences des diverses expositions,
- les mesures à prendre, en fonction de l'endroit de l'intervention sur l'ouvrage et notamment en terme de protection, pour réduire les risques liés à des expositions défavorables, voire pour les éviter, ainsi que pour procéder à des réparations,
- le dimensionnement.

weitergehender Forschungsbedarf:

En plus de la validation pour d'autres adhésifs, les besoins évoqués concernent a) le développement de modèles analytiques et numériques de simulation du comportement de l'adhésif sous actions multi-axiales quasi-statiques (y compris effets du vieillissement et de l'eau), b) des investigations complémentaires du comportement à la fatigue des adhésifs et joints collés sous le spectre complet des sollicitations pouvant intervenir dans un pont, c) des d'investigations complémentaires du comportement des joints collés, à court et long terme, notamment aux interfaces entre les éléments de renforcement en béton, acier ou CFRP et en tenant compte des effets du gel et des sels de déverglaçage.

Einfluss auf Normenwerk:

Les résultats de la recherche devraient servir à la redéfinition des standards des SN EN 1504-4 et 1504-6, auxquelles se réfère la SIA 269/2 pour la température de transition vitreuse, et à compléter la SIA 166 à son article 5.3.2.1.

Der Präsident/die Präsidentin der Begleitkommission:

Name: Putallaz **Vorname:** Jean-Christophe

Amt, Firma, Institut: Service des routes, transports et cours d'eau, DTEE, Etat du Valais

Unterschrift des Präsidenten/der Präsidentin der Begleitkommission:

Sion, le 03.10.2017

Index of research reports on the subject of road

The list of the recently published final reports can be downloaded at
www.astra.admin.ch (Forschung im Strassenwesen --> Downloads --> Formulare)